

Use of supercritical carbon dioxide for decellularization of porcine trachea in an attempt to generate a tissue-engineered tracheal substitute

Use of supercritical carbon dioxide for decellularization of porcine trachea in an attempt to generate a tissue-engineered tracheal substitute

by

Daniëlle van Dis

in partial fulfilment of the requirements for the degree of

Master of Science
in Biomedical Engineering

at the Delft University of Technology,
to be defended publicly on Friday, July 23, 2021 at 09:30

Supervisors:	Dr. E. Oosterwijk	Radboud University Medical Centre
	R. de Wit	Radboud University Medical Centre
	Dr. ir. E.L. Fratila-Apachitei	Delft University of Technology
Thesis committee:	Prof. dr. ir. A.A. Zadpoor	Delft University of Technology
	Dr. ir. E.L. Fratila-Apachitei	Delft University of Technology
	Dr. E. Oosterwijk	Radboud University Medical Centre
	Dr. M.M.A. Verstegen	Erasmus Medical Centre

An electronic version of this thesis is available at <http://repository.tudelft.nl/>.

Abstract

Purpose: Patients with tracheal lesions that exceed half of the trachea's total length require a tracheal substitute. Tissue engineering, using either synthetic materials or decellularized tracheal tissue, opens up new possibilities for generating tracheal substitutes. Decellularization, a procedure in which the tissue's immunogenic cellular material is removed while the extracellular matrix (ECM) is preserved, seems the most promising approach. The majority of tracheal decellularization methods, however, are reliant on harsh chemicals and require lengthy wash procedures, resulting in damage to the ECM. To address these issues, a supercritical carbon dioxide (scCO₂) decellularization approach has been suggested as an alternative solution due to its ability to both decellularize and sterilize tissues while leaving no toxic residues and requiring less treatment time. Therefore, the aim of this thesis was to compare scCO₂ treatment with a chemical decellularization method, which is the current gold standard reported in literature, for creating a decellularized porcine tracheal scaffold with good cytocompatibility.

Methods: A total of five different protocols were tested that varied in decellularization and sterilization methods used. Decellularization efficiency was evaluated in terms of DNA content, histological appearance, and retention of ECM components. Additionally, mechanical tensile testing and scanning electron microscopy were used to assess the effects of the different decellularization protocols. Further, decellularized scaffolds were recellularized with fibrin-encapsulated porcine adipose derived stem cells to assess the cytocompatibility of the scaffolds.

Results: The highest reduction in DNA content was observed when samples were subjected to the vacuum-assisted detergent-enzymatic method (DEM), followed by sterilization with gamma irradiation, and when samples were subjected to scCO₂ treatment, followed by washing with sodium hydroxide. The latter protocol, however, also negatively impacted the ECM, whereas good preservation of ECM components was seen with the DEM protocol. DNA and histological analysis showed that treatment with scCO₂ in combination with a hydrogen peroxide (H₂O₂) washing step was unable to completely decellularize porcine tracheas. Static surface seeding of the decellularized scaffolds led to poor cell adherence. Cells encapsulated in fibrin and seeded on the tracheal scaffolds were able to adhere and survive, showing the cytocompatibility of the decellularized scaffolds.

Conclusions: Decellularization with scCO₂ in combination with a H₂O₂ washing step was not successful in completely decellularizing the porcine tracheas, and possibly requires the use of a co-solvent or secondary agent for successful decellularization. For recellularization of decellularized tracheal scaffolds, the use of fibrin as a cell carrier is an effective and simple seeding method. The findings in this thesis open up new avenues for potential optimizations in future research.

Contents

Abstract	i
List of Figures	iv
List of Tables	viii
1 Introduction	1
2 Materials and Methods	5
2.1 Assessment of decellularization efficiency	5
2.1.1 Trachea harvesting and decellularization	5
2.1.2 Biochemical analyses	6
2.1.3 Histological evaluation	6
2.1.4 Immunohistochemistry	7
2.1.5 Scanning electron microscopy	7
2.1.6 Mechanical tests	7
2.1.7 Mechanical testing of separate tissue components	8
2.2 Recellularization analysis	11
2.2.1 Isolation and cell culture of porcine adipose-derived stem cells	11
2.2.2 <i>In vitro</i> cell seeding	12
2.2.3 Cell metabolic assay	12
2.2.4 Histology	13
2.3 Bioreactor culture	13
2.4 Statistical analysis	14
3 Results	15
3.1 Decellularization efficiency	15
3.2 Evaluation of ECM integrity	15
3.3 Scanning electron microscopy	17
3.4 Mechanical properties	17
3.4.1 Force-displacement and stress-stretch curves	17
3.4.2 Hyperelastic modelling	22
3.5 Cytocompatibility of decellularized tracheal scaffolds	24
3.6 Bioreactor culture	26
4 Discussion	27
4.1 Decellularization efficacy	27
4.2 Impact of sterilization	28
4.3 Recellularization of decellularized scaffolds	29
4.4 Limitations and future perspectives	31
5 Conclusion	33
Bibliography	34
A Optimization of Static Seeding	43
A.1 Materials and Methods	43
A.1.1 Static surface seeding with hbSMCs of a dry scaffold	43
A.1.2 Static surface seeding with hbSMCs of a pre-wetted scaffold	43
A.1.3 Static surface seeding with hADSCs of a pre-wetted scaffold	44
A.1.4 Static seeding with progenitor cells isolated from porcine pleura, trachea, pericard and adipose tissue	44
A.1.5 Pre-wetting with FCS	44
A.1.6 Using Whatman paper	44

A.2 Results & Discussion 45

List of Figures

1.1	Tissue layers present in the trachea.	1
1.2	Phase diagram for CO ₂ . T_c and p_c are the temperature and pressure of CO ₂ beyond the critical values, respectively. Above these values CO ₂ becomes a supercritical fluid.	3
2.1	Samples of native trachea (A), trachea decellularized using scCO ₂ (III) method (B) and trachea decellularized using DEM-gamma method (C). In (A1–C1) and in (A2–C2) the front view and side view, respectively, of the composite tissue samples are depicted. In A3–C3 the cartilage samples are shown. In (D) a sample under uniaxial tension can be seen. (E) shows a schematic overview of the tracheal samples under uniaxial tension. Cartilage is depicted in light grey, and connective tissue is depicted in black. The composite tissue (connective tissue) sample is subjected to uniaxial tension in the axial direction, whereas the cartilage sample is subjected to uniaxial tension in the circumferential direction.	9
2.2	Schematic illustration of the static seeding method using fibrin gel as a cell carrier. First, cells are suspended in fibrogen solution. Subsequently, thrombin is added and the cell-fibrin suspension is pipetted on the scaffold.	12
2.3	Overview of the bioreactor setup. In (A1) the three bioreactor chambers are depicted and in (A2) a closeup of one of the chambers with a scaffold strip clamped (white arrow) in the chamber can be seen (A2). In (B) an overview of the bioreactor program with 10% cyclic uniaxial strain with a frequency of 0.25 Hz in accordance with the respiratory rate in adults is depicted.	13
3.1	Efficacy of porcine trachea decellularized with scCO ₂ or DEM. (A-F) H&E staining of decellularized and native porcine trachea. Tissue decellularized with scCO ₂ (I) (A) and DEM-gamma (E) show complete removal of cellular nuclei. No nuclei are visible in the lacunae (black arrow with o). In the scCO ₂ (II) (B) and scCO ₂ (III) (C) groups both cells in the outer tissue layers as well as chondrocytes in the cartilage tissue are depicted (indicated with * and black arrow with •, respectively), although to a lesser extent as in native tracheal tissue (F). (G) DNA content was measured in native tracheal tissue and following decellularization. A significant reduction in DNA content was seen in all samples, except scCO ₂ (III), compared to native trachea. # = significant difference (S.D.) from scCO ₂ (II), scCO ₂ (III) and native trachea ($p < 0.001$); \$ = S.D. from DEM-ethanol ($p < 0.05$); & = S.D. from DEM-gamma ($p < 0.001$), ‡ = S.D. from native trachea ($p < 0.05$), ⊙ = S.D. from DEM-gamma ($p < 0.001$), ¥ = S.D. from DEM-gamma ($p < 0.01$); • = S.D. from native trachea ($p < 0.001$). (H) Macroscopic images of the decellularized and native tracheal samples. Decellularized tracheal samples had a colourless appearance.	16
3.2	Glycosaminoglycan (GAG) content of decellularized tracheal matrices. Native porcine trachea stained with alcian blue (F1,F2) compared to tracheal matrices decellularized with scCO ₂ (I) (A1,A2), scCO ₂ (II) (B1,B2), scCO ₂ (III) (C1,C2), DEM-ethanol (D1,D2) and DEM-gamma (E1,E2). The black arrows indicate the territorial matrix which is the area around the lacunae of the chondrocytes. Trachea in the scCO ₂ (I) group show complete loss of GAGs. Some of the other decellularized matrices (B,D,E) show a less intense staining compared to native trachea (F). Matrices from the scCO ₂ (III) group (C) show retention of GAGs. (G) Quantitative analysis of sulphated GAGs in decellularized and native tracheal tissue. A significant reduction in sGAG content is seen in the scCO ₂ (I) and DEM-gamma groups when compared to native trachea. # = significant difference (S.D.) from scCO ₂ (II), scCO ₂ (III), DEM-ethanol and native trachea ($p < 0.001$), \$ = S.D. from DEM-gamma ($p < 0.05$), ‡ = S.D. from DEM-ethanol ($p < 0.01$), ⊙ = S.D. from DEM-gamma ($p < 0.001$), ¥ = S.D. from native trachea ($p < 0.01$).	18

3.3	Native and decellularized trachea stained with Picrosirius red and Gomori's trichrome to evaluate the preservation of collagen in the ECM. Native porcine trachea (F1,F2,F3) are compared to tracheal matrices decellularized with scCO ₂ (I) (A1,A2,A3), scCO ₂ (II) (B1,B2,B3), scCO ₂ (III) (C1,C2,C3), DEM-ethanol (D1,D2,D3) and DEM-gamma (E1,E2,E3). Only a clear reduction in staining intensity can be observed in the samples decellularized with scCO ₂ (I). Collagen is mostly preserved in the other groups.	19
3.4	Immunohistological staining for collagen type II of tracheal samples from each treatment group; treated with (A) scCO ₂ (I), (B) scCO ₂ (II), (C) scCO ₂ (III), (D) DEM-ethanol, (E) DEM-gamma, and (F) untreated. Collagen type II was preserved in all groups.	20
3.5	Scanning electron microscopy (SEM) of tracheal samples. The luminal surfaces and outer surfaces of tracheal matrices decellularized with scCO ₂ (I) (A1–A4), scCO ₂ (II) (B1–B4), scCO ₂ (III) (C1–C4), DEM-ethanol (D1–D4) and DEM-gamma (E1–E4) are shown.	21
3.6	Biomechanical properties of porcine tracheal scaffolds following decellularization. (A) Average force-displacement curves of decellularized tissue samples tested. (B) Maximum force of the decellularized tracheas. # = significant difference (S.D.) from scCO ₂ (III) and DEM-ethanol ($p < 0.001$), \$ = S.D. from native trachea ($p < 0.01$), ‡ = S.D. from scCO ₂ (III) ($p < 0.001$), ∅ = S.D. from DEM-ethanol ($p < 0.01$), & = S.D. from native trachea ($p < 0.05$), ¥ = S.D. from DEM-gamma ($p < 0.01$), % = S.D. from DEM-gamma ($p < 0.01$), † = S.D. from native trachea ($p < 0.05$).	21
3.7	Cauchy stress-stretch data for cartilage and composite tissue (connective tissue) samples from (A) native trachea ($n = 4$ and $n = 2$ for cartilage and connective tissue samples, respectively), (B) trachea decellularized with the DEM-gamma method ($n = 3$ for both cartilage and connective tissue samples), and (C) trachea decellularized with the scCO ₂ (III) method ($n = 5$ and $n = 3$ for cartilage and connective tissue samples, respectively). Cartilage shows a linear response in all groups. The connective tissue in the native and scCO ₂ (III) groups show typical stiffening behavior. In (D) the tensile elastic modulus of the different cartilage samples is depicted. No statistical differences were seen between groups ($p > 0.05$).	22
3.8	Fit of the Yeoh hyperelastic model to the experimental Cauchy stress-stretch data obtained from uniaxial tensile testing for cartilage and connective tissue (composite tissue) samples from (A) native trachea, (B) trachea decellularized with the DEM-gamma method, and (C) trachea decellularized with the scCO ₂ (III). The model reflects the stress-stretch behavior of the different tissue types accurately.	23
3.9	Histological staining and metabolic activity (WST-1 assay) were used to evaluate the attachment and proliferation of cells seeded on decellularized tracheal scaffolds. (A) Proliferation (WST-1 assay) of pADSCs seeded on decellularized tracheal scaffolds and cultured in proliferation medium over a 10 day culture period ($n = 1$). A decline in metabolic activity was seen in the scCO ₂ (III) group, whereas an increase in metabolic activity was seen in the DEM-ethanol group. (B) Proliferation of pADSCs seeded on decellularized tracheal scaffolds and cultured in chondrogenic differentiation medium over a 7 day culture period. The results of three separate experiments are depicted ($n = 1$, $N = 3$). Metabolic activity did not decrease significantly over time, indicating the cells were able to proliferate and survive on all scaffolds. (C) Representative images of the H&E staining of the cell seeded constructs in chondrogenic differentiation medium at day 7.	24

- 3.10 Histological staining was used to evaluate the attachment of cells seeded on tracheal scaffolds that had been decellularized using various methods. Representative images of the H&E staining of the cell seeded constructs decellularized with the (A) DEM-ethanol, (B) DEM-gamma and (C) scCO₂(III) methods and cultured for 21 days in chondrogenic differentiation medium ($n = 1$ for each group). Cells in the DEM-ethanol and scCO₂(III) groups depicted a spindle-shape and elongated morphology. Minimal cell infiltration was seen. Alcian blue staining was used to visualize GAGs and as such evaluate the chondrogenic potential of the cells seeded on the constructs decellularized with (D) DEM-ethanol, (E) DEM-gamma, and (F) scCO₂(III) methods and cultured for 21 days in chondrogenic differentiation medium. A slightly enhanced blue staining was seen from day 7 to day 21, especially in the scCO₂(III) group, suggesting the production of GAGs and thus chondrogenic differentiation. 25
- A.1 Human bladder smooth muscle cell (hbSMC) seeding of decellularized tracheal scaffolds. All scaffolds were seeded with 5×10^5 hbSMCs at passages 6 and 9 ($n = 3$ for each group). (A) Metabolic activity (WST-1 assay) and (B) cell proliferation (PicoGreen) were measured and compared on day 0 (24 hours) and day 7 after seeding. Data were expressed as mean \pm SD. Results display that the metabolic activity of the cells is low and did not increase over time, indicating that the cells were not able to adhere on the scaffolds. DNA quantification, which is assumed proportional to cell number, showed a DNA amount of less than 50 ng/mg scaffold in all scaffolds, indicating a low cell number. Besides, DNA content decreased over time in all scaffolds. * $p < 0.05$; ** $p < 0.01$; *** $p < 0.001$. 45
- A.2 Human bladder smooth muscle cell (hbSMC) seeding of decellularized tracheal scaffolds pre-wetted in SMC medium or FNC coating mix. All scaffolds were decellularized with the scCO₂(III) method and seeded with 5×10^5 hbSMCs. (A) WST-1 assay displays absorbance values close to zero, indicating low metabolic activity of the seeded cells. (B) After 7 days of culture, H&E staining demonstrated that there were no cells on the surface of the scaffolds. 46
- A.3 Proliferation (WST-1 assay) of (A) human adipose derived stem cells (hADSCs) seeded on tracheal scaffolds decellularized with the scCO₂(III) method cultured for up to 7 days and (B) hADSCs seeded in a 24 well plate after 24 hours of incubation. Bars represent the results of one experiment ($n = 1$). 47
- A.4 Proliferation (WST-1 assay) of (A) porcine progenitor cells (isolated from pleura, pericard, trachea and adipose tissue) seeded on tracheal scaffolds decellularized with the scCO₂(III) and DEM-ethanol methods after 1 day and 7 day proliferation. Bars represent the results of one experiment ($n = 1$). (B) H&E staining images of decellularized tracheal constructs seeded with porcine progenitor cells isolated from pleura, pericard, trachea and adipose tissue and cultured for up to 7 days. The images of the DEM-ethanol scaffold seeded with progenitor cells isolated from pericard tissue at day 0 is a top view. 48
- A.5 Comparison of recellularized decellularized tracheal scaffolds with porcine adipose derived stem cell (pADSC). Cell suspensions of pADSCs ($5 \times 10^5 / \text{cm}^2$) were pipetted on scaffold punches placed on a double layer of autoclaved Whatman paper. After 24 hours, medium was changed to differentiation medium or the cell-seeded constructs were continuously cultured in proliferation medium. (A) Proliferation of the seeded cells was assessed with the WST-1 assay. The WST-1 assay mainly shows a decline in metabolic activity from day 0 to day 7, both when cultured in (A1) proliferation medium as well as in (A2) chondrogenic differentiation medium. (B) Images of pADSCs cultured on decellularized tracheal scaffolds at 0 and 7 days and stained with H&E. Some cell adherence on the DEM-ethanol scaffolds after 7 day proliferation was seen. The results of one experiment ($n = 1$) are depicted. 49
- A.6 24 hours (day 0) and 7 days after porcine adipose derived stem cell (pADSC) seeding onto DEM-ethanol and scCO₂(III) decellularized tracheal scaffolds that were incubated in 100% fetal calf serum (FCS) overnight, (A) the proliferation (WST-1 assay) of the cells was measured and (B) H&E images were taken. The results of one experiment ($n = 1$) are depicted. 50

- A.7 Comparison of decellularized tracheal scaffolds seeded with fibrin encapsulated porcine adipose derived stem cell (pADSC). pADSCs ($5 \times 10^5 / \text{cm}^2$) were suspended in fibrinogen and, after addition of thrombin, pipetted on scaffold punches. After 24 hours, medium was changed to differentiation medium or the cell-seeded constructs were continuously cultured in proliferation medium. (A) Proliferation of the seeded cells was assessed with the WST-1 assay. Results of the cell-seeded constructs when cultured in (A1) proliferation medium or in (A2) chondrogenic differentiation medium are displayed. (B) Images of fibrin-encapsulated pADSCs cultured on decellularized tracheal scaffolds at 0 and 7 days and stained with H&E. The results of one experiment ($n = 1$) are depicted. 51

List of Tables

2.1	Decellularization protocols used.	5
2.2	Hyperelastic materials models used in this thesis. The strain energy function and related Cauchy stress equation for an incompressible isotropic material subjected to uniaxial tension are provided for each model.	11
2.3	Parameters of the different groups used in the seeding experiments.	12
3.1	Different hyperelastic models were used to fit the experimentally obtained stress-stretch data of the different decellularized tracheal tissue components. In the table the coefficient of determination, R^2 , for each model and tissue type is displayed.	23

Introduction

Tracheal lesions are uncommon, yet they pose a significant challenge for thoracic surgeons [1]. At first, the trachea was considered to be a simple structure to reconstruct [2]. However, published work to date has shown that the trachea's complex structure makes tracheal reconstruction a significant challenge.

The trachea is a hollow framework comprised of a series of 18 to 22 C-shaped cartilaginous rings that are interconnected with ligaments (Figure 1.1) [3, 4]. Posteriorly, the semi-circular cartilaginous rings are bridged by trachealis muscle [4]. The fibrocartilaginous structure is key for maintaining an open conduit and providing the trachea with the necessary longitudinal stability for neck movement, voice, and swallowing [4, 5]. The internal mucosal lining is perfused by blood vessels that penetrate the inter-cartilaginous ligaments [5]. This mucosal lining is comprised of pseudostratified epithelium, which aids in mucosal secretion clearance and serves as a barrier against infection [4, 6]. The epithelium rests on the basement membrane, a specialized form of extracellular matrix (ECM) that acts as a barrier for epithelial cell attachment and proliferation [2, 7]. The underlying lamina propria is comprised of many elastic fibers and forms, together with the basement membrane and the epithelium, the mucosa [4]. Underneath the mucosa is the submucosa which is comprised of loose areolar connective tissue in which seromucous tubular glands reside [2, 4]. The outer connective tissue layer of the trachea is called the adventitia, and houses fibroblasts, nerves, lymphatics and blood vessels [2, 4].

Tracheal lesions can be divided into two categories, namely acquired and congenital lesions. Tracheomalacia and congenital tracheal stenosis are the two most common congenital tracheal lesions [9]. Congenital tracheal stenosis affects around one in every 64,500 live births, whereas the incidence rate of tracheomalacia is unknown [9, 10]. Iatrogenic injury during or after tracheostomy or endotracheal intubation are the most common causes of acquired benign tracheal stenosis [11, 12]. The estimated incidence rate of adult post-intubation laryngotracheal stenosis is around 4.9 people per million per

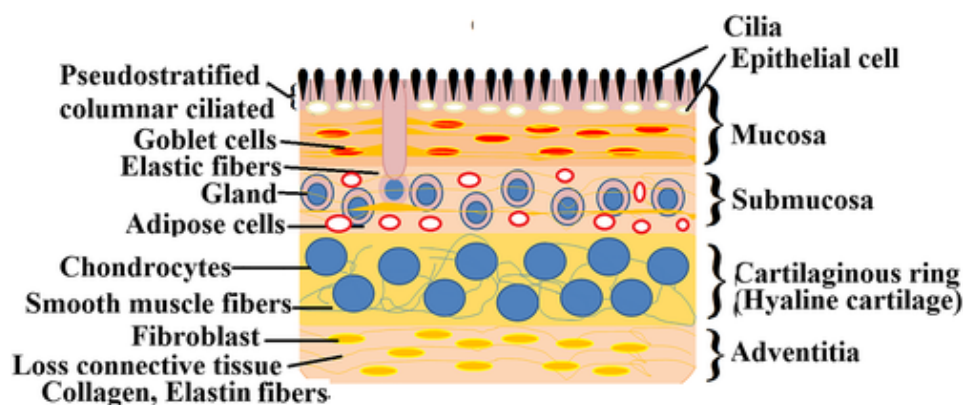


Figure 1.1: Tissue layers present in the trachea. Obtained from [8].

year [13]. Other etiologies for acquired tracheal stenosis are infection, external trauma and autoimmune diseases [2, 14]. Tracheal malignancies are rare, affecting approximately 1.4 to 2.6 people per million per year [15, 16]. Squamous cell carcinoma and adenoid cystic carcinoma are the two most prevalent histological types, accounting for approximately 60% of all primary tumors in the trachea [15].

Short-segment tracheal lesions, e.g. comprising less than 50% of the length of the trachea, can be repaired using a variety of methods, of which tracheal resection accompanied by direct end-to-end anastomosis is the gold standard [5]. This curative procedure is often successful with low mortality rates [17, 18]. Yet, anastomotic complications such as granulation at the anastomosis site, stenosis, and separation may occur after resection [18]. While these complications are rare, they can cause significant morbidity [18]. Diabetes mellitus, reoperation, the need for pre-operative tracheostomy, laryngotracheal resection, pediatric patients, and resections ≥ 4 cm are all risk factors that increase the complication rate, as identified by Wright et al. [18]. Other treatment options are required for these so-called complicated short-segment tracheal lesions [5]. Common treatment options include the use of cartilage grafts, anterior tracheoplasty, and free tracheal autografts, all with their own advantages and disadvantages [5].

Resection is no longer an option for long-segment tracheal lesions, characterized as lesions that are longer than half the tracheal length in adults or one third the tracheal length in children, since it would result in high mechanical stress at the anastomosis site [19]. However, there are few other options for this particular patient group. Temporary treatment options for long-segment tracheal lesions include mechanical dilatation, laser treatment and stent placement [20, 21]. Palliative stenting has numerous disadvantages, including granulation formation, loss of mucocilliary transport, infection and stent displacement [22]. Furthermore, these temporary treatment options often require repetitive treatment due to, e.g., excessive scar tissue formation and restenosis [20].

Curative treatment of long-segment tracheal lesions, however, remains an unresolved issue that necessitates the use of a tracheal substitute [5, 23]. The ideal trachea substitute, according to Belsey, Grillo and many other researchers in the field, should be laterally rigid, longitudinally flexible, airtight, biocompatible, nonimmunogenic, nontoxic and expandable [23–25].

Over the years, extensive research has been invested into trying to find the ideal tracheal substitute. These techniques were classified into five categories by Grillo: foreign materials, nonviable tissues, autogenous tissues, tracheal transplantation and tissue engineering [23]. Synthetic prostheses have been linked to many problems, including graft migration, dislodgement, erosion of surrounding tissue, obstruction with granulation tissue and infection [23, 26]. Implantation of nonviable tissues led to scar tissue formation and necrosis of the epithelium and cartilaginous rings [27, 28]. Tracheal transplantation necessitates life-long immunosuppressive therapy which is especially undesirable for cancer patients and lacks sufficient revascularization resulting in stenosis and obstruction [25]. Conduit allografts and autografts (such as esophagus, bowel, aorta, and trachea) used for tracheal replacement often have poor mechanical properties, are limited by the lack of donors, and are associated with remodeling after implantation, resulting in formation of scar tissue, obstruction and eventually graft failure [23]. Furthermore, due to the poor mechanical properties of these allografts, additional stent placement is required, which is again associated with complications such as inflammation and infection [25]. Reconstruction with autogenous tissue either as patches or as a tubular structure, e.g. skin flaps supported with cartilage strips [29], have also shown limited success due to failure of healing [23]. Tissue engineering (TE) seems to be a more attractive option for regenerating a tracheal substitute. However, no clinical successes involving tissue-engineered structures have been reported to date, and there are still several hurdles to overcome in this field.

The so-called TE triad forms the basis of TE research and is comprised of three main elements: cells, signaling molecules, and a scaffold [8, 30, 31]. In this context, the scaffold, in combination with the signaling molecules, provides the structural and mechanical support and modulates cellular behavior [30, 31]. In tracheal TE, two main material types for preparation of scaffolds can be distinguished, namely synthetic materials and decellularized tracheal tissue [32]. Synthetic polymeric scaffolds have several advantages. They are simple to sterilize and manufacture, eliminate the need for donor tissue

and can be tailored to fit the patient's specific needs [32, 33]. Another major advantage is that the scaffold's properties are relatively easy to control and can be adjusted to regulate cell behavior [30, 32, 33]. To date, however, synthetic scaffolds show poor outcomes *in vivo*, mainly as a result of delayed epithelialization and lack of revascularization [34, 35]. This is largely attributed to the poor biocompatibility of synthetic scaffolds and the absence of the unique ECM composition of the native trachea [36, 37].

Decellularization of tracheal donor tissue is considered more interesting. The aim of the decellularization procedure is to eliminate any cells and cellular material that could potentially cause an adverse immune response when the scaffold is implanted *in vivo*, while preserving as much of the biochemical and structural composition of native extracellular matrix (ECM) as possible [30, 36]. Decellularized scaffolds have been shown to possess anti-inflammatory properties and promote constructive tissue remodeling upon implantation; a process that includes the formation of “*de novo*, site-appropriate tissue” [37–39].

Chemical, enzymatic and physical methods, or a combination of these methods, are utilized to decellularize the native tissue [30]. Subsequently, the decellularized tissue can be recellularized with autologous cells to create a functional, patient-specific tissue [30]. A major drawback, however, is that for obtaining decellularized tracheal scaffolds donor tissue is still required [36]. Furthermore, variability in donor tissue results in low reproducibility [40].

Currently, decellularized tracheal scaffolds are often prepared by the so-called detergent-enzymatic method (DEM), which makes use of the detergent sodium deoxycholate (SDC) and the enzyme deoxyribonuclease (DNase) to remove cells and cellular remnants from the tissue [41–43]. Although this method has proven to be effective, the decellularization process takes several weeks to complete and has been shown to result in loss of ECM components, such as collagen and glycosaminoglycans (GAGs) [41, 42]. In 2015, Lange et al. published a modification of the DEM, namely an accelerated vacuum-assisted decellularization protocol, which resulted in a significant reduction in treatment time and increased reproducibility [44, 45]. However, this method still requires the use of chemicals and enzymes in the decellularization process, which has several drawbacks. Detergents are strongly cytotoxic, and if residual chemicals are present in the tissue, they could be toxic to host cells when implanted *in vivo* or impair cellular growth when the scaffold is recellularized [30, 46, 47]. Furthermore, since residual nucleases are difficult to remove from tissue, lengthy, time consuming wash procedures are needed to limit the risk of an adverse immune response [47, 48]. Along with this, chemical and enzymatic decellularization approaches almost certainly result in (some) disruption of ECM ultrastructure proteins and require an additional sterilization step [30, 47–49].

Thus, innovative, safer decellularization strategies that eliminate the use of harsh chemicals are needed [50]. In recent years, supercritical carbon dioxide (scCO₂) has been used as an alternative decellularization approach. scCO₂ is a fluid state of CO₂, that occurs when CO₂ is compressed and heated above its critical pressure and temperature (304.2 K and 7.38 MPa, respectively) (Figure 1.2) [51].

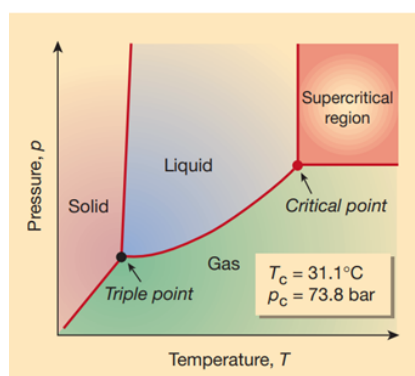


Figure 1.2: Phase diagram for CO₂. T_c and p_c are the temperature and pressure of CO₂ beyond the critical values, respectively. Above these values CO₂ becomes a supercritical fluid. Obtained from [51].

scCO₂ possesses the attractive properties of being relatively inert, nontoxic, environmentally friendly, inexpensive, readily available in nature and nonflammable [48, 50]. Along with this, scCO₂ holds a unique combination of gas-like and liquid-like properties, meaning scCO₂ exhibits liquid-like density but low viscosity and high diffusivity [48, 51]. Because of these unique properties, along with its zero surface tension, scCO₂ can serve as a good solvent and permeate dense matrices, without leaving behind any toxic traces inside the tissue or affecting the material's mechanical properties [30, 50–52]. Another great advantage of scCO₂ is that it is also an effective sterilization technique, eliminating the need for an additional sterilization step [48].

Hence, it was hypothesized that with a scCO₂ decellularization approach an off-the-shelf, sterile, decellularized tracheal substitute could be obtained in less time than when using the vacuum-assisted decellularization method. Therefore, the aim of this thesis was to assess the potential of using scCO₂ for decellularizing porcine tracheal tissue. For this purpose, three objectives were defined: (1) analyze and compare the efficiency of scCO₂ decellularization of porcine trachea with the vacuum-assisted decellularization method, (2) assess the biocompatibility of the decellularized tracheal matrices by recellularizing the scaffolds with stem cells, and (3) study the effect of cyclic loading on the chondrogenic phenotype of the cells seeded on the decellularized matrices.

2

Materials and Methods

2.1. Assessment of decellularization efficiency

2.1.1. Trachea harvesting and decellularization

Tracheas from landrace pigs involved in unrelated experiments with planned termination were used for decellularization. The approximate length of each trachea was 10 cm. The tracheas were decellularized by the vacuum-assisted detergent-enzymatic method (DEM) or the supercritical carbon dioxide (scCO₂) method and were sterilized using various procedures. A total of six groups were defined and are displayed in table 2.1. These groups will be addressed in this thesis as scCO₂(I), scCO₂(II), scCO₂(III), DEM-ethanol, DEM-gamma and native trachea.

Decellularization process with scCO₂

Tracheal scaffolds that were decellularized using scCO₂ were prepared by HCM Medical (Nijmegen, the Netherlands). In brief, the tracheas were washed, cut into smaller pieces and treated with scCO₂. During scCO₂ processing, the temperature was set at 37°C at a pressure of 250 bar for a time period of 12 hours and a constant flow of CO₂ was used. After scCO₂ processing, tissues were washed with 25% hydrogen peroxide (H₂O₂) for 60 minutes and multiple times with water afterwards. For the scCO₂(I) method, this was followed by an additional washing step with 1.25 M sodium hydroxide (NaOH) for 30 minutes and several washes in water. For all tissues, the pH value of the last washing step was set at 7.4 ± 0.2. Subsequently, all tissues were freeze dried under vacuum conditions for 3 days. The first drying step was set at a temperature of -20°C, followed by drying steps at -5°C and 20°C. Following freeze drying, scaffolds were sterilized using either gamma irradiation at a minimum dose of 25 kGy (methods scCO₂(I) and scCO₂(II)) or scCO₂ (method scCO₂(III)). For sterilization with scCO₂ the temperature was set at 35°C at a pressure of 160 bar for 4 hours, and peracetic acid was used as a co-solvent.

Table 2.1: Decellularization protocols used.

Group	Decellularization protocol	Sterilization method
scCO ₂ (I)	scCO ₂ +H ₂ O ₂ +NaOH+freeze drying	Gamma irradiation
scCO ₂ (II)	scCO ₂ +H ₂ O ₂ +freeze drying	Gamma irradiation
scCO ₂ (III)	scCO ₂ +H ₂ O ₂ +freeze drying	scCO ₂
DEM-ethanol	Freeze+thaw+Triton X-100/SDC +DNase/RNase	70% ethanol
DEM-gamma	Freeze+thaw+Triton X-100/SDC +DNase/RNase	Gamma irradiation
Native trachea	Control; untreated trachea	-

Chemical decellularization

Decellularization of porcine tracheas using the vacuum-assisted DEM was performed by a PhD student at the department following the protocol as described by Lange et al. [44]. In brief, tracheal tissue was frozen at -80°C and subsequently thawed at room temperature (RT) for 1 to 2 hours. After thawing, the tissue was incubated in a solution containing the detergents 0.25% Triton X-100 and 0.25% sodium deoxycholate (SDC) for 24 hours and incubated in DNase (2 kU/mL) and RNase (100 $\mu\text{g}/\text{mL}$) for 2×24 hours, with washing steps in between the incubation steps. The complete decellularization protocol was performed in a container in which a vacuum to <1000 Pa was created. After decellularization, tissues in the DEM-gamma group were sent to HCM Medical (Nijmegen, the Netherlands), where the scaffolds were freeze-dried and sterilized with gamma irradiation using the same procedure as described in the section *Decellularization process with scCO_2* .

2.1.2. Biochemical analyses

Decellularized and native tracheal tissues were cut with a 6-mm biopsy punch and weighed to determine their dry weight. Subsequently, samples were incubated with phosphate buffered saline (PBS) for 24 hours. After 24 hours, any excess water was removed with Whatman paper and the weight of the samples was determined. Next, samples were digested in a phosphate buffer (0.1 M sodium phosphate buffer, 5 mM L-cystein, and 5 mM EDTA) containing 140 $\mu\text{g}/\text{mL}$ papain (from papaya latex, Sigma-Aldrich) for 16 hours at 60°C to completely digest the tissue samples. Subsequently, samples were left to cool to RT before being centrifuged at 13,000 rpm for 10 minutes. The supernatant of each sample was collected and stored at -20°C until further analysis.

The Quant-iT PicoGreen dsDNA Assay Kit (Thermo Fisher Scientific) was used to quantify dsDNA contents. PicoGreen is a highly sensitive fluorescent probe that only fluoresces when bound to dsDNA, making it ideal as a marker for cell numbers [53]. In brief, 28 μL of standards and samples were added to a 96-well plate, to which 72 μL of PicoGreen solution and 100 μL of Tris-EDTA buffer was added. After the plate was incubated in the dark for 10 minutes, the fluorescence was measured using a microplate reader (Wallac 1420 Victor) at excitation/emission wavelengths of 485/525 nm. DNA contents were determined in relation to the standard curve and normalised to the wet weight of the samples.

GAG contents were quantified using the dimethyl-methylene blue (DMMB) assay. This colorimetric assay employs the dye 1,9-dimethyl-methylene blue, which binds to negatively charged sulfated GAGs (sGAGs), causing a metachromatic shift [54]. In brief, 10 μL of diluted sample was mixed with 200 μL of DMMB reagent (38.45 $\mu\text{mol}/\text{L}$ 1,9-dimethyl-methylene blue (Sigma-Aldrich), 40.5 mmol/L NaCl, 40.5 mmol/L glycine; pH 3.0). Absorbance values were measured immediately at a wavelength of 525 nm using a Benchmark Plus microplate reader (Bio-Rad) and the GAG concentration of the samples was determined from a standard curve obtained from bovine tracheal chondroitin 4-sulfate (Biocolor).

2.1.3. Histological evaluation

Scaffold punches from each group were embedded in Tissue-Tek (O.C.T. Compound) and frozen in isopentane well cooled on dry ice for histological analysis. Next, 5 μm sections of the Tissue-Tek blocks containing the scaffolds were prepared on a cryostat and mounted on SuperFrost Plus slides (Thermo Fisher Scientific). Sections were fixed in 4% paraformaldehyde, washed with PBS and subsequently stained with Hematoxylin and Eosin (H&E), Alcian Blue, Picrosirius red and Gomori's trichrome. The staining procedures can be found below. Following histological staining, slides were dehydrated through a series of ethanol solutions, cleared in two changes of xylene and mounted with Permount mounting medium (Thermo Fisher Scientific). All stained sections were analyzed using a light microscope (Leica DMI1).

H&E stain. For H&E staining, sections were stained for 10 minutes with hematoxylin. Following that, the sections were rinsed in running tap water for 10 minutes before being stained with 0.5% eosin in 96% ethanol for 5 minutes. With H&E staining, nuclei stain purple and the cytoplasm and ECM stain pink.

Alcian blue stain. To detect the presence of sGAGs, Alcian blue staining was performed. Sections were stained with a solution of 1% Alcian Blue 8GX (pH 2.5; Sigma-Aldrich) dissolved in 3% (v/v)

aqueous acetic acid for 1 hour. After washing in distilled water for 5 minutes, all sections were counterstained with hematoxylin for 3 minutes and washed in running tap water for 5 minutes. With this stain, sGAGs stain turquoise-blue, and the intensity of staining can give an estimation of the amount of sGAGs present in the tissue.

Picosirius red stain. To assess collagen in the decellularized tissues, sections were stained with Sirius Red (Direct Red 80, Sigma-Aldrich). In brief, sections were stained in hematoxylin and washed under running tap water. Sections were then incubated in 0.1% (w/v) sirius red in picric acid for 1 hour, followed by two changes in 0.5% (v/v) acetic acid solution. With this staining, collagen stains red and nuclei stain black.

Gomori's trichrome stain. Sections were stained with Van Gomori trichrome at the Pathology department of the Radboud University Medical Center (Nijmegen, the Netherlands) to also assess collagen in the matrices. In brief, sections were stained in Harris hematoxylin for 5 minutes and rinsed in running tap water for 5 to 10 minutes. After briefly rinsing the slides in distilled water, sections were stained in trichrome solution (chromotrope 2R, fast green FCF, phosphotungstic acid, deionized water, and acetic acid) for 20 minutes. Subsequently, slides were briefly incubated in 0.25% (v/v) acetic acid solution. Gomori's trichrome stains connective tissues containing collagen green-blue, such as the basement membrane, cytoplasm and muscle fibers red-purple and nuclei blue-black.

2.1.4. Immunohistochemistry

For immunostaining, decellularized and native tracheal samples were embedded in Tissue-Tek (O.C.T. Compound) and frozen in isopentane cooled on dry ice. Samples were cryosectioned at a thickness of 5 μm and fixed with 100% pre-cooled acetone (-20°C) for 10 minutes. Endogenous peroxidase activity was blocked by incubating the sections in 1% (v/v) H_2O_2 solution in PBS for 10 minutes at RT, followed by 30 minutes of treatment with 10% (v/v) normal goat serum in a solution of 1% (w/v) bovine serum albumin/phosphate buffered saline (BSA/PBS) to block non-specific protein binding sites. Subsequently, sections were incubated with the anti-Collagen type 2 primary antibody (1:400, COL2A1, Santa Cruz Biotechnology, sc-52658) overnight at 4°C in a humidified chamber. Next, sections were rinsed with PBS and incubated for 30 minutes at RT with the secondary antibody (Powervision Poly-Horseradisch peroxidase (HRP)-anti Mouse/Rabbit/Rat IgG, Immunologic), followed by color development with 3,3'-Diaminobenzidine (bright-DAB, Immunologic). Lastly, sections were counterstained with hematoxylin, dehydrated in a graded series of ethanol solutions (30–100%), cleared in two changes of xylene and mounted with Permount mounting medium (Fisher Scientific). Images were taken with a light microscope (Leica DMI1). Both the primary and the secondary antibodies were diluted in 1% (w/v) BSA/PBS, and the primary antibody was omitted as a negative control.

2.1.5. Scanning electron microscopy

Images of the luminal and outer surfaces of the decellularized tracheal scaffolds were taken with scanning electron microscopy (SEM) by a researcher at the lab to compare the surface-topography after each decellularization method. Samples were fixed in a solution containing 2% (v/v) glutaraldehyde (Merck) in 0.1 mM phosphate buffer for at least 1 hour, and washed in 0.1 M phosphate buffer for 1 hour. Following that, samples were dehydrated in a graded series of ethanol (30–100%), followed by an overnight incubation in 100% ethanol. Next, samples were critical point dried (Polaron), mounted on a SEM stub, sputter coated with gold-palladium (Edward Scancoat 6) for 60 seconds and analyzed with a scanning electron microscope (Zeiss Sigma 300).

2.1.6. Mechanical tests

Uniaxial tensile tests were used to assess the mechanical properties of native and decellularized tracheal scaffolds ($n = 3$ for each group). Mechanical testing was performed at the Department of Dentistry of the Radboud University Medical Center (Nijmegen, the Netherlands) with a tensile-testing device (Lloyd instruments) equipped with a 100 N load cell. Scaffold samples (average length 19–22 mm) were clamped into the sample holders which had sandpaper pieces glued on to prevent the samples from slipping. After applying a 1 N pre-load, samples were stretched with a strain rate of 1 mm/s at RT. The samples were subjected to increasing uniaxial tensile testing until they ruptured, as shown by a loss of load and tears in the tissue [42, 55]. All samples were tested in the axial direction.

2.1.7. Mechanical testing of separate tissue components

The mechanical behavior of the separate components of the trachea was also characterized by uniaxial tensile testing. The tests performed and the hyperelastic modelling were mainly based on previous work by Safshekan et al. [3, 56].

Sample preparation

For mechanical testing, tracheal samples from native trachea, the scCO₂(III) group, and the DEM-gamma group were obtained (Figure 2.1). Cartilage and composite tissue samples from each group were cut by hand and stored in 0.9% physiological saline solution at 4°C for a maximum of 36 hours. Prior to mechanical testing, samples were stored at RT for 3 hours. The composite tissue samples consisted of both hyaline cartilage tissue and connective tissue [3]. The assumption is that the cartilaginous regions are rigid and that the connective tissue sections are mainly responsible for the deformation observed during tensile testing [3].

Tensile testing

Mechanical testing was again performed at the Department of Dentistry of the Radboud University Medical Center (Nijmegen, the Netherlands). A tensile tester (Lloyd instruments) equipped with a 100 N load cell was used. Sandpaper pieces were glued on the tensile tester's sample holders to prevent the samples from slipping. Before testing, each sample was photographed and an electric digital caliper was used to measure the initial length of each sample (defined as the grip-to-grip distance). ImageJ software was used to calculate the width and thickness of each sample. The tissue samples were considered to be incompressible. Composite tissue samples were subjected to six preconditioning cycles at a strain rate of 3 mm/min followed by an increased uniaxial tension at a strain rate of 1 mm/min until rupture occurred [3], indicated by loss of load and the presence of tears in the tissue [42, 55]. Uniaxial tension was applied to the cartilage samples at a strain rate of 0.5 mm/min until the samples ruptured [3]. Composite and cartilage tissue samples were subjected to uniaxial tension in the axial direction and circumferential direction, respectively. The force (N) and displacement (mm) data of each tissue sample were recorded by the tensile tester and exported to Excel to calculate Cauchy stress-stretch data. The stretch λ was calculated as:

$$\lambda = \frac{L_0 + \Delta L}{L_0} \quad (2.1)$$

Where ΔL represents the displacement or change in length and L_0 represents the original length of the tissue sample. The Cauchy stress σ was calculated, assuming incompressibility, according to [3]:

$$\sigma = \frac{F}{A_0} \lambda \quad (2.2)$$

Where F is the recorded tensile force, and A_0 is the initial cross-sectional area of the tissue sample.

Hyperelastic modelling

Hyperelastic materials are a subclass of elastic materials that generally experience large (finite) strains [58, 59]. They are described by the nonlinear theory of elasticity [59, 60]. This theory employs a strain-energy function for describing the nonlinear mechanical behavior of hyperelastic materials. The majority of research consider tracheal tissues to be hyperelastic [61].

Based on previous literature [3, 56], the trachea is regarded an incompressible and isotropic material in this thesis. This section will provide a brief summary of the various hyperelastic models utilized in this thesis as well as the nonlinear elasticity theory for incompressible isotropic materials. This section is mainly based on the book by Holzapfel [58] and the articles by Martins et al. [59] and Safshekan et al. [3].

The strain-energy function (Ψ) of an isotropic material is determined by the strain invariants, such that:

$$\Psi_{isotropic} = \Psi(I_1, I_2, I_3) \quad (2.3)$$

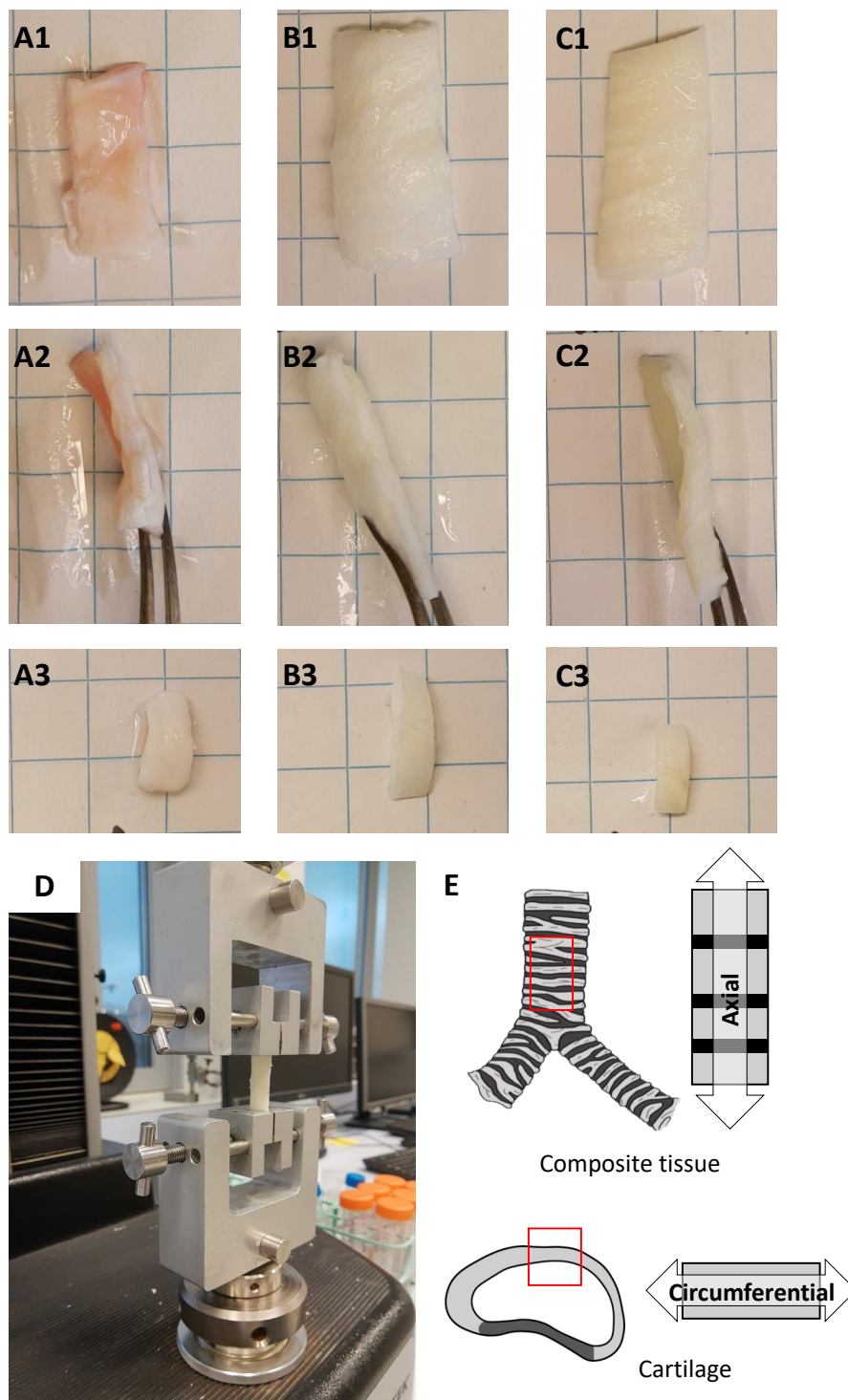


Figure 2.1: Samples of native trachea (A), trachea decellularized using scCO₂(III) method (B) and trachea decellularized using DEM-gamma method (C). In (A1–C1) and in (A2–C2) the front view and side view, respectively, of the composite tissue samples are depicted. In A3–C3 the cartilage samples are shown. In (D) a sample under uniaxial tension can be seen. (E) shows a schematic overview of the tracheal samples under uniaxial tension. Cartilage is depicted in light grey, and connective tissue is depicted in black. The composite tissue (connective tissue) sample is subjected to uniaxial tension in the axial direction, whereas the cartilage sample is subjected to uniaxial tension in the circumferential direction. The image of the trachea in (E) is adapted from [57]. The rest of the images in (E) are adapted from/inspired by [56].

in which

$$\begin{aligned} I_1 &= \sum_{i=1}^3 \lambda_i^2 \\ I_2 &= \sum_{i,j=1}^3 \lambda_i^2 \lambda_j^2, \quad i \neq j \\ I_3 &= \prod_{i=1}^3 \lambda_i^2 \end{aligned} \quad (2.4)$$

in which λ_1 , λ_2 and λ_3 are the principal stretches. As a result, the strain energy function may also be described as a function of the stretches in the following way:

$$\Psi_{isotropic} = \Psi(\lambda_1, \lambda_2, \lambda_3) \quad (2.5)$$

The deformation gradient, a second-order tensor, defines the overall state of a finite deformation:

$$F_{aA} = \frac{\partial x_a}{\partial X_A}; \quad a, A = 1, 2, 3. \quad (2.6)$$

Where, x and X are the point coordinates in the deformed and reference configurations, respectively. When a hyperelastic material is subjected to uniaxial tension in the x_1 direction, the deformation gradient \mathbf{F} becomes

$$[\mathbf{F}] = \begin{bmatrix} \lambda & 0 & 0 \\ 0 & \frac{1}{\sqrt{\lambda}} & 0 \\ 0 & 0 & \frac{1}{\sqrt{\lambda}} \end{bmatrix} \quad (2.7)$$

Assuming that $\lambda_1 = \lambda$ and observing that due to the incompressibility condition

$$J = \prod_{i=1}^3 \lambda_i = \det(\mathbf{F}) = 1, \quad (2.8)$$

we can express that: $\lambda_2 = \lambda_3 = \frac{1}{\sqrt{\lambda}}$.

Using Equation (2.7), the Right ($[\mathbf{C}]$) and Left ($[\mathbf{b}]$) Cauchy-Green tensors can then be defined as:

$$[\mathbf{C}] = [\mathbf{F}]^T [\mathbf{F}] = \begin{bmatrix} \lambda^2 & 0 & 0 \\ 0 & \lambda^{-1} & 0 \\ 0 & 0 & \lambda^{-1} \end{bmatrix} \quad (2.9)$$

$$[\mathbf{b}] = [\mathbf{F}][\mathbf{F}]^T = \begin{bmatrix} \lambda^2 & 0 & 0 \\ 0 & \lambda^{-1} & 0 \\ 0 & 0 & \lambda^{-1} \end{bmatrix} \quad (2.10)$$

and are equal. Subsequently, we can define the invariants using Equation (2.9):

$$\begin{aligned} I_1 &= \text{tr}(\mathbf{C}) \\ I_2 &= \frac{1}{2}(\text{tr}(\mathbf{C}))^2 - \text{tr}(\mathbf{C}^2) \\ I_3 &= \det(\mathbf{C}). \end{aligned} \quad (2.11)$$

And,

$$\begin{aligned} I_1 &= \lambda^2 + \frac{2}{\lambda} \\ I_2 &= 2\lambda + \frac{1}{\lambda^2} \\ I_3 &= 1. \end{aligned} \quad (2.12)$$

The principal Cauchy stresses can both be expressed as a function of the invariants as well as as a function of the stretches. For an incompressible isotropic hyperelastic material subjected to uniaxial tension we know that $\sigma_2 = \sigma_3 = 0$ and $J = 1$. As such, the Cauchy stress as a function of the stretches can be written as:

$$\sigma_1 = \lambda_1 \frac{\partial \Psi}{\partial \lambda_1} - \lambda_3 \frac{\partial \Psi}{\partial \lambda_3} \quad (2.13)$$

The strain-energy function only depends on the two principal invariants I_1 and I_2 , as a result of the kinematic constraint $I_3 = \det(\mathbf{C}) = \det(\mathbf{b}) = 1$. As stated by Holzapfel [58], the Cauchy stress is then formulated as:

$$\boldsymbol{\sigma} = -p\mathbf{I} + 2 \frac{\partial \Psi}{\partial I_1} \mathbf{b} - 2 \frac{\partial \Psi}{\partial I_2} \mathbf{b}^{-1} \quad (2.14)$$

In the case of uniaxial tension, the Cauchy stress as a function of the invariants is given by:

$$\boldsymbol{\sigma} = 2 \left(\lambda^2 - \frac{1}{\lambda} \right) \left(\frac{\partial \Psi}{\partial I_1} + \frac{1}{\lambda} \frac{\partial \Psi}{\partial I_2} \right). \quad (2.15)$$

The different hyperelastic material models utilized in this thesis are described in Table 2.2. For each model, the strain energy function and Cauchy stress equation for an incompressible isotropic material subjected to uniaxial tension are presented [3, 59]. These formulations are based on Equations (2.13) and (2.15). To fit the stress-stretch data acquired in the tests, these hyperelastic material models were used. The curve fitting toolbox in MATLAB R2021a, which is based on the Levenberg-Marquardt algorithm, was used to fit the stress-stretch data [3].

2.2. Recellularization analysis

2.2.1. Isolation and cell culture of porcine adipose-derived stem cells

Porcine adipose-derived stem cells (pADSCs) were isolated from porcine subcutaneous adipose tissue by a researcher at the lab. In brief, adipose tissue obtained from landrace pigs was finely minced and digested via collagenase type II treatment. After separation of the adipocytes from the stromal vascular fraction (SVF) containing the pADSCs by centrifugation and filtration, adipocytes were discarded and the SVF pellet was resuspended in culture medium, seeded into culture flasks and cryopreserved until use. In a previous study, the potential of the isolated pADSCs to differentiate into osteoblasts, chondrocytes and adipocytes was already demonstrated.

For the seeding experiments, cryopreserved vials containing the pADSCs at passage 2 were seeded in culture flasks and cultured under standard conditions (37°C, 5% CO₂) in α -minimum essential medium (α -MEM, Thermo Fisher Scientific) supplemented with 1% (v/v) penicillin/streptomycin (P/S, Thermo Fisher Scientific) and 10% (v/v) fetal calf serum (FCS, Sigma Aldrich). Medium was replaced every

Table 2.2: Hyperelastic materials models used in this thesis. The strain energy function and related Cauchy stress equation for an incompressible isotropic material subjected to uniaxial tension are provided for each model. Adapted from and based on [3, 59].

Model	Strain Energy Function	Cauchy Stress
Neo-Hookean	$\Psi = c_1(I_1 - 3)$	$\sigma = 2 \left(\lambda^2 - \frac{1}{\lambda} \right) c_1$
Mooney-Rivlin	$\Psi = \sum_{i=1}^2 c_i(I_i - 3)$	$\sigma = 2 \left(\lambda^2 - \frac{1}{\lambda} \right) (c_1 + c_2 \frac{1}{\lambda})$
Yeoh	$\Psi = \sum_{i=1}^3 c_i(I_1 - 3)^i$	$\sigma = 2 \left(\lambda^2 - \frac{1}{\lambda} \right) (c_1 + 2c_2(I_1 - 3) + 3c_3(I_1 - 3)^2)$
Fung	$\Psi = \frac{c_1}{2c_2} (e^{c_2(I_1-3)} - 1)$	$\sigma = c_1 \left(\lambda^2 - \frac{1}{\lambda} \right) e^{c_2(I_1-3)}$
Ogden	$\Psi = \sum_{i=1}^3 \frac{c_i(2i-1)}{c_{2i}} (\lambda_1^{c_{2i}} + \lambda_2^{c_{2i}} + \lambda_3^{c_{2i}} - 3)$	$\sigma = c_1(\lambda^{c_2} - 2^{-1+c_2} \lambda^{-c_2/2}) + c_3(\lambda^{c_4} - 2^{-1+c_4} \lambda^{-c_4/2}) + c_5(\lambda^{c_6} - 2^{-1+c_6} \lambda^{-c_6/2})$
Humphrey	$\Psi = c_1(e^{c_2(I_1-3)} - 1)$	$\sigma = 2 \left(\lambda^2 - \frac{1}{\lambda} \right) c_1 c_2 e^{c_2(I_1-3)}$
Veronda-Westmann	$\Psi = c_1[e^{\alpha(I_1-3)} - 1] - \frac{c_1 c_2}{2} (I_2 - 3)$	$\sigma = 2 \left(\lambda^2 - \frac{1}{\lambda} \right) c_1 c_2 (e^{c_2(I_1-3)} - \frac{1}{2\lambda})$

Table 2.3: Parameters of the different groups used in the seeding experiments.

Group	Scaffold type	Culture Media Type	<i>n</i>
DEM-ethanol	DEM sterilized with 70% ethanol	Growth	1
DEM-ethanol	DEM sterilized with 70% ethanol	Chondrogenic	3
scCO ₂ (III)	scCO ₂ sterilized with scCO ₂	Growth	1
scCO ₂ (III)	scCO ₂ sterilized with scCO ₂	Chondrogenic	3
DEM-gamma	DEM sterilized with gamma irradiation	Chondrogenic	3

3 to 4 days and cells were passaged at 80% confluence. Passage 5 (P5) cells were harvested via trypsinisation and used for consecutive experiments.

2.2.2. *In vitro* cell seeding

Prior to conducting the following seeding experiments, the efficiency of a series of seeding methods was evaluated. The seeding methods used and the obtained results are depicted in Appendix A.

Seeding onto the decellularized tracheal scaffolds was evaluated using a total of five groups, as depicted in Table 2.3. Decellularized tracheal scaffolds were cut with a 12-mm biopsy punch and incubated in 0.9% physiological saline solution for a minimum of 24 hours and cell culture medium for a minimum of 24 hours before cell seeding. Punches from the DEM-ethanol group were also sterilized with 70% ethanol for a minimum of 24 hours prior to incubation in 0.9% physiological saline solution and culture medium. Prior to seeding, the scaffold punches were placed in 6-well low-attachment plates (Corning Life Sciences (VWR)) with the outer surface facing upwards.

pADSCs were seeded onto the scaffolds by using fibrin gel as a cell carrier, at a seeding density of 500,000 cells per cm² of scaffold. Fibrinogen solution (from bovine plasma, Sigma-Aldrich) was prepared by reconstitution in 0.9% NaCl to a final concentration of 10 mg/mL and passed through a 0.22- μ m filter (Whatman) for sterilization. For each 12-mm scaffolds punch, 5.65×10^5 cells pADSCs were resuspended in 100 μ L fibrinogen solution (10 mg/mL) and mixed with 2.2 μ L thrombin (from bovin plasma, 50 U/mL, Sigma-Aldrich), and pipetted on the outer (abluminal) surface of the scaffold (Figure 2.2). The cell-fibrin suspension was allowed to polymerize for approximately 3 minutes, after which culture medium was added. After 24 hours of culture, seeded scaffolds were either treated with chondrogenic differentiation medium (high-glucose Dulbecco's Modified Eagle's Medium (Invitrogen) supplemented with 1% insulin-transferrin-selenious acid mix (ITS), 50 nM dexamethasone, 50 μ g/mL L-ascorbic acid 2-phosphate, 40 μ g/mL L-proline, 100 μ g/mL sodium pyruvate, 10 ng/mL TGF- β 3 (Thermo Fisher Scientific) and 1% (v/v) P/S), or were continuously cultured in standard culture medium.

2.2.3. Cell metabolic assay

To evaluate the cell seeding efficiency, the metabolic activity of the seeded cells was determined on days 1, 7 and 21 after seeding, using the 4-[3-(4-iodophenyl)-2-(4-nitrophenyl)-2H-5-tetrazolio]-1,3-

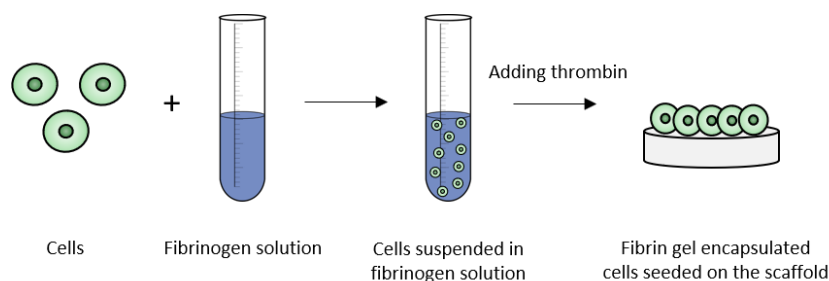


Figure 2.2: Schematic illustration of the static seeding method using fibrin gel as a cell carrier. First, cells are suspended in fibrinogen solution. Subsequently, thrombin is added and the cell-fibrin suspension is pipetted on the scaffold. Adapted from [62].

benzene Disulfonate (WST-1) assay. The WST-1 assay is a cell metabolic activity assay that measures the absorbance of formazan dye, which is formed by cleavage of the tetrazolium salt WST-1. At the predetermined time points, the scaffold punches ($n = 1$ or $n = 3$) were transferred into a fresh 24-well plate and 700 μL of RPMI medium containing 10% (v/v) FCS supplemented with 70 μL of WST-1 reagent (1:10 ratio) was added to each well. After 1 hour of incubation in a 37°C humidified 5% CO_2 incubator, the absorbance of the resulting formazan dye was measured at a wavelength of 450 nm using a microplate reader (Wallac 1420 Victor). Absorbance values were plotted and the value of the blanking well was subtracted.

2.2.4. Histology

Presence of vital cells on the scaffolds and the production of GAGs was examined via H&E staining and alcian blue staining, according to the protocols described in Section 2.1.3.

2.3. Bioreactor culture

Tracheal scaffold samples decellularized with the sc CO_2 (III) method were cut into strips measuring 2 cm in length and 1.5 cm in width ($n = 3$). Following cutting, the tracheal strips were washed with 0.9% physiologic saline solution (at least 2×1 hour and once overnight), followed by an overnight incubation in culture medium. Next, the strips were placed in a bioreactor chamber, under sterile conditions, and fixed with clamps on both ends (Figure 2.3). Subsequently, each scaffold strip was seeded statically with 1.5×10^6 pADSCs (seeding density of 5×10^5 cells per cm^2) resuspended in 300 μL fibrinogen solution (10 mg/mL) and mixed with 6,6 μL thrombin (from bovine plasma, 50 U/mL, Sigma-Aldrich), according to the protocol described in Section 2.2.2. Seeding was performed in the bioreactor chamber to avoid manipulation of the scaffolds as much as possible.

Subsequently, each bioreactor chamber was filled with approximately 60 mL α -MEM medium supplemented with 1% (v/v) P/S and 10% (v/v) FCS, and closed. Next, approximately 150 mL complete α -MEM medium was added to each bottle connected to a bioreactor chamber and the scaffold strips were cultured under static conditions (37°C, 5% CO_2) for 3 days. After 3 days of culture, culture medium was replaced with chondrogenic differentiation medium and the seeded scaffold strips were placed in the bioreactor. The scaffold strips were cultured under dynamic conditions for 15 days by subjecting them to cyclic uniaxial strain (10% stretch with a frequency of 0.25 Hz in accordance with the respiratory rate in adults) (Figure 2.3.B). A control scaffold strip was cultured under static conditions. After 15 days of culture, the scaffold strips were harvested and analyzed.

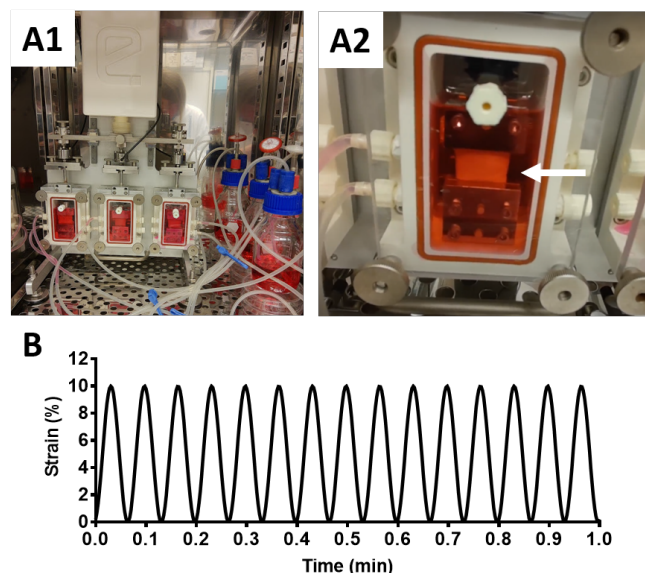


Figure 2.3: Overview of the bioreactor setup. In (A1) the three bioreactor chambers are depicted and in (A2) a closeup of one of the chambers with a scaffold strip clamped (white arrow) in the chamber can be seen (A2). In (B) an overview of the bioreactor program with 10% cyclic uniaxial strain with a frequency of 0.25 Hz in accordance with the respiratory rate in adults is depicted.

2.4. Statistical analysis

Statistical analyses were performed with Graphpad Prism (version 7.00). Unless stated otherwise, experiments were carried out in triplicate ($n = 3$). Data are presented as the mean or the mean \pm standard deviation. $p < 0.05$ was used to denote statistical significance. To compare groups, one-way-analysis-of-variance (ANOVA) followed by a Bonferroni's post-hoc comparisons test was employed. If the homogeneity of variances assumption could not be met, the Dunnett T3 post-hoc test was used.

3

Results

3.1. Decellularization efficiency

In 2011, Crapo et al. suggested three criteria that could be used for evaluating the efficacy of decellularization [47]. These criteria are as follows:

- no visible nuclear material remain in 4',6-diamidino-2-phenylindole (DAPI-) or H&E-stained tissue sections
- the total amount of dsDNA in dry ECM is less than 50 ng
- there are no DNA fragments longer than 200 base pairs

H&E staining and DNA quantification were used in this thesis to test the first two criteria and, as such, evaluate the efficacy of the five different decellularization methods studied (Table 2.1).

Representative images of the H&E staining of native and decellularized tracheal samples are shown in Figure 3.1. For each decellularization protocol, an image focusing on the luminal surface (Figure 3.1.A1,B1,C1,D1,E1,F1) and an image focusing on the cartilage (Figure 3.1.A2,B2,C2,D2,E2,F2) are shown. As depicted in Figure 3.1, the native porcine tracheal tissues contained an intact cartilage matrix, with chondrocytes packed inside the lacunae. A high number of cells could be detected in the mucosal and connective tissue layers. Compared with the native trachea group, the scCO₂(I) and DEM-gamma decellularization methods were able to remove all visible cellular components, including the chondrocytes in the hyaline cartilage matrix. H&E staining depicted completely clear lacunae in these groups. In the DEM-ethanol group, efficacy of decellularization varied between samples. In some samples almost complete removal of cellular and nuclear content was depicted, whereas in other samples intact nuclei were still visible, mainly in the cartilaginous region (data not shown). Images (B) and (C) in figure 3.1 show that tissue samples after treatment with either the scCO₂(II) method or the scCO₂(III) method contain visible cells, both on the luminal surface as well as in the cartilaginous region, although to a lesser extent than in the native trachea samples. These results indicate that these two methods resulted in partial decellularization of the tracheal samples, but incomplete cellular removal.

DNA quantification supported these findings and is presented in Figure 3.1.G. As depicted in Figure 3.1.G, samples from the scCO₂(I) and DEM-gamma groups depicted the lowest DNA values. The DNA content of the samples from the DEM-ethanol group was highly dependent on the sample analyzed; variations from 1.80–70.30 ng DNA per mg wet weight were seen. The results further depict that the DNA content in all groups, except scCO₂(III), was significantly lower than in the native trachea group (Figure 3.1.G: native trachea 69.58 ± 12.11 ng/mg vs. scCO₂(I) 16.62 ± 4.04 ng/mg vs. scCO₂(II) 40.98 ± 5.44 ng/mg vs. DEM-ethanol 43.65 ± 19.04 ng/mg vs. DEM-gamma 10.90 ± 2.00 ng/mg, $p < 0.05$).

3.2. Evaluation of ECM integrity

Alcian blue staining of decellularized and native trachea samples is presented in Figure 3.2. As can be seen in Figure 3.2.F, native trachea was rich in sulfated GAGs (sGAGs). A more intense blue staining can be found in the central core of the native cartilage, indicating that this area contains a higher

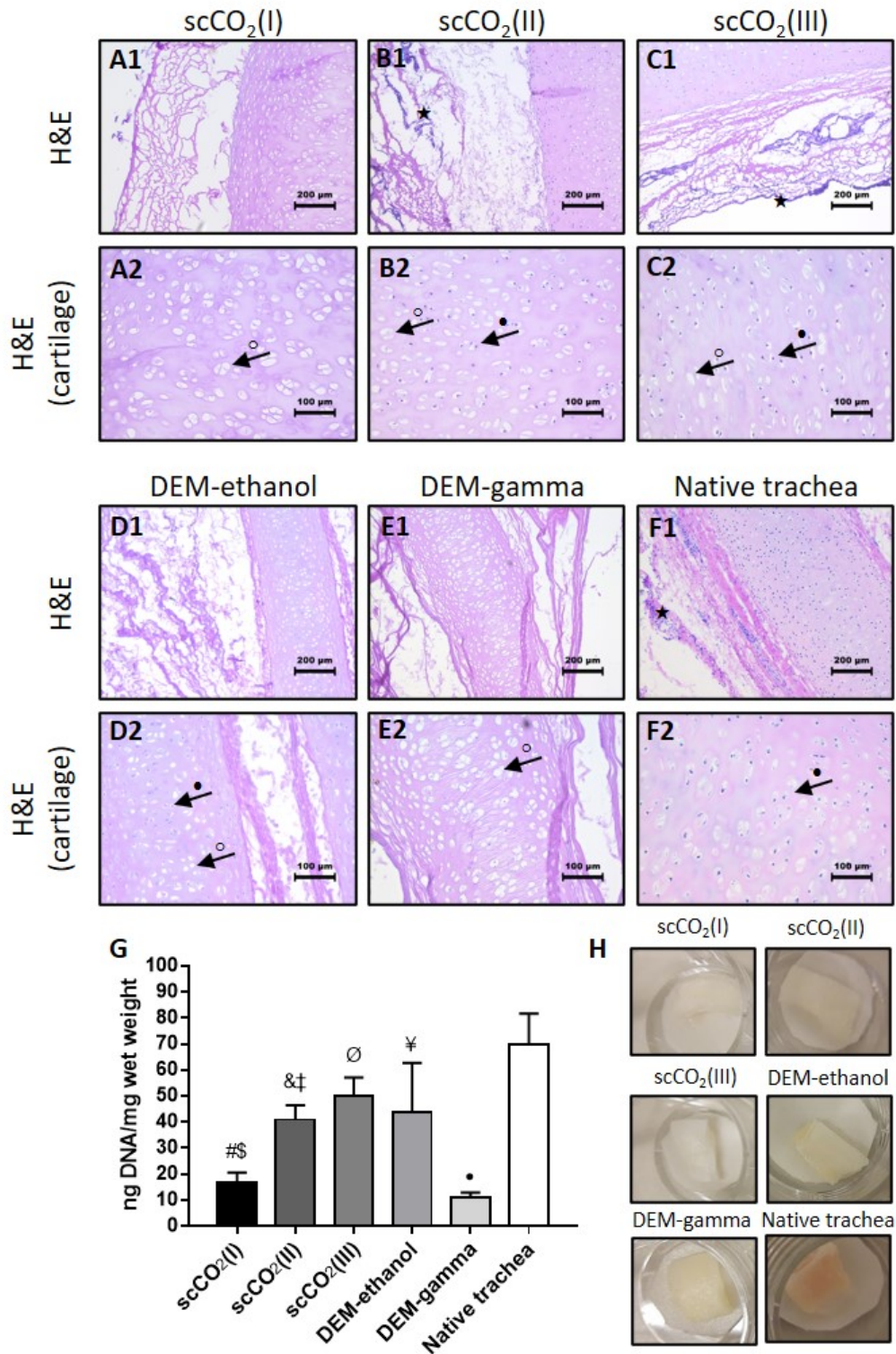


Figure 3.1: Efficacy of porcine trachea decellularized with scCO₂ or DEM. (A-F) H&E staining of decellularized and native porcine trachea. Tissue decellularized with scCO₂(I) (A) and DEM-gamma (E) show complete removal of cellular nuclei. No nuclei are visible in the lacunae (black arrow with o). In the scCO₂(II) (B) and scCO₂(III) (C) groups both cells in the outer tissue layers as well as chondrocytes in the cartilage tissue are depicted (indicated with * and black arrow with ●, respectively), although to a lesser extent as in native tracheal tissue (F). (G) DNA content was measured in native tracheal tissue and following decellularization. A significant reduction in DNA content was seen in all samples, except scCO₂(III), compared to native trachea. # = significant difference (S.D.) from scCO₂(II), scCO₂(III) and native trachea ($p < 0.001$); \$ = S.D. from DEM-ethanol ($p < 0.05$); & = S.D. from DEM-gamma ($p < 0.001$), ‡ = S.D. from native trachea ($p < 0.05$), ∘ = S.D. from DEM-gamma ($p < 0.001$), ¥ = S.D. from DEM-gamma ($p < 0.01$); • = S.D. from native trachea ($p < 0.001$). (H) Macroscopic images of the decellularized and native tracheal samples. Decellularized tracheal samples had a colourless appearance.

amount of GAGs. Alcian blue staining also revealed that the sGAG content was best preserved in the scCO₂(III) group following decellularization. In the scCO₂(I) group, on the other hand, complete loss of sGAGs could be depicted, as indicated by loss of blue staining (Figure 3.2.A). Alcian blue staining also depicted a noticeable reduction of staining in the scCO₂(II), DEM-ethanol and DEM-gamma groups (Figure 3.2.B,D,E).

However, quantitative analysis revealed no significant differences in sGAG content between the scCO₂(II), scCO₂(III), DEM-ethanol and native trachea groups (Figure 3.2.G: native trachea 37.73 ± 5.27 µg/mg vs. scCO₂(II) 30.73 ± 8.62 µg/mg vs. scCO₂(III) 43.83 ± 8.71 µg/mg vs. DEM-ethanol 26.00 ± 12.15 µg/mg, $p > 0.5$). The results did reveal that there was a significant loss of sGAG content in the DEM-gamma group when compared to the native trachea group (DEM-gamma 20.35 ± 1.59 µg/mg, $p < 0.01$ significant difference from native trachea). Furthermore, a reduction of 88% in sGAG content was seen in the scCO₂(I) group (scCO₂(I) 4.51 ± 1.83 µg/mg, $p < 0.001$ significant difference from native trachea), which is expected from the staining results.

The presence of collagen types I and III in the trachea's ECM was demonstrated with Picrosirius red and Gomori's trichrome staining. Collagen type I is the most abundant collagen type in the ECM of the human trachea [63]. Picrosirius red staining displayed no substantial differences in staining intensity amongst the different groups, suggesting that decellularization did not affect the collagen content of the scaffolds (Figure 3.3.B-F). Only the samples treated with scCO₂(I) showed a clear reduction in staining intensity (Figure 3.3.A). Gomori's trichrome staining did show some noticeable differences between the different decellularization groups. As shown in Figure 3.3.F3, the native trachea clearly depicts a blue-green staining in the tissues surrounding the cartilage, indicating collagen containing connective tissue. Similarly, the DEM-ethanol group depicts this blue-green staining in the perichondrium (dense connective tissue that surrounds the cartilage), which is known to contain collagen type I (Figure 3.3.D3). This staining, however, is not evident in the other decellularization groups, suggesting some loss of collagen in these groups. Since the basement membrane contains collagen type III fibers, it could also indicate (partial) loss of the basement membrane in these groups.

Collagen type II, which is only found in the cartilage, accounts for 10 to 30% of the ECM in the human native trachea [2, 63]. Figure 3.4 displays the presence of collagen type II in the decellularized and native matrices. Native trachea depicted high staining intensity, especially in the territorial matrix (the area immediately surrounding chondrocytes), which was also observed in the cartilage matrix of the scCO₂(III) scaffold samples. The staining further indicated that collagen type II was retained in all groups after decellularization.

3.3. Scanning electron microscopy

Scanning electron microscopy (SEM) images clearly showed that the epithelium was removed in all decellularized scaffolds (Figure 3.5). The luminal surfaces of the samples from the DEM-ethanol and DEM-gamma groups looked visibly different than the luminal surfaces of the samples from the scCO₂ groups. At higher magnification, gaps and a meshwork of fibers could be depicted on the luminal surfaces of the scCO₂(II), scCO₂(III) and DEM-gamma scaffolds (Figure 3.5.B2,C2), whereas the DEM-ethanol group seemed to have a more smooth appearance (Figure 3.5.D2). This suggests that the constructs from the DEM-ethanol group have an (partially) intact basement membrane, whereas the basement membrane is (partially) destructed in the other groups. SEM images of the outer surfaces of the matrices also depicted some differences between the scaffolds. The fibers in the scCO₂(III) group seemed to have a more loose appearance and the scCO₂(I) group shows a disrupted surface, whereas the surface in the DEM-gamma group is more smooth.

3.4. Mechanical properties

3.4.1. Force-displacement and stress-stretch curves

Uniaxial tensile tests were performed to evaluate the possible effects of the decellularization and sterilization processes on the mechanical properties of the scaffolds. The average force-displacement curves for the tissue samples tested are depicted in Figure 3.6.

When compared to native tissue samples, decellularized tissues samples from the scCO₂(III) and DEM-ethanol groups showed comparable characteristics. No significant differences in the maximum force were seen between the native trachea samples (8.79 ± 0.86 N) and samples from the DEM-ethanol (10.55 ± 0.87 N) and scCO₂(III) (10.48 ± 0.45 N) groups ($p > 0.05$). The force-displacement

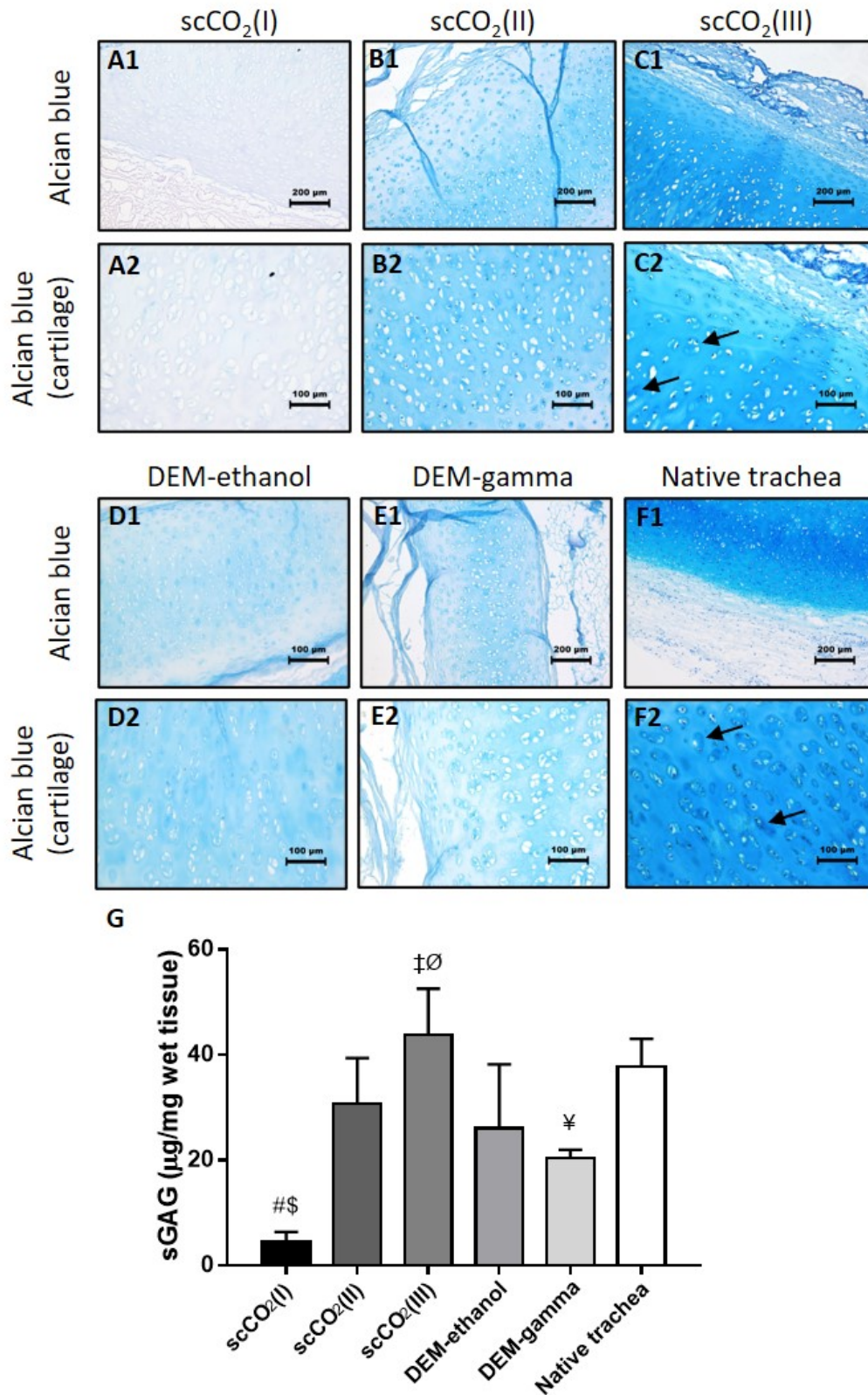


Figure 3.2: Glycosaminoglycan (GAG) content of decellularized tracheal matrices. Native porcine trachea stained with alcian blue (F1,F2) compared to tracheal matrices decellularized with scCO₂(I) (A1,A2), scCO₂(II) (B1,B2), scCO₂(III) (C1,C2), DEM-ethanol (D1,D2) and DEM-gamma (E1,E2). The black arrows indicate the territorial matrix which is the area around the lacunae of the chondrocytes. Trachea in the scCO₂(I) group show complete loss of GAGs. Some of the other decellularized matrices (B,D,E) show a less intense staining compared to native trachea (F). Matrices from the scCO₂(III) group (C) show retention of GAGs. (G) Quantitative analysis of sulphated GAGs in decellularized and native tracheal tissue. A significant reduction in sGAG content is seen in the scCO₂(I) and DEM-gamma groups when compared to native trachea. # = significant difference (S.D.) from scCO₂(II), scCO₂(III), DEM-ethanol and native trachea ($p < 0.001$), \$ = S.D. from DEM-gamma ($p < 0.05$), ‡ = S.D. from DEM-ethanol ($p < 0.01$), ∅ = S.D. from DEM-gamma ($p < 0.001$), ¥ = S.D. from native trachea ($p < 0.01$).

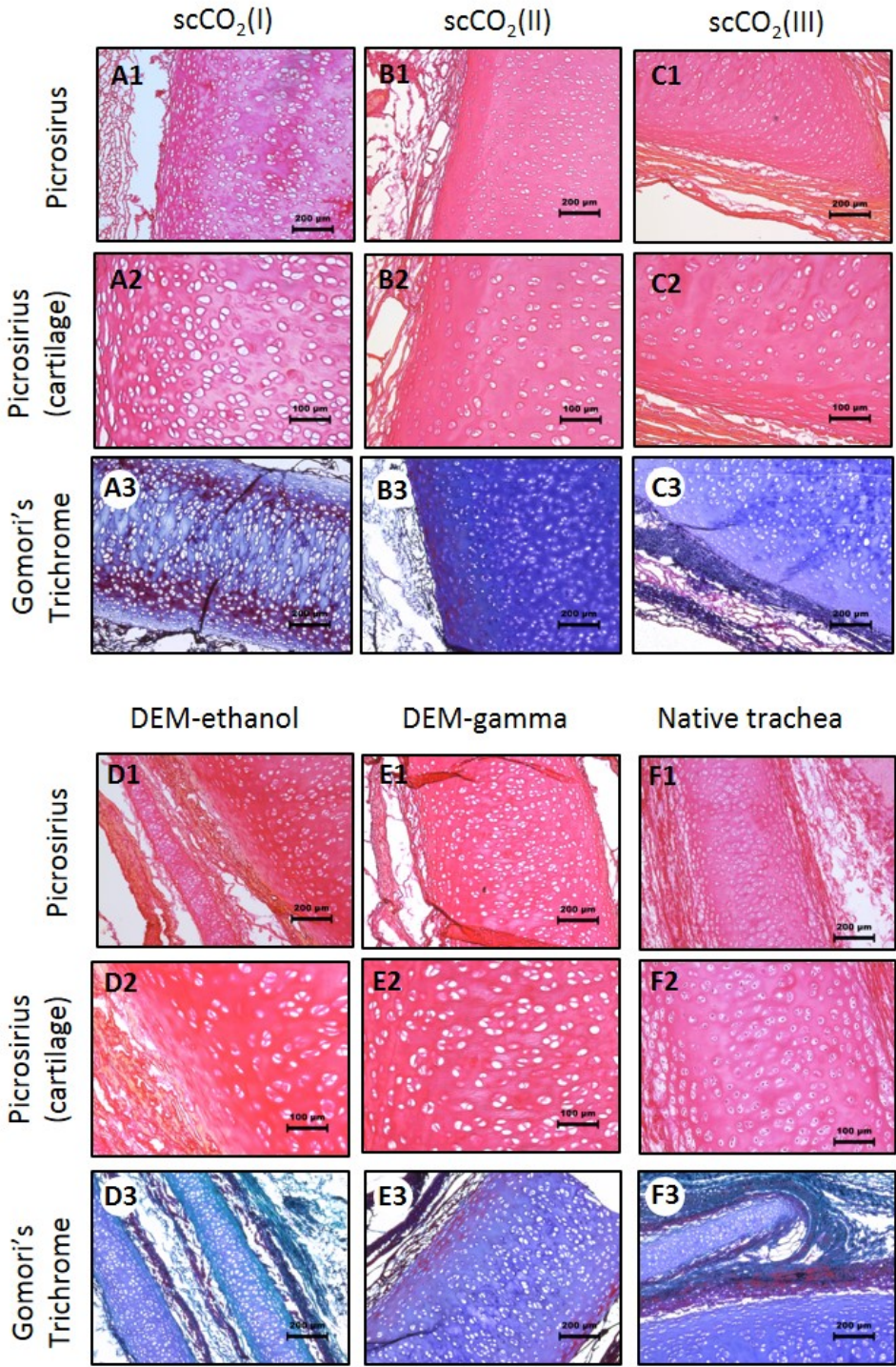


Figure 3.3: Native and decellularized trachea stained with Picrosirius red and Gomori's trichrome to evaluate the preservation of collagen in the ECM. Native porcine trachea (F1,F2,F3) are compared to tracheal matrices decellularized with scCO₂(I) (A1,A2,A3), scCO₂(II) (B1,B2,B3), scCO₂(III) (C1,C2,C3), DEM-ethanol (D1,D2,D3) and DEM-gamma (E1,E2,E3). Only a clear reduction in staining intensity can be observed in the samples decellularized with scCO₂(I). Collagen is mostly preserved in the other groups.

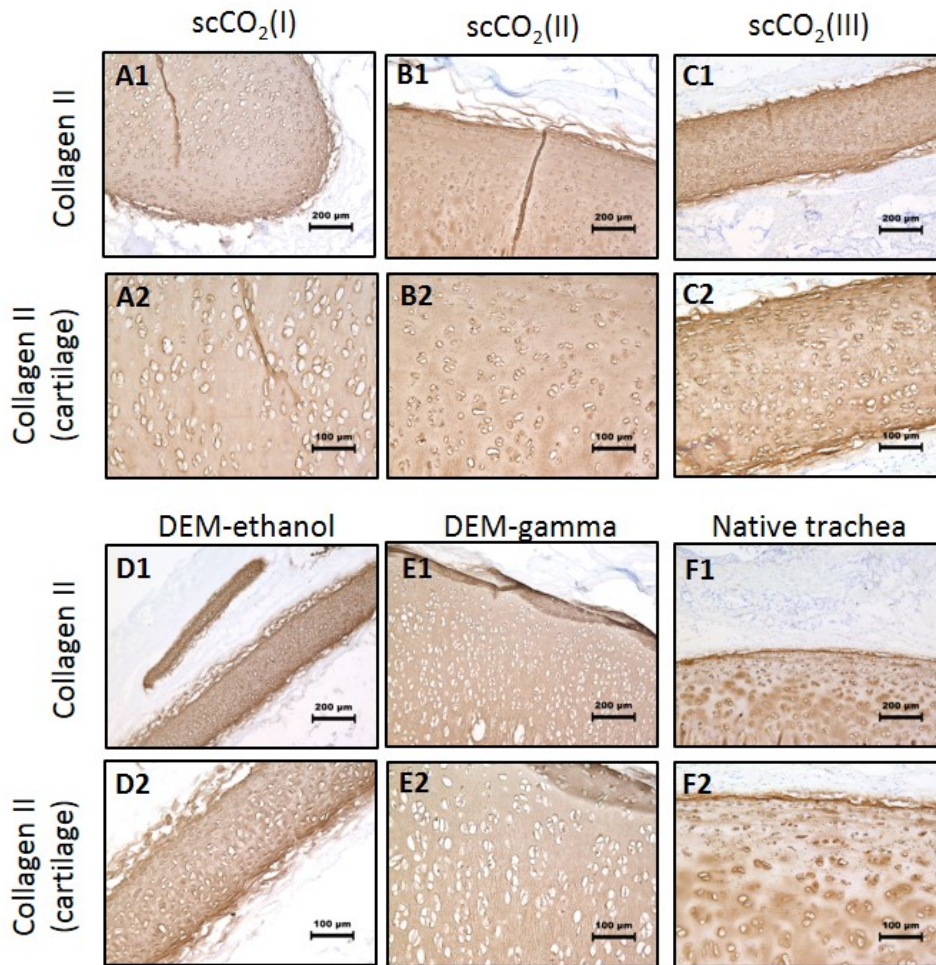


Figure 3.4: Immunohistological staining for collagen type II of tracheal samples from each treatment group; treated with (A) $\text{scCO}_2(\text{I})$, (B) $\text{scCO}_2(\text{II})$, (C) $\text{scCO}_2(\text{III})$, (D) DEM-ethanol, (E) DEM-gamma, and (F) untreated. Collagen type II was preserved in all groups.

curves of the $\text{scCO}_2(\text{III})$ and DEM-ethanol samples did have a higher slope than the curve of the native tracheal samples. Furthermore, the maximum force decreased significantly in the tissue samples from groups $\text{scCO}_2(\text{I})$ ($1.34 \pm 0.86 \text{ N}$), $\text{scCO}_2(\text{II})$ ($4.17 \pm 1.36 \text{ N}$) and DEM-gamma ($4.65 \pm 1.37 \text{ N}$) compared to native trachea ($p < 0.01$, $p < 0.05$ and $p < 0.05$, respectively).

Tensile testing of single tracheal components, namely cartilage and composite (connective tissue) tissue samples, was also performed. For cartilage samples, tensile tests up to 20% strain were performed, which is considered to completely cover the physiological conditions of tracheal cartilage [3]. Under normal physiological conditions, the stretch of tracheal cartilage is lower than 1.05 [3,64]. Tensile tests up to 50% strain were conducted for the composite tissue samples, in accordance to the experiments reported by Safshekan et al. [3]. Figure 3.7 illustrates the average stress-strain curves obtained by tensile testing of native, $\text{scCO}_2(\text{III})$ and DEM-gamma tracheal samples. In MATLAB R2021a, a code was implemented to obtain the mean of the samples' stress-strain curves after interpolating them to the same stretch values. To compare the obtained experimental data to data from literature, the Young's modulus of the cartilage samples was calculated assuming elastic behavior and considering a strain of a maximum of 5% [64].

The stress-strain curves of the cartilage samples show that cartilage had the highest stiffness and was found to be linear up to 10%–20% stretch in all groups. In the decellularization groups, the curves bent slightly at higher stretch rates. The Young's modulus for native porcine tracheal cartilage was found to be $1.17 \pm 0.17 \text{ MPa}$ (Figure 3.7.D). This value is comparable to results found in literature. Wang et al., for instance, reported a Young's modulus of $1.74 \pm 0.85 \text{ MPa}$ for porcine tracheal cartilage [65], whereas a range of 1–15 MPa was reported by Rains et al. for human tracheal cartilage [66]. There

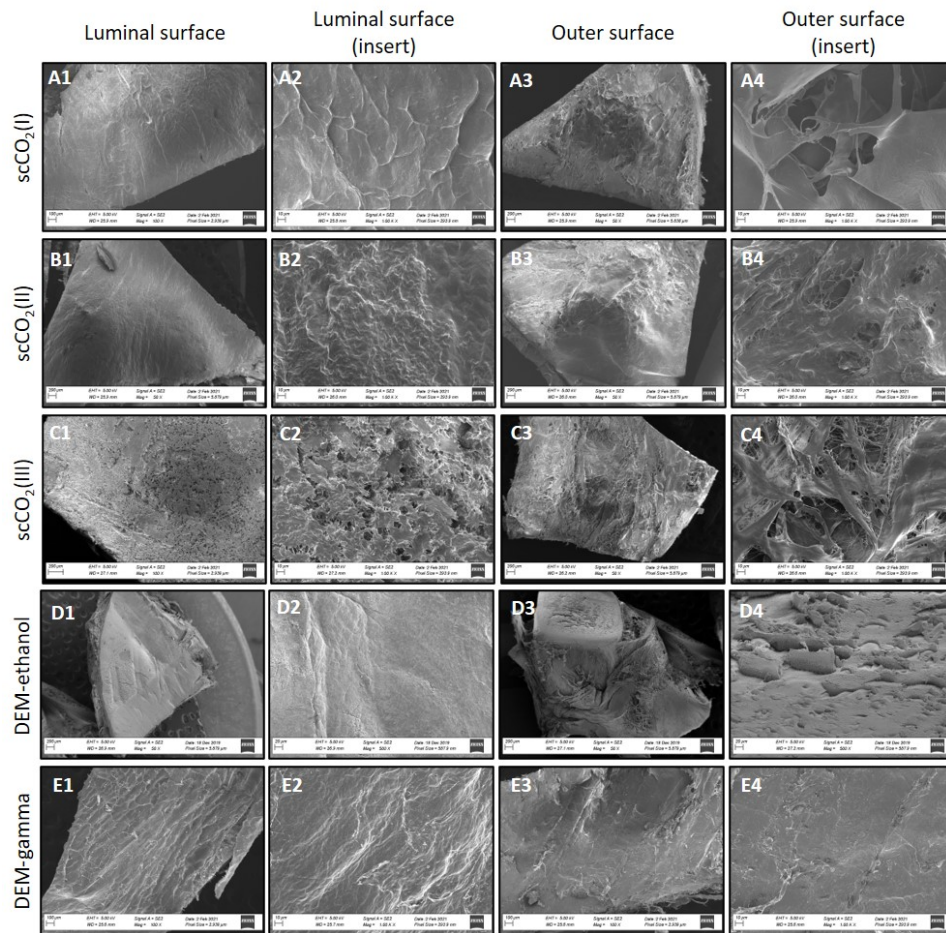


Figure 3.5: Scanning electron microscopy (SEM) of tracheal samples. The luminal surfaces and outer surfaces of tracheal matrices decellularized with scCO_2 (I) (A1–A4), scCO_2 (II) (B1–B4), scCO_2 (III) (C1–C4), DEM-ethanol (D1–D4) and DEM-gamma (E1–E4) are shown.

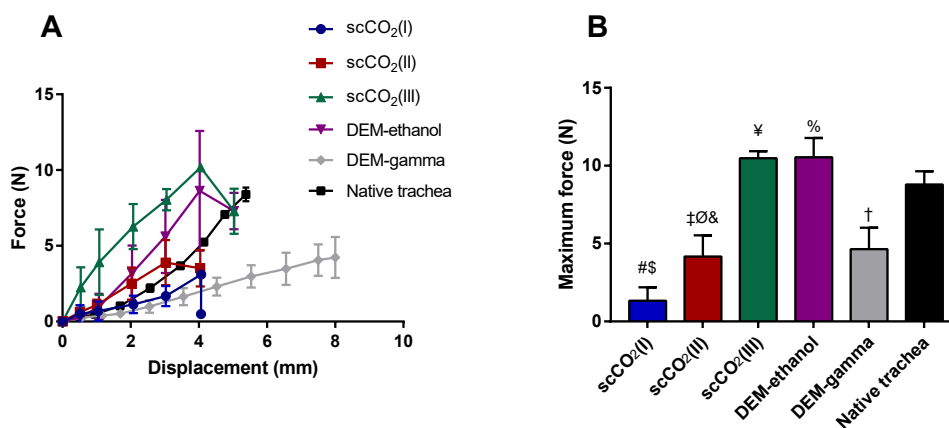


Figure 3.6: Biomechanical properties of porcine tracheal scaffolds following decellularization. (A) Average force-displacement curves of decellularized tissue samples tested. (B) Maximum force of the decellularized tracheas. # = significant difference (S.D.) from scCO_2 (III) and DEM-ethanol ($p < 0.001$), \$ = S.D. from native trachea ($p < 0.01$), ‡ = S.D. from scCO_2 (III) ($p < 0.001$), ⊙ = S.D. from DEM-ethanol ($p < 0.01$), & = S.D. from native trachea ($p < 0.05$), ¥ = S.D. from DEM-gamma ($p < 0.01$), % = S.D. from DEM-gamma ($p < 0.01$), † = S.D. from native trachea ($p < 0.05$).

were no statistical differences in the tensile modulus between the three different groups ($p > 0.05$).

The native connective tissue's average stress-strain curve is typical for soft tissues: it displays non-linear stiffening behavior (incremental Young's modulus when the stretch is increased) (Figure 3.7.A) [3]. The scCO₂(III) connective tissue samples showed a similar average stress-strain curve, but the standard deviations are much higher. Interestingly, the average curve of the DEM-gamma connective tissue samples lacked this non-linear stiffening behavior. The curve had a more linear response and loss of load was depicted at a lower strain value (~40%) than in the other two groups (~50%).

3.4.2. Hyperelastic modelling

The Cauchy stress-stretch data of the different tracheal samples of the native and decellularized tracheal tissues obtained with uniaxial tensile testing were fitted with different hyperelastic models. In Table 3.1 the goodness of fit results for seven hyperelastic models are shown. The table shows the coefficient of determination R^2 , which runs from 0 to 1 and is an estimate of the model's goodness of fit to the data. A R^2 of 1 represents a perfect fit. When all models were compared, the fitting curves of the Yeoh, Fung and Ogden models best represented the experimental data ($R^2 \geq 0.99$). Overall, the Yeoh model showed the highest coefficient of determination for all three tissue types. Figure 3.8

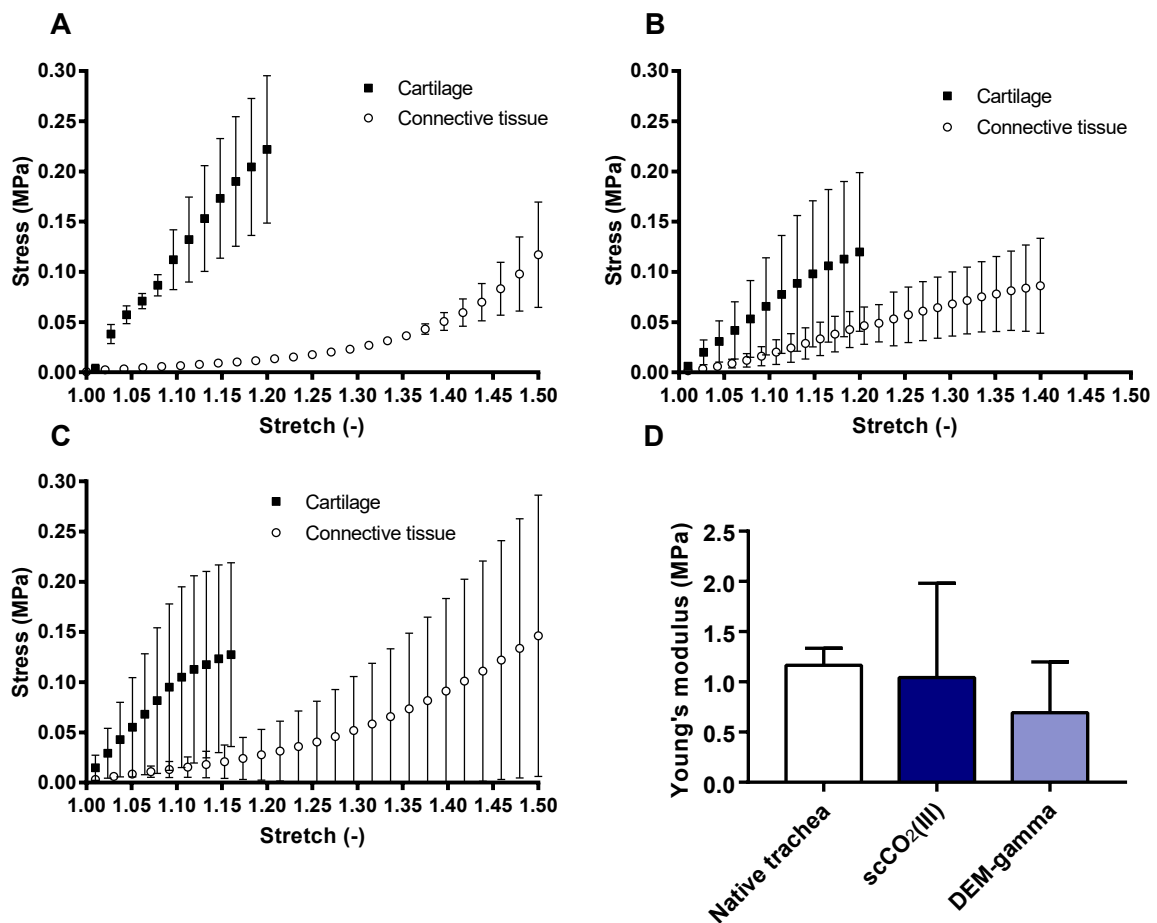


Figure 3.7: Cauchy stress-stretch data for cartilage and composite tissue (connective tissue) samples from (A) native trachea ($n = 4$ and $n = 2$ for cartilage and connective tissue samples, respectively), (B) trachea decellularized with the DEM-gamma method ($n = 3$ for both cartilage and connective tissue samples), and (C) trachea decellularized with the scCO₂(III) method ($n = 5$ and $n = 3$ for cartilage and connective tissue samples, respectively). Cartilage shows a linear response in all groups. The connective tissue in the native and scCO₂(III) groups show typical stiffening behavior. In (D) the tensile elastic modulus of the different cartilage samples is depicted. No statistical differences were seen between groups ($p > 0.05$).

Table 3.1: Different hyperelastic models were used to fit the experimentally obtained stress-stretch data of the different decellularized tracheal tissue components. In the table the coefficient of determination, R^2 , for each model and tissue type is displayed.

Model	Cartilage			Connective Tissue		
	Native trachea	DEM-gamma	scCO ₂ (III)	Native trachea	DEM-gamma	scCO ₂ (III)
Mooney-Rivlin	1.000	0.998	0.995	0.930	0.998	0.990
Yeoh	0.999	1.000	0.998	1.000	1.000	0.999
Fung	1.000	0.998	0.994	0.994	0.998	0.998
Neo-Hookean	0.979	0.986	0.999	0.995	0.998	0.888
Humphrey	0.951	0.989	0.952	0.999	0.998	0.999
Ogden	0.997	0.998	0.994	0.998	0.999	1.000
Veronda-Westmann	0.951	0.972	0.994	0.959	0.989	0.995

depicts the curve fitting results of the Yeoh model for the different tracheal tissues. It is demonstrated that the model reflects the stress-stretch behavior of the different tissues accurately, similar to what was depicted by Safshekan et al. [3]. Only in the native trachea cartilage stress-stretch curve a deviation from the fitted curve can be seen at a stretch from 1.0–1.05.

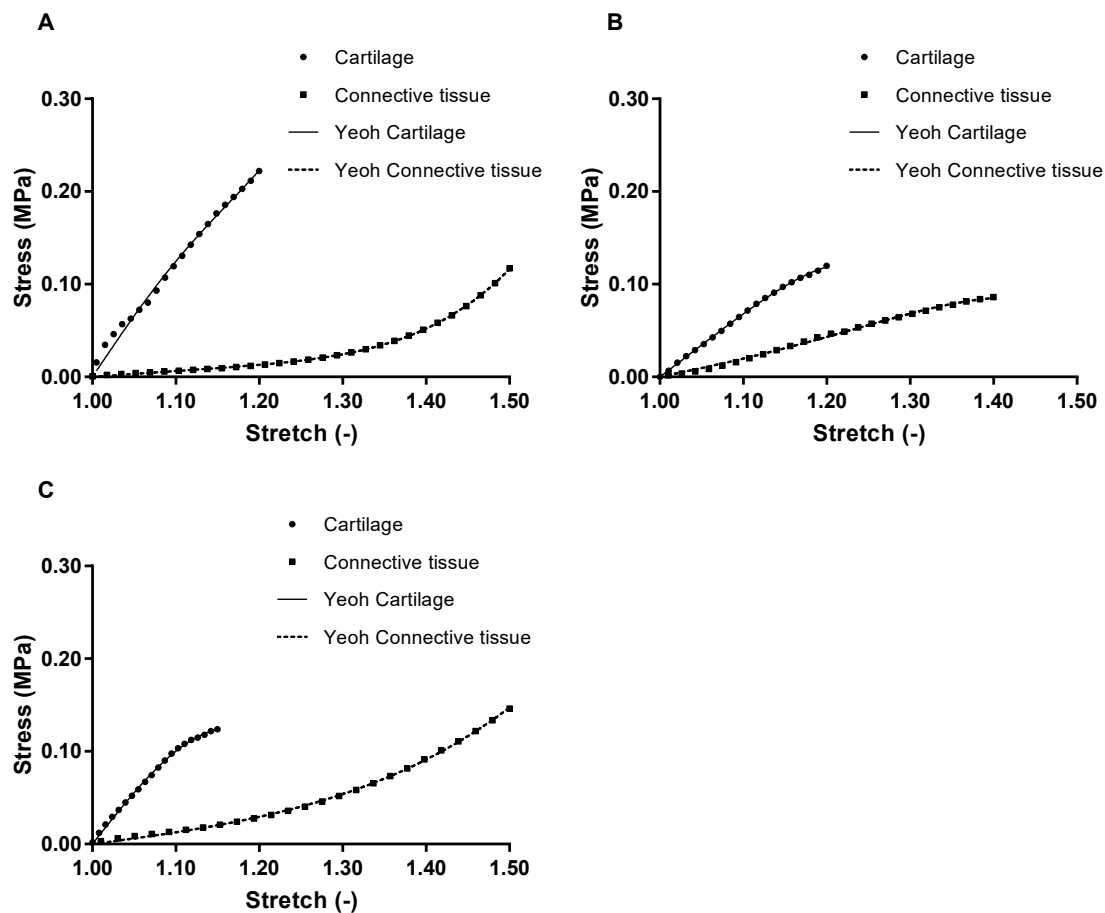


Figure 3.8: Fit of the Yeoh hyperelastic model to the experimental Cauchy stress-stretch data obtained from uniaxial tensile testing for cartilage and connective tissue (composite tissue) samples from (A) native trachea, (B) trachea decellularized with the DEM-gamma method, and (C) trachea decellularized with the scCO₂(III). The model reflects the stress-stretch behavior of the different tissue types accurately.

3.5. Cytocompatibility of decellularized tracheal scaffolds

To be clinically useful, decellularized tracheas must maintain the ability to support cells [45]. Therefore, cells from various cell types were seeded on the decellularized tracheal scaffolds to assess the ability of the scaffolds to support cell attachment and growth. When cells were seeded directly onto the decellularized scaffolds, by dropping a concentrated cell suspension on the top of the scaffolds, (almost) no cell attachment could be depicted and metabolic activity of the cells was low (Appendix A).

To increase seeding efficiency, fibrin gel-encapsulated pADSCs at passage 5 were seeded onto the decellularized tracheal scaffolds. After seeding, scaffolds were cultured in proliferation and chondrogenic differentiation medium under static conditions for 7 and 21 days.

Fibrin gel-encapsulated pADSCs cultured in proliferation medium showed a decline in metabolic activity over the 10 day culture period in the scCO₂(III) group, whereas an increase was seen in the DEM-ethanol group (Figure 3.9.A). A similar trend was seen when scaffolds were pre-wetted with 100% FCS and seeded with a static seeding method (Appendix A). The metabolic activity of fibrin gel-encapsulated

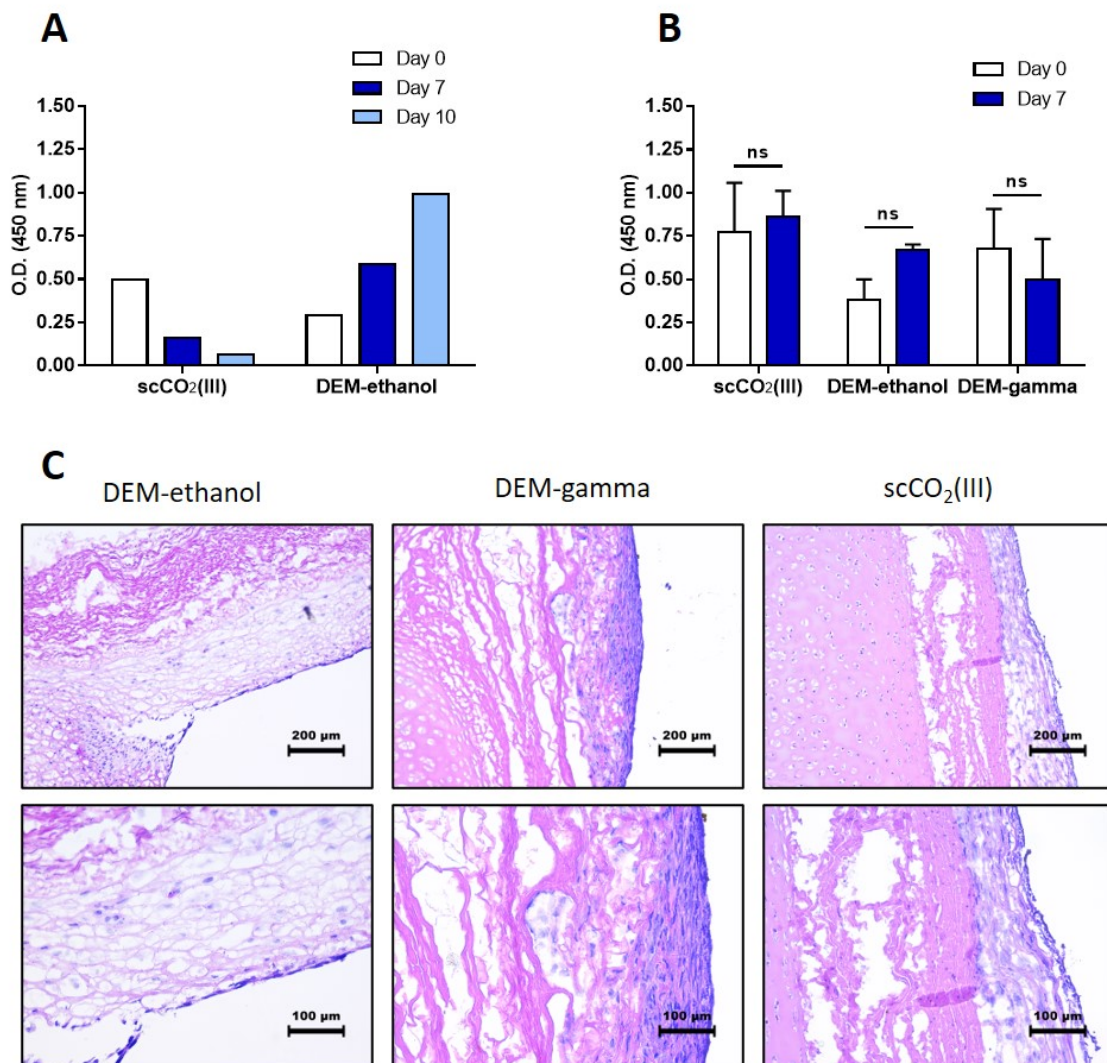


Figure 3.9: Histological staining and metabolic activity (WST-1 assay) were used to evaluate the attachment and proliferation of cells seeded on decellularized tracheal scaffolds. (A) Proliferation (WST-1 assay) of pADSCs seeded on decellularized tracheal scaffolds and cultured in proliferation medium over a 10 day culture period ($n = 1$). A decline in metabolic activity was seen in the scCO₂(III) group, whereas an increase in metabolic activity was seen in the DEM-ethanol group. (B) Proliferation of pADSCs seeded on decellularized tracheal scaffolds and cultured in chondrogenic differentiation medium over a 7 day culture period. The results of three separate experiments are depicted ($n = 1$, $N = 3$). Metabolic activity did not decrease significantly over time, indicating the cells were able to proliferate and survive on all scaffolds. (C) Representative images of the H&E staining of the cell seeded constructs in chondrogenic differentiation medium at day 7.

pADSCs cultured in chondrogenic differentiation medium did not significantly decrease over the 7 day culture period in all groups (Figure 3.9.B). A trend of increasing metabolic activity was seen in the scCO₂(III) and DEM-ethanol groups, although this was not statistically significant.

After 7 days of culture, H&E staining of the cell seeded scaffolds cultured in chondrogenic differentiation medium revealed the formation of a cell layer across the surfaces of the scaffolds (Figure 3.9.C). Cells on the surface appeared to have a spindle-shape, elongated morphology, whereas cells deeper in the fibrin gel had a more round morphology. No clear differences could be depicted between the various groups. After 21 days of culture, more cells had a spindle-shape and elongated morphology and, the cells were evenly distributed on the surfaces of the scaffolds (Figure 3.10.A–C). Cells in the DEM-gamma group were more clustered in one location and had a more spherical morphology. Cell infiltration into the ECM of the scaffolds was very limited.

Overall, these results indicated that both the scCO₂ and chemically decellularized tracheal scaffolds supported the attachment and growth of fibrin gel-encapsulated ADSCs under chondrogenic culture conditions. Alcian blue staining further indicated the production of GAGs by slightly enhanced blue staining from day 7 to day 21 around the surface of the scaffolds under chondrogenic culture conditions, suggesting that the ADSCs differentiated into chondrocytes (Figure 3.10.D–F).

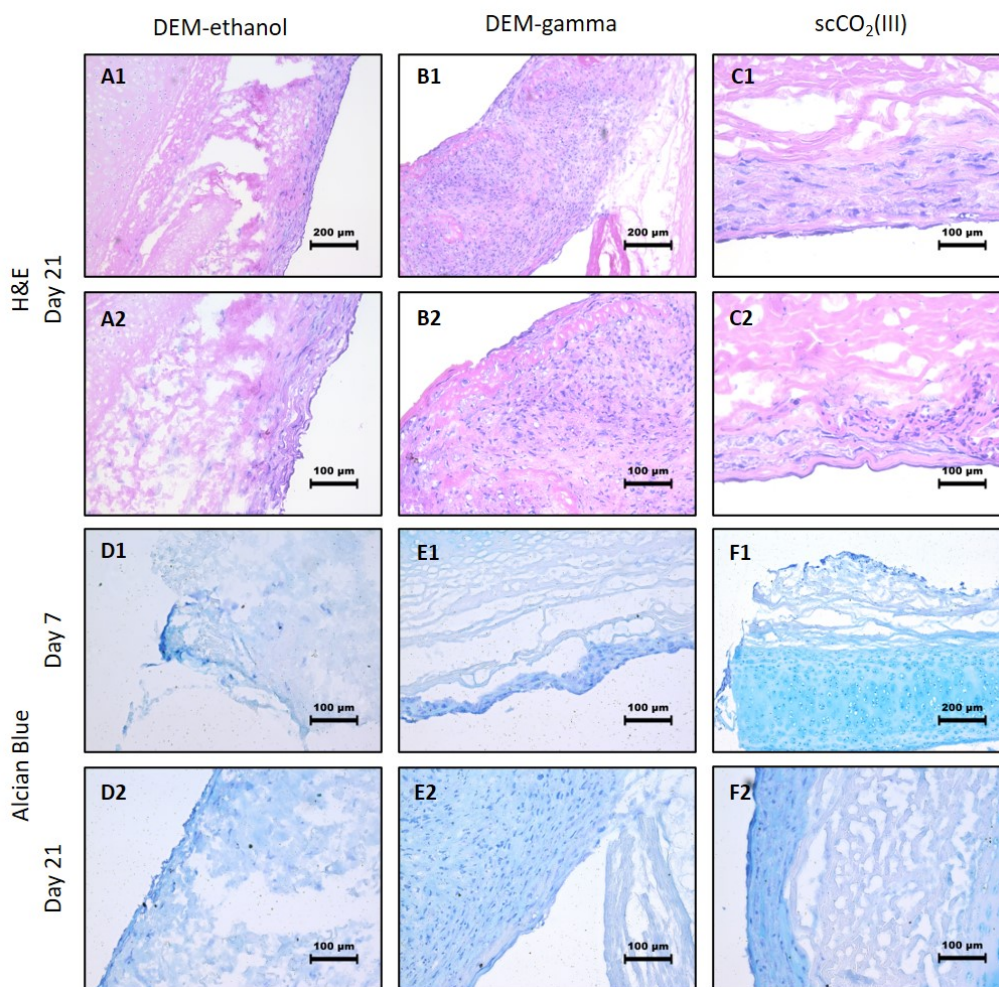


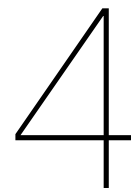
Figure 3.10: Histological staining was used to evaluate the attachment of cells seeded on tracheal scaffolds that had been decellularized using various methods. Representative images of the H&E staining of the cell seeded constructs decellularized with the (A) DEM-ethanol, (B) DEM-gamma and (C) scCO₂(III) methods and cultured for 21 days in chondrogenic differentiation medium ($n = 1$ for each group). Cells in the DEM-ethanol and scCO₂(III) groups depicted a spindle-shape and elongated morphology. Minimal cell infiltration was seen. Alcian blue staining was used to visualize GAGs and as such evaluate the chondrogenic potential of the cells seeded on the constructs decellularized with (D) DEM-ethanol, (E) DEM-gamma, and (F) scCO₂(III) methods and cultured for 21 days in chondrogenic differentiation medium. A slightly enhanced blue staining was seen from day 7 to day 21, especially in the scCO₂(III) group, suggesting the production of GAGs and thus chondrogenic differentiation.

3.6. Bioreactor culture

The trachea is subjected to many mechanical forces during respiration [67]. These mechanical loads allow the trachea to maintain its function and integrity. Mechanical loading, in addition to the TE triad, is thought to be critical in creating native-like tissue, particularly in cartilage TE [31]. Mechanical loading has, for instance, been shown to increase *in vitro* chondrogenesis of human mesenchymal stem cells [31]. Loading of the matrix increased the expression and production of ECM components, and, therefore, improved mechanical properties. As such, it is hypothesized that preconditioning of recellularized decellularized scaffolds, by creating an environment that closely mimics the native local environment, could generate more functional organs for *in vivo* implantation [31]. This concept has primarily been investigated in the context of articular cartilage TE. Whether mechanical loading of mesenchymal stem cells seeded on decellularized tracheal scaffolds will result in functional improvement is currently unknown. To study this hypothesis, this bioreactor experiment was conducted.

It was hypothesized that stimulation of the tracheal constructs with cyclic uniaxial tensile strain for 21 days would lead to an increased chondrogenic phenotype compared to the statically treated seeded scaffolds, resulting in improved mechanical properties of the constructs. In comparison to statically treated constructs, the loaded tracheal constructs were thought to have higher proteoglycan and collagen contents.

Unfortunately, the bioreactor experiments were accompanied with many difficulties, including leakage of medium, malfunctioning of the pump, and contamination. As a result, the data obtained were not reliable and are therefore not discussed.



Discussion

The trachea's primary functions include conducting air into the lungs, humidification and warming of the inspired air, and mucociliary clearance [68]. The trachea has a complex anatomy that allows it to perform these tasks, making regeneration of the trachea a major challenge. Long-segment tracheal lesions can only be cured by tracheal replacement with a substitute [25]. The most promising approach for obtaining a functional tissue substitute seems to be the process of decellularization. Successful decellularization is characterized by the elimination of (nearly) all cellular material while mimimizing alterations to the ECM structure [30]. The ECM is a complex, tissue-specific three-dimensional network made up of functional and structural proteins and serves a structural role while also directing and regulating cellular survival, behavior and phenotype [37, 69]. In addition, the ECM is continuously remodeled by the cells that reside in the matrix [37, 69]. As Badylak et al. point out, this synergistic relationship between the ECM and its residing cells is one of the great advantages of decellularized scaffolds over synthetic scaffolds [69].

Detergents and enzymes are often used for decellularization, similar for the trachea, and have been shown to be effective in removing cells and genetic material from biological tissues. However, detergents such as SDC have a negative impact on the ECM's physical, biochemical, and structural properties, which can be detrimental to cell repopulation [70]. A scCO₂ decellularization approach could be an interesting alternative, as scCO₂ possesses some attractive properties including non toxicity, natural availability and the ability to permeate dense matrices [48, 50, 52]. Therefore, the aim of this thesis was to investigate the potential of scCO₂ decellularization as a novel method for decellularization of porcine trachea and compare it to a vacuum-assisted chemical-enzymatic decellularization method. The effects of scCO₂ treatment without addition of a co-solvent, as well as the effects of scCO₂ treatment with an additional washing step with NaOH, were investigated. Furthermore, sterilization with scCO₂ was compared with sterilization with gamma irradiation. Decellularization efficiency was assessed in terms of removal of cellular components, retention of mechanical properties and preservation of ECM components and ultrastructure. Furthermore, the cytocompatibility of the scaffolds was evaluated and a methodology for reseeding the decellularized scaffolds with porcine ADSCs was identified.

4.1. Decellularization efficacy

The elimination of cellular components and genetic material from the ECM is an important criterion for decellularization. Based on the criteria set by Crapo et al. [47], scCO₂ followed by a H₂O₂ washing step (groups scCO₂(II) and scCO₂(III)) was not successful in completely decellularizing porcine trachea in this study. A significant amount of DNA was still present after decellularization, and histological analysis also demonstrated cells and cellular content remaining in the tissue. This is consistent with a previous study on the decellularization of articular cartilage using only scCO₂ [71]. On the other hand, decellularization with scCO₂ followed by the H₂O₂ washing step and an additional washing step with NaOH (group scCO₂(I)) led to complete removal of cells and cellular debris but was particularly detrimental to the ECM, as evidenced by substantial loss of GAGs and collagen. This loss of GAGs is in line with previous findings [72–74]. Schneider et al., for instance, compared 24 different decellularization protocols for decellularizing articular cartilage and found that NaOH led to the highest reduction in GAG

content [74]. In contrast to the scCO₂(II) and scCO₂(III) groups, chemical treatment of porcine trachea (groups DEM-ethanol and DEM-gamma) was found to be effective in removing cells and cellular debris. This is also in line with two previous studies using the same protocol [44,45]. Furthermore, most ECM components were preserved after chemical treatment, although some loss in GAGs was observed. This is also comparable to the results obtained by Lange et al. [44]. In their study 40-60% of the GAG content was maintained, whereas in this thesis approximately 69% of the GAG content was preserved in the DEM-ethanol samples. In the study of Butler et al., on the other hand, the vacuum-assisted chemical method did not result in a decline in GAG content [45]. Overall, this chemical method, which could be considered the gold standard, depicted the best effect from the decellularization methods presented in this thesis.

Inadequate decellularization with the scCO₂ approach, without a washing step with NaOH, may be caused by a variety of factors. Rapid depressurization is thought to be important for removing cells and cellular debris [48]. According to Topuz et al., the retention of cellular remnant inside the tissue may thus be attributed to a low rate of gas discharge [48]. Furthermore, studies on the ability of scCO₂ to remove DNA are inconclusive. Sawada et al., for instance, found that only scCO₂ with ethanol as an additive effectively removed cellular content from porcine aorta, while scCO₂ alone did not [75]. To explain this, supercritical extraction of cells or cellular remnants has been suggested as one of the mechanisms of action of scCO₂ decellularization [47,50]. Since CO₂ itself is a nonpolar molecule, only a small amount of the polar cellular material will dissolve in pure scCO₂, as explained by Sawada et al. and Casali et al. [50,75]. As such, it has been recommended to use a polar co-solvent that is soluble in CO₂, such as ethanol, in the decellularization process. Using ethanol as a co-solvent has yielded promising results for several other scientists as well [76-78]. However, the use of ethanol has been shown to cause tissue dehydration [75]. Besides, porcine aorta were not successfully decellularized in the study by Casali et al., despite the inclusion of ethanol in the decellularization process [50]. Only when porcine aorta were treated with the detergent sodium dodecyl sulfate (SDS) directly followed by scCO₂ processing, effective decellularization was accomplished. Similarly, chemical decellularization methods were combined with scCO₂ in the study of Ling et al. for the decellularization of cancellous bone [79]. As such, Casali et al. hypothesized that scCO₂ may not be able to fully permeate the cell membrane, resulting in incomplete cell elimination [50]. Duarte et al. support this theory, explaining that while studies on the mechanism of scCO₂ sterilization show that scCO₂ can infiltrate the cell membrane, the extent of this penetration might not be adequate enough to result in complete cell removal [80]. In their study, they therefore used freeze-thawing prior to decellularization to induce cell lysis and combined scCO₂ with Tri(n-butyl) phosphate (TnBP) to improve decellularization efficacy.

Based on the literature, future experiments on the decellularization of tracheal tissue could thus explore the use of a freeze-thawing method, the use of a co-solvent and the combination of a secondary agent like TnBP and scCO₂ processing. Furthermore, parameters of the scCO₂ process, such as temperature, pressure, treatment time, use of co-solvents and gas output rate could be adjusted in future experiments to gain a better understanding of the working mechanism of scCO₂ decellularization of tracheal tissue.

4.2. Impact of sterilization

Besides comparing scCO₂ decellularization with chemical decellularization, various sterilization methods were also studied. Commonly used terminal sterilization methods for ECM scaffolds include electron beam irradiation, gamma irradiation and ethylene oxide exposure [47,81,82]. However, these conventional sterilization methods have certain drawbacks. Ethylene oxide, for instance, is a toxic compound that can significantly alter the mechanical properties of the ECM [83,84]. Gamma irradiation has also been shown to compromise the tissue's ultrastructure leading to altered mechanical properties as well as reduced cell adhesion [47,85,86]. Tissue structural changes are dose dependent and are believed to be caused in part by cross-linking of structural components like collagen [82,86,87]. In studies utilizing decellularized tracheas, antibiotics [55,88-91], peracetic acid and ethanol [92,93], and gamma irradiation [93-95] are mostly used as sterilization and disinfection methods. However, information on the effects of these sterilization methods on decellularized tracheal scaffolds is very limited. Only one study has been conducted on the effects of gamma irradiation on the ultrastructure of decellularized tracheas [94]. Johnson et al. demonstrated that sterilizing mice tracheas with 25 kGy gamma irradiation resulted in degradation of the tissue's ultrastructure, including disorganization

of collagen fibers and lacunal degeneration [94].

Sterilization using scCO₂ has been suggested as an alternative. The low critical temperature of CO₂ (31.1°C) makes sterilization with scCO₂ an ideal method for sensitive materials [96]. Treatment with scCO₂ has, for instance, been used for sterilization of heart valves [96], lung tissue [97], and bone [98]. In these studies scCO₂ treatment was found to be an efficient sterilization technique, and did not impact the properties and composition of the tissues.

In this thesis, sterilization of porcine tracheal scaffolds was achieved using 25 kGy gamma irradiation or scCO₂ in conjunction with peracetic acid, as it has been suggested that scCO₂ sterilization requires a co-solvent to efficiently inactivate bacterial endospores [96]. Subsequently, the mechanical characteristics and ECM ultrastructure of these scaffolds were evaluated. The maximum force of most scaffolds was found to be declined after decellularization and sterilization when compared to native trachea. The maximum force was not altered when scaffolds were decellularized and sterilized with scCO₂ (scCO₂(III)), whereas scaffolds decellularized with scCO₂ but sterilized with gamma irradiation (scCO₂(II)) did show a significant decline in maximum force. This difference between scCO₂(II) and scCO₂(III) could thus potentially be explained by the different sterilization methods used, since, as already discussed in the preceding text, gamma irradiation negatively impacts the mechanical properties of biological tissues, whereas scCO₂ does not.

The stress-strain curves of native trachea and tracheas treated with the scCO₂(III) and DEM-gamma methods also depicted some noticeable differences. The samples treated with DEM-gamma already depicted loss of load at 40% strain, while the native and scCO₂(III) treated samples depicted loss of load after 50% strain. Furthermore, no clear stiffening behavior could be depicted in the stress-strain curve of the DEM-gamma treated samples, whereas this behavior was more clear in the curves of the native and scCO₂(III) treated samples. Gamma irradiation has been shown to affect collagen fibers by cross-linking of collagen molecules in the presence of free radicals or by splitting polypeptide chains [99]. The decrease in elasticity in the gamma-irradiated samples is thus likely attributable to irradiation-induced collagen damage. These results are consistent with the findings obtained by Gouk et al., who demonstrated that gamma irradiation of acellular human tissue matrix resulted in a decreased toe region length and declined ultimate strain [85]. Similarly, the different sterilization procedures used can clarify the variations in DNA content and ECM components seen in the histological and quantitative data (scCO₂(II) vs. scCO₂(III) and DEM-gamma vs. DEM-ethanol). Gamma irradiation sterilization generally resulted in lower DNA content and less retention of ECM components. The reduced DNA content seen following gamma irradiation could also be explained by the fact that gamma irradiation causes DNA damage, which is its main mode of action for inactivation of microorganisms. DNA fragmentation has been shown to influence the accuracy of DNA content measurement, implying that the smaller DNA fragments due to DNA damage are simply not measured by the PicoGreen assay [100].

4.3. Recellularization of decellularized scaffolds

Decellularized scaffolds were seeded with pADSCs to assess cytocompatibility and recellularization efficacy. Unseeded scaffolds have been shown to be more prone to induce graft failure as a result of leakage and granulations as well as eliciting a local immune response [32]. Additionally, the trachea's complex structure necessitates recellularization, most likely with multiple cell types to regenerate a functional tracheal scaffold. The most frequently used cell types for recellularization include respiratory epithelial cells, chondrocytes, and mesenchymal stem cells [32]. In this thesis, ADSCs were mainly used for the recellularization experiments because of their many advantages. ADSCs are a popular cell source due to their relative abundance and accessibility [101]. Furthermore, mesenchymal stem cells have the ability to differentiate towards different lineages and produce immunomodulatory factors [32].

Initial static seeding results demonstrated poor survival of cells. When fibrin was used as a cell carrier and scaffolds were cultured under chondrogenic conditions, both scCO₂ decellularized and chemically decellularized scaffolds supported the viability and attachment of pADSCs, as demonstrated with WST-1 assay and H&E staining.

Fibrin is a naturally occurring biopolymer that is formed when thrombin converts fibrinogen to cross-linked fibrin [102–104]. Together, these molecules play important roles in blood coagulation and wound healing. Fibrin gel has been mainly used as a cell carrier in cardiovascular TE [104, 105]. Fibrin has the benefit over other gels in that it can be easily isolated from the patient's own blood and thus used

as an autologous material [104, 105]. Another advantage of using gel as a cell carrier that has been mentioned in the literature is that freshly formed ECM components do not permeate straight into the surrounding medium, but can accumulate in the extracellular space [104, 105].

According to the findings in this thesis, seeding the scaffolds with fibrin-encapsulated cells resulted in the formation of confluent cell layers, whereas with the other static seeding methods tested hardly any cells adhered to the scaffolds. Fibrin mimics the ECM and entraps cells onto the scaffold, which could explain why this seeding method was effective [106]. When static droplet seeding is used, the cell suspension spills over the scaffold's edges more quickly. Static surface seeding has been found to be inefficient in other studies as well, with seeding efficiencies ranging from 10–25% [106].

The inefficiency of the static seeding methods used could also be explained by the nature of the scaffold. Hamilton et al. found that only few cells covered the surface of tracheal scaffolds decellularized with DEM and seeded with bronchial epithelial cells, while a large number of live cells were found on the surface of decellularized dermis scaffolds [107].

The higher seeding efficiency seen in the scaffolds cultured in chondrogenic differentiation medium in comparison to scaffolds cultured in proliferation medium could be explained by a faster formation of ECM. When no degradation inhibitors are used, fibrin will degrade rapidly (within several days), due to cell-associated enzymatic activities [104]. The fibrin can then be replaced by newly synthesized ECM. It is likely that ADSCs in chondrogenic differentiation medium will start producing ECM components faster, entrapping the cells in this newly formed matrix, whereas (loosely-attached) cells in proliferation medium might be lost in the surrounding medium when fibrin starts to degrade. The differences in surface topographies seen with SEM could explain why cells seeded onto a DEM-ethanol decellularized scaffold and cultured in proliferation medium showed cell adherence and proliferation while cells seeded onto a scCO₂(III) decellularized scaffold and cultured in proliferation medium did not. Decellularization and sterilization with scCO₂ (scCO₂(III)) resulted in collagen with a more loose and fibrous appearance, possibly inhibiting cellular adherence.

Future experiments can be performed comparing culturing with and without the use of fibrin degradation inhibitors, to determine the influence on cell differentiation and production of ECM. Additionally, cell mediators such as growth factors may be incorporated into the fibrin gel to provide the cells with a more tissue-specific environment, and thereby potentially improve cell function [105].

Overall, seeding tracheal scaffolds using fibrin as a cell carrier provided a fast and easy seeding method that can be used to obtain a higher cell seeding efficiency. The seeded cells did seem to concentrate on the surface of the decellularized scaffolds and also after 21 days of culture, there was only minimal infiltration of cells into the ECM of the tracheal scaffolds. It is possible that cells will infiltrate the scaffold after a longer *in vitro* culture period. Additional long-term *in vitro* experiments are needed to determine if this is indeed the case.

However, research has shown that the dense ECM of the trachea hinders migration of cells into the scaffold. Several studies have been conducted in an effort to improve cell infiltration and repopulation of decellularized cartilage matrices. Here, the porosity of a scaffold is an important property that influences cell ingrowth. There have been reports of GAGs being intentionally removed to increase porosity of the decellularized scaffolds and thus enhance cellular infiltration [73, 74, 108]. Bautista et al., for instance, used the enzyme chondroitinase ABC in their decellularization protocol to remove GAGs from porcine articular cartilage [108]. Nevertheless, removal of GAGs did not result in successful recellularization [74, 108, 109]. Another approach for enhancing cellular ingrowth was to use a needle to create microchannels into the scaffold [109, 110]. This method facilitated the migration of cells into the scaffolds and allowed for the production of ECM components in these "openings". Others have shown that laser surface modification improved cell adhesion and infiltration into the scaffolds, and supported deposition of cartilage-specific matrix components [111, 112]. Furthermore, dynamic cell seeding methods have also been proposed to facilitate cell infiltration. Examples include centrifugal seeding and seeding inside a bioreactor [113, 114]. However, to date it is unclear if and which dynamic seeding methods improve cellular infiltration in decellularized tracheal scaffolds and lead to improved functional outcome *in vivo*.

The approach suggested by Aoki et al. eliminates the need for cartilage regeneration [115]. They propose to partially decellularize the tracheal scaffolds, thereby removing the epithelium but leaving the cartilage matrix intact. It is hypothesized that this "hybrid graft" will not lead to an immune response when implanted *in vivo* due to the immunoprivileged nature of cartilage. They further explain that this concept would simplify the recellularization process as the cartilage is kept alive. scCO₂ might be a

promising method for this interesting concept, but that is also something that the future holds. Aspects like terminal sterilization were, for instance, not discussed in the article.

Besides improving recellularization efficiency of decellularized scaffolds, mechanical loading of cell-seeded constructs is also an important topic. Choi et al. define mechanical loading as the fourth primary approach in cartilage TE, in addition to the three approaches cells, scaffold, and growth factors [31]. In cartilage TE, many studies have already been conducted on the importance of mechanical loading for the generation of tissue-engineered constructs that better mimic native tissue [31, 116, 117]. Application of mechanical loads has been shown to enhance chondrogenesis *in vitro*. Cao et al., for example, showed that dynamic compressive loading of bone marrow mesenchymal stem cells encapsulated in a collagen hydrogel resulted in chondrogenic differentiation, increased ECM production and improved mechanical properties [118]. Similar results were reported by other authors in the field [119]. To the author's knowledge, the importance of mechanical conditioning in the field of tracheal TE has not received much attention yet. By applying cyclic strain that mimics the respiratory rate in humans to cell-seeded decellularized tracheal constructs in a bioreactor, we wanted to investigate the effects on cellular behavior and phenotype. It was hypothesized that the loaded cell-seeded constructs would depict an enhanced chondrogenic phenotype. Future experiments with the bioreactor should determine whether mechanical loading of cell-seeded decellularized tracheal scaffolds results in increased production of ECM components and, as a result, improved mechanical properties to fulfill the requirements for clinical success. Furthermore, the hyperelastic modelling findings may be utilized to generate a finite-element model of the bioreactor system.

4.4. Limitations and future perspectives

In the following bullet points some limitations of this thesis are addressed:

- Only histological staining was used in this thesis to estimate the preservation of collagen. In a future study, a biochemical assay could be used to quantify the collagen content, which could provide a more precise picture.
- Another limitation was that preservation of the basement membrane was not assessed. A co-seeding strategy has been suggested due to the trachea's complex structure. Absence or disruption of the basement membrane could impede epithelial cell adherence [2, 107]. Furthermore, this membrane is known to act as a protective barrier, and its absence can result in undesirable invasion of cells into the submucosa [2].
- Uniaxial tensile tests of the single trachea components were carried out with native tracheal samples that were stored in the freezer (-80°C) for over 2 years. The effects of long-term storage on the mechanical properties and structure of tracheal constructs remain unclear. Long-term storage of decellularized tracheal scaffolds at -80°C for 6 months showed no difference in mechanical properties compared to freshly decellularized tracheal scaffolds [120]. Cryopreservation of tracheal grafts is, however, associated with cartilage damage [121]. Long-term storage of native tracheal samples could explain why the tensile modulus of native cartilage was on the lower end of the spectrum as compared to other studies. In the study by Safshekan et al., for instance, a much higher Young's modulus of 16.92 ± 8.76 MPa for human tracheal cartilage was reported [3]. More research on the differences between long-term stored and fresh native trachea is therefore needed.
- Furthermore, only uniaxial tensile testing was assessed in this study. Uniaxial tensile testing does not account for all the complex mechanical forces that the trachea normally experiences during respiration. It is important for tracheal functionality *in vivo* to closely match the mechanical properties of a tissue-engineered tracheal scaffold to native trachea [67]. A mismatch in mechanical properties can result in granulation at the anastomosis sites and, eventually, graft failure. In their review, Boazak et al. therefore emphasize the importance of conducting both longitudinal tensile and lateral (radial) compression tests as well as compliance tests [67]. These tests, when combined, will provide further detail on the tissue-engineered trachea's extensibility, tubular resistance to collapse, and ability to withstand and flex in the presence of physiologic transmural pressures [67]. It is therefore proposed that more mechanical tests are conducted in future experiments to gain a greater understanding of the mechanical performance of the trachea after decellularization.

- Moreover, most seeding experiments tested only one sample per time point, to limit the amount of animal tissue used. This affects the interpretation of the published data, as the results are more prone to errors. However, given the general difficulties associated with static seeding of scaffolds in other studies, as well as the fact that static seeding was repeated multiple times, it is not believed that the low sample size changes the general conclusion of the seeding experiments.
- Lastly, tissue sterility was not validated. While the scaffolds demonstrated cytocompatibility, future experiments could focus on the efficacy of the sterilization technique used by employing several tests [96]. Along with this, the effect of scCO₂ decellularization alone, without the additional sterilization step used in this thesis could be studied, and the effect of different parameters, including temperature, pressure, treatment time could be evaluated to assess the effect on sterilization efficacy.

5

Conclusion

The current study evaluated the potential of scCO₂ processing for decellularization and sterilization of porcine tracheas as an alternative to methods described in the literature, which often use harsh chemicals. The analyses performed in this thesis revealed that decellularization with scCO₂ in combination with a H₂O₂ washing step, without the use of a co-solvent, was not successful in completely decellularizing the porcine tracheas. The vacuum-assisted DEM, considered the gold standard, depicted the best effect from the decellularization methods presented in this thesis. However, this chemical method is still a time-consuming process, taking several days to complete. Further investigation is therefore suggested to determine whether scCO₂ decellularization combined with a co-solvent or secondary agent can result in successful decellularization. Sterilization and decellularization of tracheas in a one-step procedure could then also be assessed further. Seeding with fibrin-encapsulated stem cells was identified as an effective and easy seeding method and demonstrated that cells were able to adhere to the decellularized scaffolds.

Together with the future directions outlined in this thesis, the results in this thesis open up new avenues for potential optimizations. It is believed that the many advantages associated with scCO₂ processing could, in the future, streamline the process of decellularizing tracheas to achieve successful decellularization in a shorter time period and with less post-processing steps, thereby creating an off-the-shelf template for tracheal TE purposes.

Bibliography

- [1] M. Torre, M. Carlucci, and V. Jasonni, "Tracheal Lesions," in *Pediatric Thoracic Surgery* (M. Lima, ed.), pp. 205–215, Springer Milan, 2013.
- [2] M. den Hondt, *From bed to bench: towards the creation of a tissue-engineered trachea*. PhD thesis, KU Leuven, Jan. 2018.
- [3] F. Safshekan, M. Tafazzoli-Shadpour, M. Abdouss, and M. Shadmehr, "Mechanical Characterization and Constitutive Modeling of Human Trachea: Age and Gender Dependency.," *Materials (Basel)*, vol. 9, p. 456, June 2016.
- [4] T. Prange, "Chapter 48 - Trachea," in *Equine Surgery (Fifth Edition)* (J. A. Auer, J. A. Stick, J. M. Kümmeler, and T. Prange, eds.), pp. 797–804, W.B. Saunders, fifth edition ed., 2019.
- [5] M. Den Hondt and J. J. Vranckx, "Reconstruction of defects of the trachea," *Journal of Materials Science: Materials in Medicine*, vol. 28, no. 24, 2017.
- [6] C. Crowley, M. Birchall, and A. M. Seifalian, "Trachea transplantation: from laboratory to patient," *Journal of Tissue Engineering and Regenerative Medicine*, vol. 9, no. 4, pp. 357–367, 2015.
- [7] B. Brown, K. Lindberg, J. Reing, D. Stolz, and S. Badylak, "The basement membrane component of biologic scaffolds derived from extracellular matrix," *Tissue engineering*, vol. 12, no. 3, pp. 519–526, 2006.
- [8] A. Dhasmana, A. Singh, and S. Rawal, "Biomedical grafts for tracheal tissue repairing and regeneration "Tracheal tissue engineering: an overview",," *Journal of Tissue Engineering and Regenerative Medicine*, vol. 14, no. 5, pp. 653–672, 2020.
- [9] P. Varela, M. Torre, C. Schweiger, and H. Nakamura, "Congenital tracheal malformations," *Pediatric Surgery International*, vol. 34, pp. 701–713, July 2018.
- [10] P. Herrera, C. Caldarone, V. Forte, P. Campisi, H. Holtby, P. Chait, P. Chiu, P. Cox, S. Yoo, D. Manson, and P. Kim, "The current state of congenital tracheal stenosis," *Pediatric surgery international*, vol. 23, no. 11, pp. 1033–1044, 2007.
- [11] G. Galluccio, G. Lucantoni, P. Battistoni, G. Paone, S. Batzella, V. Lucifora, and R. D. Iacono, "Interventional endoscopy in the management of benign tracheal stenoses: definitive treatment at long-term follow-up," *European Journal of Cardio-Thoracic Surgery*, vol. 35, pp. 429–433, Mar. 2009.
- [12] N. A. Rahman, O. Fruchter, D. Shitrit, B. D. Fox, and M. R. Kramer, "Flexible bronchoscopic management of benign tracheal stenosis: long term follow-up of 115 patients," *Journal of Cardio-thoracic Surgery*, vol. 5, Jan. 2010.
- [13] S. Nouraei, E. Ma, A. Patel, D. Howard, and G. Sandhu, "Estimating the population incidence of adult post-intubation laryngotracheal stenosis," *Clinical Otolaryngology*, vol. 32, pp. 411–412, 2007.
- [14] C. Aravena, F. A. Almeida, S. Mukhopadhyay, S. Ghosh, R. R. Lorenz, S. C. Murthy, and A. C. Mehta, "Idiopathic subglottic stenosis: a review," *Journal of Thoracic Disease*, vol. 12, pp. 1100–1111, Nov. 2020.
- [15] J. Honings, J. A. A. M. van Dijck, A. F. T. M. Verhagen, H. F. M. van der Heijden, and H. A. M. Marres, "Incidence and Treatment of Tracheal Cancer: A Nationwide Study in The Netherlands," *Annals of Surgical Oncology*, vol. 14, pp. 968–976, 2007.

- [16] A. I. Urdaneta, J. B. Yu, and L. D. Wilson, "Population based cancer registry analysis of primary tracheal carcinoma," *American Journal of Clinical Oncology*, vol. 34, no. 1, pp. 32–37, 2011.
- [17] S. Timman, C. Schoemaker, W. Li, H. Marres, J. Honings, W. Morshuis, E. van der Heijden, and A. Verhagen, "Functional outcome after (laryngo)tracheal resection and reconstruction for acquired benign (laryngo)tracheal stenosis," *Annals of Cardiothoracic Surgery*, vol. 7, pp. 227–236, Mar. 2018.
- [18] C. D. Wright, H. C. Grillo, J. C. Wain, D. R. Wong, D. M. Donahue, H. A. Gaissert, and D. J. Mathisen, "Anastomotic complications after tracheal resection: Prognostic factors and management," *The Journal of Thoracic and Cardiovascular Surgery*, vol. 128, no. 5, pp. 731–739, 2004.
- [19] K. A. Kucera, A. E. Doss, S. S. Dunn, L. A. Clemson, and J. B. Zwischenberger, "Tracheal Replacements: Part 1," *ASAIO Journal*, vol. 53, pp. 497–505, July 2007.
- [20] A. D. Dikina, H. A. Strobel, B. P. Lai, M. W. Rolle, and E. Alsberg, "Engineered cartilaginous tubes for tracheal tissue replacement via self-assembly and fusion of human mesenchymal stem cell constructs," *Biomaterials*, vol. 52, pp. 452–462, 2015.
- [21] A. Siciliani, E. A. Rendina, and M. Ibrahim, "State of the art in tracheal surgery: a brief literature review," *Multidisciplinary Respiratory Medicine*, vol. 13, Sept. 2018.
- [22] E. Folch and C. Keyes, "Airway stents," *Annals of Cardiothoracic Surgery*, vol. 7, no. 2, pp. 273–283, 2018.
- [23] H. C. Grillo, "Tracheal replacement: a critical review," *The Annals of Thoracic Surgery*, vol. 73, no. 6, pp. 1995–2004, 2002.
- [24] R. Belsey, "Resection and reconstruction of the intrathoracic trachea," *The British Journal of Surgery*, vol. 38, pp. 200–205, Oct. 1950.
- [25] H. Etienne, D. Fabre, A. Gomez Caro, F. Kolb, S. Mussot, O. Mercier, D. Mitilian, F. Stephan, E. Fadel, and P. Darteville, "Tracheal replacement," *European Respiratory Journal*, vol. 51, no. 2, 2018.
- [26] A. E. Doss, S. S. Dunn, K. A. Kucera, L. A. Clemson, and J. B. Zwischenberger, "Tracheal Replacements: Part 2," *ASAIO Journal*, vol. 53, pp. 631–639, Sept. 2007.
- [27] J. P. Jacobs, M. J. Elliott, M. P. Haw, C. M. Bailey, and C. Herberhold, "Pediatric tracheal homograft reconstruction: A novel approach to complex tracheal stenoses in children," *The Journal of Thoracic and Cardiovascular Surgery*, vol. 112, pp. 1549–1560, Dec. 1996.
- [28] M. Elliott, M. Haw, J. Jacobs, C. Bailey, J. Evans, and C. Herberhold, "Tracheal reconstruction in children using cadaveric homograft trachea," *European Journal of Cardiothoracic Surgery*, vol. 10, no. 9, pp. 707–712, 1996.
- [29] D. Fabre, S. Singhal, V. De Montpreville, B. Decante, S. Mussot, O. Chataigner, O. Mercier, F. Kolb, P. G. Darteville, and E. Fadel, "Composite cervical skin and cartilage flap provides a novel large airway substitute after long-segment tracheal resection," *The Journal of Thoracic and Cardiovascular Surgery*, vol. 138, pp. 32–39, July 2009.
- [30] A. Gilpan and Y. Yang, "Decellularization Strategies for Regenerative Medicine: From Processing Techniques to Applications," *BioMed Research International*, vol. 2017, 2017.
- [31] J. R. Choi, K. W. Yong, and J. Y. Choi, "Effects of mechanical loading on human mesenchymal stem cells for cartilage tissue engineering," *Journal of Cellular Physiology*, vol. 233, no. 3, pp. 1913–1928, 2018.
- [32] E. F. Maughan, R. E. Hynds, T. J. Proctor, S. M. Janes, M. Elliott, M. A. Birchall, M. W. Lowdell, and P. D. Coppi, "Autologous Cell Seeding in Tracheal Tissue Engineering," *Current Stem Cell Reports*, vol. 3, pp. 279–289, 2017.

- [33] F. N. Alaribe, S. L. Manoto, and S. C. Motaung, "Scaffolds from biomaterials: advantages and limitations in bone and tissue engineering," *Biologia*, vol. 71, no. 4, pp. 353–366, 2016.
- [34] V. Pepper, C. A. Best, K. Buckley, C. Schwartz, E. Onwuka, N. King, A. White, S. Dharmadhikari, S. D. Reynolds, J. Johnson, J. Grischkan, C. K. Breuer, and T. Chiang, "Factors Influencing Poor Outcomes in Synthetic Tissue-Engineered Tracheal Replacement," *Otolaryngology–Head and Neck Surgery*, vol. 161, pp. 458–467, Apr. 2019.
- [35] T. Chiang, V. Pepper, C. Best, E. Onwuka, and C. K. Breuer, "Clinical Translation of Tissue Engineered Trachea Grafts," *Annals of Otology, Rhinology & Laryngology*, vol. 125, no. 11, pp. 873–885, 2016.
- [36] S. Bogan, G. Teoh, and M. Birchall, "Tissue Engineered Airways: A Prospects Article," *Journal of Cellular Biochemistry*, vol. 117, pp. 1497–505, July 2016.
- [37] B. N. Brown and S. F. Badylak, "Extracellular matrix as an inductive scaffold for functional tissue reconstruction," *Translational Research*, vol. 163, no. 4, pp. 268–285, 2014. Regenerative Medicine: The Hurdles and Hopes.
- [38] A. Petrosyan, S. Da Sacco, N. Tripuraneni, U. Kreuser, M. Lavarreda-Pearce, R. Tamburrini, R. E. De Filippo, G. Orlando, P. Cravedi, and L. Perin, "A step towards clinical application of acellular matrix: A clue from macrophage polarization," *Matrix Biology*, vol. 57-58, pp. 334–346, Jan. 2017.
- [39] M. Pinto, E. Rios, A. Silva, S. Neves, H. Caires, A. Pinto, C. Durães, F. Carvalho, A. Cardoso, N. Santos, C. Barrias, D. Nascimento, P. P. do Ó, M. Barbosa, F. Carneiro, and M. Oliveira, "Decellularized human colorectal cancer matrices polarize macrophages towards an anti-inflammatory phenotype promoting cancer cell invasion via CCL18," *Biomaterials*, vol. 124, pp. 211–224, 2017.
- [40] J. Liao, B. Xu, R. Zhang, Y. Fan, H. Xie, and X. Li, "Applications of decellularized materials in tissue engineering: advantages, drawbacks and current improvements, and future perspectives," *Journal of Materials Chemistry B*, vol. 8, pp. 10023–10049, Oct. 2020.
- [41] L. Partington, N. Mordan, C. Mason, J. Knowles, H.-W. Kim, M. Lowdell, M. Birchall, and I. Wall, "Biochemical changes caused by decellularization may compromise mechanical integrity of tracheal scaffolds," *Acta Biomaterialia*, vol. 9, no. 2, pp. 5251–5261, 2013.
- [42] S. Baiguera, P. Jungebluth, A. Burns, C. Mavilia, J. Haag, P. De Coppi, and P. Macchiarini, "Tissue engineered human tracheas for in vivo implantation," *Biomaterials*, vol. 31, no. 34, pp. 8931–8938, 2010.
- [43] M. T. Conconi, P. D. Coppi, R. D. Liddo, S. Vigolo, G. F. Zanon, P. P. Parnigotto, and G. G. Nussdorfer, "Tracheal matrices, obtained by a detergent-enzymatic method, support in vitro the adhesion of chondrocytes and tracheal epithelial cells," *Transplant International*, vol. 18, no. 6, pp. 727–734, 2005.
- [44] P. Lange, K. Greco, L. Partington, C. Carvalho, S. Oliani, M. A. Birchall, P. D. Sibbons, M. W. Lowdell, and T. Ansari, "Pilot study of a novel vacuum-assisted method for decellularization of tracheae for clinical tissue engineering applications," *Journal of Tissue Engineering and Regenerative Medicine*, vol. 11, no. 3, pp. 800–811, 2017.
- [45] C. R. Butler, R. E. Hynds, C. Crowley, K. H. Gowers, L. Partington, N. J. Hamilton, C. Carvalho, M. Platé, E. R. Samuel, A. J. Burns, L. Urbani, M. A. Birchall, M. W. Lowdell, P. De Coppi, and S. M. Janes, "Vacuum-assisted decellularization: an accelerated protocol to generate tissue-engineered human tracheal scaffolds," *Biomaterials*, vol. 124, pp. 95–105, 2017.
- [46] K. H. Hussein, K.-M. Park, K.-S. Kang, and H.-M. Woo, "Biocompatibility evaluation of tissue-engineered decellularized scaffolds for biomedical application," *Materials Science and Engineering: C*, vol. 67, pp. 766–778, 2016.

- [47] P. M. Crapo, T. W. Gilbert, and S. F. Badylak, "An overview of tissue and whole organ decellularization processes," *Biomaterials*, vol. 32, no. 12, pp. 3233–3243, 2011.
- [48] B. Topuz, G. Günal, S. Guler, and H. M. Aydin, "Chapter 4 - Use of supercritical CO₂ in soft tissue decellularization," in *Cell-derived Matrices - Part B* (D. Caballero, S. C. Kundu, and R. L. Reis, eds.), vol. 157 of *Methods in Cell Biology*, pp. 49–79, Academic Press, 2020.
- [49] J. Chakraborty, S. Roy, and S. Ghosh, "Regulation of decellularized matrix mediated immune response," *Biomaterials Science*, vol. 8, no. 5, pp. 1194–1215, 2020.
- [50] D. M. Casali, R. M. Handleton, T. Shazly, and M. A. Matthews, "A novel supercritical CO₂-based decellularization method for maintaining scaffold hydration and mechanical properties," *The Journal of Supercritical Fluids*, vol. 131, pp. 72–81, 2018.
- [51] W. Leitner, "Designed to dissolve," *Nature*, vol. 405, pp. 129–130, May 2000.
- [52] A. Harris, J. Lacombe, S. Liyanage, M. Han, E. Wallace, S. Karsunky, N. Abidi, and F. Zenhausern, "Supercritical carbon dioxide decellularization of plant material to generate 3D biocompatible scaffolds," *Scientific Reports*, vol. 11, no. 3643, 2021.
- [53] A. Dragan, J. Casas-Finet, E. Bishop, R. Strouse, M. Schenerman, and C. Geddes, "Characterization of PicoGreen Interaction with dsDNA and the Origin of its Fluorescence Enhancement upon Binding," *Biophysical Journal*, vol. 99, no. 9, pp. 3010–3019, 2010.
- [54] C. J. Billington, "Cartilage proteoglycan release assay," in *Matrix Metalloproteinase Protocols* (I. M. Clark, ed.), pp. 451–456, Totowa, NJ: Humana Press, 2001.
- [55] F. Sun, Y. Jiang, Y. Xu, H. Shi, S. Zhang, X. Liu, S. Pan, G. Ye, W. Zhang, F. Zhang, and C. Zhong, "Genipin cross-linked decellularized tracheal tubular matrix for tracheal tissue engineering applications," *Scientific Reports*, vol. 6, Apr. 2016.
- [56] F. Safshekan, M. Tafazzoli-Shadpour, M. Abdouss, M. B. Shadmehr, and F. Ghorbani, "Finite element simulation of human trachea: Normal vs. surgically treated and scaffold implanted cases," *International Journal of Solids and Structures*, vol. 190, pp. 35–46, 2020.
- [57] H. R. Hoogenkamp, *Novel Collagen-based Scaffolds For Hollow Organ Regeneration*. PhD thesis, Radboud University Nijmegen, 2015.
- [58] G. A. Holzapfel, *Nonlinear Solid Mechanics: A Continuum Approach for Engineering Science*. John Wiley & Sons, 2000.
- [59] P. A. L. S. Martins, R. M. N. Jorge, and A. J. M. Ferreira, "A comparative study of several material models for prediction of hyperelastic properties: Application to silicone-rubber and soft tissues," *Strain*, vol. 42, no. 3, p. 135–147, 2006.
- [60] C. Wex, S. Arndt, A. Stoll, C. Bruns, and Y. Kupriyanova, "Isotropic incompressible hyperelastic models for modelling the mechanical behaviour of biological tissues: a review," *Biomedical Engineering / Biomedizinische Technik*, vol. 60, no. 6, 2015.
- [61] S. J. Hollister, M. P. Hollister, and S. K. Hollister, "Computational modeling of airway instability and collapse in tracheomalacia," *Respiratory Research*, vol. 18, no. 1, 2017.
- [62] Y. Li, H. Meng, Y. Li, and B. P. Lee, "Fibrin gel as an injectable biodegradable scaffold and cell carrier for tissue engineering," *The Scientific World Journal*, pp. 685–690, Mar. 2015.
- [63] S. R. Cohen, N. Perelman, V. Mahnovski, M. E. Nimni, and D. T. Cheung, "Whole organ evaluation of collagen in the developing human larynx and adjoining anatomic structures (hyoid and trachea)," *Annals of Otolaryngology, Rhinology & Laryngology*, vol. 102, no. 9, pp. 655–659, 1993.
- [64] O. Trabelsi, A. Del Palomar, J. López-Villalobos, A. Ginel, and M. Doblaré, "Experimental characterization and constitutive modeling of the mechanical behavior of the human trachea," *Medical Engineering & Physics*, vol. 32, pp. 76–82, Jan. 2010.

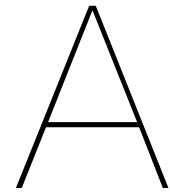
- [65] J. Wang, P. Mesquida, and T. Lee, "Young's modulus measurement on pig trachea and bronchial airways," *Annu Int Conf IEEE Eng Med Biol Soc*, pp. 2089–92, 2011.
- [66] J. Rains, J. Bert, C. Roberts, and P. Paré, "Mechanical properties of human tracheal cartilage," *Journal of Applied Physiology*, vol. 72, no. 1, pp. 219–225, 1985.
- [67] E. M. Boazak and D. T. Auguste, "Trachea Mechanics for Tissue Engineering Design," *ACS Biomaterials Science & Engineering*, vol. 4, no. 4, pp. 1272–1284, 2018.
- [68] B. E. Brand-Saberi and T. Schäfer, "Trachea: Anatomy and Physiology," *Thoracic Surgery Clinics*, vol. 24, pp. 1–5, Feb. 2014.
- [69] S. F. Badylak, D. Taylor, and K. Uygun, "Whole-Organ Tissue Engineering: Decellularization and Recellularization of Three-Dimensional Matrix Scaffolds," *Annual Review of Biomedical Engineering*, vol. 13, no. 1, pp. 27–53, 2011.
- [70] I. Sherifi, M. Bachy, T. Laumonier, H. Petite, and D. Hannouche, "Use of supercritical carbon dioxide technology for fabricating a tissue engineering scaffold for anterior cruciate ligament repair," *Scientific Reports*, vol. 10, Aug. 2020.
- [71] J. Antons, M. Marascio, P. Aeberhard, G. Weissenberger, N. Hirt-Burri, L. Applegate, P. Bourban, and D. Pioletti, "Decellularised tissues obtained by a CO₂-philic detergent and supercritical CO₂," *European Cells & Materials*, vol. 4, pp. 81–95, Sept. 2018.
- [72] D. Herbage, J. Bouillet, and J. Bernengo, "Biochemical and physicochemical characterization of pepsin-solubilized type-II collagen from bovine articular cartilage," *Biochemical Journal*, vol. 161, pp. 303–312, Feb. 1977.
- [73] S. Schwarz, A. F. Elsaesser, L. Koerber, E. Goldberg-Bockhorn, A. M. Seitz, C. Bermueller, L. Dürselen, A. Ignatius, R. Breiter, and N. Rotter, "Processed xenogenic cartilage as innovative biomatrix for cartilage tissue engineering: effects on chondrocyte differentiation and function," *Journal of Tissue Engineering and Regenerative Medicine*, vol. 9, no. 12, pp. E239–E251, 2015.
- [74] C. Schneider, J. Lehmann, G. J. van Osch, F. Hildner, A. Teuschl, X. Monforte, D. Miosga, P. Heimel, E. Priglinger, H. Redl, S. Wolbank, and S. Nürnberger, "Systematic Comparison of Protocols for the Preparation of Human Articular Cartilage for Use as Scaffold Material in Cartilage Tissue Engineering," *Tissue Engineering Part C: Methods*, vol. 22, no. 12, pp. 1095–1107, 2016.
- [75] K. Sawada, D. Terada, T. Yamaoka, S. Kitamura, and T. Fujisato, "Cell removal with supercritical carbon dioxide for acellular artificial tissue," *Journal of Chemical Technology & Biotechnology*, vol. 83, no. 6, pp. 943–949, 2008.
- [76] S. Guler, B. Aslan, P. Hosseinian, and H. M. Aydin, "Supercritical Carbon Dioxide-Assisted Decellularization of Aorta and Cornea," *Tissue Engineering Part C: Methods*, vol. 23, no. 9, pp. 540–547, 2017.
- [77] J. K. Wang, B. Luo, V. Guneta, L. Li, S. E. M. Foo, Y. Dai, T. T. Y. Tan, N. S. Tan, C. Choong, and M. T. C. Wong, "Supercritical carbon dioxide extracted extracellular matrix material from adipose tissue," *Materials Science and Engineering: C*, vol. 75, pp. 349–358, 2017.
- [78] Y.-H. Huang, F.-W. Tseng, W.-H. Chang, I.-C. Peng, D.-J. Hsieh, S.-W. Wu, and M.-L. Yeh, "Preparation of acellular scaffold for corneal tissue engineering by supercritical carbon dioxide extraction technology," *Acta Biomaterialia*, vol. 58, pp. 238–243, 2017.
- [79] Y. Ling, W. Xu, L. Yang, C. Liang, and B. Xu, "Improved the biocompatibility of cancellous bone with compound physicochemical decellularization process," *Regenerative Biomaterials*, vol. 7, pp. 443–451, Oct. 2020.
- [80] M. M. Duarte, N. Ribeiro, I. V. Silva, J. R. Dias, N. M. Alves, and A. L. Oliveira, "Fast decellularization process using supercritical carbon dioxide for trabecular bone," *The Journal of Supercritical Fluids*, vol. 172, p. 105194, 2021.

- [81] M. Tao, T. Ao, X. Mao, X. Yan, R. Javed, W. Hou, Y. Wang, C. Sun, S. Lin, T. Yu, and Q. Ao, "Sterilization and disinfection methods for decellularized matrix materials: Review, consideration and proposal," *Bioactive Materials*, vol. 6, no. 9, pp. 2927–2945, 2021.
- [82] T. J. Keane, I. T. Swinehart, and S. F. Badylak, "Methods of tissue decellularization used for preparation of biologic scaffolds and in vivo relevance," *Methods*, vol. 84, pp. 25–34, 2015. *Advanced Methods for Tissue Engineering and Regenerative Medicine*.
- [83] N. Ribeiro, G. C. Soares, V. Santos-Rosales, A. Concheiro, C. Alvarez-Lorenzo, C. A. García-González, and A. L. Oliveira, "A new era for sterilization based on supercritical CO₂ technology," *Journal of Biomedical Materials Research Part B: Applied Biomaterials*, vol. 108, no. 2, pp. 399–428, 2020.
- [84] D. J. Rosario, G. C. Reilly, E. Ali Salah, M. Glover, A. J. Bullock, and S. MacNeil, "Decellularization and sterilization of porcine urinary bladder matrix for tissue engineering in the lower urinary tract," *Regenerative Medicine*, vol. 3, no. 2, pp. 145–156, 2008.
- [85] S.-S. Gouk, T.-M. Lim, S.-H. Teoh, and W. Q. Sun, "Alterations of human acellular tissue matrix by gamma irradiation: Histology, biomechanical property, stability, in vitro cell repopulation, and remodeling," *Journal of Biomedical Materials Research Part B: Applied Biomaterials*, vol. 84B, no. 1, pp. 205–217, 2008.
- [86] W. Q. Sun and P. Leung, "Calorimetric study of extracellular tissue matrix degradation and instability after gamma irradiation," *Acta Biomaterialia*, vol. 4, no. 4, pp. 817–826, 2008.
- [87] A. M. Matuska and P. S. McFetridge, "The effect of terminal sterilization on structural and biophysical properties of a decellularized collagen-based scaffold; implications for stem cell adhesion," *Journal of Biomedical Materials Research Part B: Applied Biomaterials*, vol. 103, no. 2, pp. 397–406, 2015.
- [88] S. Baiguera, C. Del Gaudio, E. Kuevda, A. Gonfiotti, A. Bianco, and P. Macchiarini, "Dynamic decellularization and cross-linking of rat tracheal matrix," *Biomaterials*, vol. 35, no. 24, pp. 6344–6350, 2014.
- [89] J. Haag, S. Baiguera, P. Jungebluth, D. Barale, C. Del Gaudio, F. Castiglione, A. Bianco, C. E. Comin, D. Ribatti, and P. Macchiarini, "Biomechanical and angiogenic properties of tissue-engineered rat trachea using genipin cross-linked decellularized tissue," *Biomaterials*, vol. 33, no. 3, pp. 780–789, 2012.
- [90] A. Batioglu-Karaaltin, E. Ovali, M. V. Karaaltin, M. Yener, M. Yılmaz, F. Eyüpoglu, Y. Z. Yılmaz, E. R. Bozkurt, N. Demir, E. Konuk, E. S. Bozdog, Özgür Yigit, and H. Cansiz, "Decellularization of Trachea With Combined Techniques for Tissue-Engineered Trachea Transplantation," *Clinical and Experimental Otorhinolaryngology*, vol. 12, no. 1, pp. 86–94, 2019.
- [91] M. Den Hondt, B. Vanaudenaerde, E. Maughan, C. Butler, C. Crowley, E. Verbeken, S. Verleden, and J. Vranckx, "An optimized non-destructive protocol for testing mechanical properties in decellularized rabbit trachea," *Acta Biomaterialia*, vol. 60, pp. 291–301, 2017.
- [92] A. Weymann, N. P. Patil, A. Sabashnikov, S. Korkmaz, S. Li, P. Soos, R. Ishtok, N. Chaimow, I. Pätzold, N. Czerny, B. Schmack, A.-F. Popov, A. R. Simon, M. Karck, and G. Szabo, "Perfusion-Decellularization of Porcine Lung and Trachea for Respiratory Bioengineering," *Artificial Organs*, vol. 39, pp. 1024–1032, Apr. 2015.
- [93] J. C. Kutten, D. McGovern, C. M. Hobson, S. A. Luffy, A. Nieponice, K. Tobita, R. J. Francis, S. D. Reynolds, J. S. Isenberg, and T. W. Gilbert, "Decellularized Tracheal Extracellular Matrix Supports Epithelial Migration, Differentiation, and Function," *Tissue Engineering Part A*, vol. 21, no. 1-2, pp. 75–84, 2015.
- [94] C. M. Johnson, D. Guo, S. Ryals, G. N. Postma, and P. M. Weinberger, "The feasibility of gamma radiation sterilization for decellularized tracheal grafts," *The Laryngoscope*, vol. 127, no. 8, pp. 258–264, 2017.

- [95] N. T. Remlinger, C. A. Czajka, M. E. Juhas, D. A. Vorp, D. B. Stolz, S. F. Badylak, S. Gilbert, and T. W. Gilbert, "Hydrated xenogeneic decellularized tracheal matrix as a scaffold for tracheal reconstruction," *Biomaterials*, vol. 31, no. 13, pp. 3520–3526, 2010.
- [96] R. S. Hennessy, S. Jana, B. J. Tefft, M. R. Helder, M. D. Young, R. R. Hennessy, N. J. Stoyles, and A. Lerman, "Supercritical Carbon Dioxide–Based Sterilization of Decellularized Heart Valves," *JACC: Basic to Translational Science*, vol. 2, no. 1, pp. 71–84, 2017.
- [97] J. L. Balestrini, A. Liu, A. L. Gard, J. Huie, K. M. Blatt, J. Schwan, L. Zhao, T. J. Broekelmann, R. P. Mecham, E. C. Wilcox, and L. E. Niklason, "Sterilization of Lung Matrices by Supercritical Carbon Dioxide," *Tissue Engineering Part C: Methods*, vol. 22, no. 3, pp. 260–269, 2016.
- [98] N. Russell, A. Rives, M. H. Pelletier, T. Wang, and W. R. Walsh, "The effect of supercritical carbon dioxide sterilization on the anisotropy of bovine cortical bone," *Cell and Tissue Banking*, vol. 16, pp. 109–121, 2015.
- [99] H. Nguyen, D. Morgan, and M. Forwood, "Sterilization of allograft bone: effects of gamma irradiation on allograft biology and biomechanics," *Cell Tissue Banking*, vol. 8, pp. 93–105, 2007.
- [100] T. Sedlackova, G. Repiska, P. Celec, T. Szemes, and G. Minarik, "Fragmentation of DNA affects the accuracy of the DNA quantitation by the commonly used methods," *Biological Procedures Online*, vol. 15, no. 1, 2013.
- [101] T. T. Y. Han, J. T. Walker, A. Grant, G. A. Dekaban, and L. E. Flynn, "Preconditioning Human Adipose-Derived Stromal Cells on Decellularized Adipose Tissue Scaffolds Within a Perfusion Bioreactor Modulates Cell Phenotype and Promotes a Pro-regenerative Host Response," *Frontiers in Bioengineering and Biotechnology*, vol. 9, p. 131, 2021.
- [102] I. Catelas, "Fibrin," in *Comprehensive Biomaterials* (P. Ducheyne, ed.), pp. 303–328, Elsevier, 2011.
- [103] T. A. Ahmed, E. V. Dare, and M. Hincke, "Fibrin: A Versatile Scaffold for Tissue Engineering Applications," *Tissue Engineering Part B: Reviews*, vol. 14, no. 2, pp. 199–215, 2008.
- [104] A. Mol, M. I. van Lieshout, C. G. Dam-de Veen, S. Neuenschwander, S. P. Hoerstrup, F. P. Baaijens, and C. V. Bouten, "Fibrin as a cell carrier in cardiovascular tissue engineering applications," *Biomaterials*, vol. 26, no. 16, pp. 3113–3121, 2005.
- [105] Q. Ye, G. Zünd, P. Benedikt, S. Jockenhoevel, S. P. Hoerstrup, S. Sakyama, J. A. Hubbell, and M. Turina, "Fibrin gel as a three dimensional matrix in cardiovascular tissue engineering," *European Journal of Cardio-Thoracic Surgery*, vol. 17, pp. 587–591, May 2000.
- [106] G. A. Villalona, B. Udelsman, D. R. Duncan, E. McGillicuddy, R. F. Sawh-Martinez, N. Hibino, C. Painter, T. Mirensky, B. Erickson, T. Shinoka, and C. K. Breuer, "Cell-Seeding Techniques in Vascular Tissue Engineering," *Tissue Engineering Part B: Reviews*, vol. 16, no. 3, pp. 341–350, 2010.
- [107] N. J. Hamilton, D. D. H. Lee, K. H. Gowers, C. R. Butler, E. F. Maughan, B. Jevans, J. C. Orr, C. J. McCann, A. J. Burns, S. MacNeil, M. A. Birchall, C. O'Callaghan, R. E. Hynds, and S. M. Janes, "Bioengineered airway epithelial grafts with mucociliary function based on collagen IV- and laminin-containing extracellular matrix scaffolds," *European Respiratory Journal*, vol. 55, June 2020.
- [108] C. Bautista, H. Park, C. Mazur, R. Aaron, and B. Bilgen, "Effects of Chondroitinase ABC-Mediated Proteoglycan Digestion on Decellularization and Recellularization of Articular Cartilage," *PLOS ONE*, vol. 11, no. 7, 2016.
- [109] L. Luo, R. Eswaramoorthy, K. Mulhall, and D. Kelly, "Decellularization of porcine articular cartilage explants and their subsequent repopulation with human chondroprogenitor cells," *Journal of the Mechanical Behavior of Biomedical Materials*, vol. 55, pp. 21–31, Mar. 2016.

- [110] L. Luo, J. Y. Chu, R. Eswaramoorthy, K. J. Mulhall, and D. J. Kelly, "Engineering Tissues That Mimic the Zonal Nature of Articular Cartilage Using Decellularized Cartilage Explants Seeded with Adult Stem Cells," *ACS Biomaterials Science & Engineering*, vol. 3, pp. 1933–1943, Sept. 2017.
- [111] Y. Xu, D. Li, Z. Yin, A. He, M. Lin, G. Jiang, X. Song, X. Hu, Y. Liu, J. Wang, X. Wang, L. Duan, and G. Zhou, "Tissue-engineered trachea regeneration using decellularized trachea matrix treated with laser micropore technique," *Acta Biomaterialia*, vol. 58, pp. 113–121, Aug. 2017.
- [112] S. Nürnberger, C. Schneider, C. Keibl, B. Schüdl, P. Heimel, X. Monforte, A. Teuschl, M. Nalbach, P. Thurner, J. Grillari, H. Redl, and S. Wolbank, "Repopulation of decellularised articular cartilage by laser-based matrix engraving," *EBioMedicine*, vol. 64, p. 103196, 2021.
- [113] Q. Zhou, X. Ye, Q. Ran, A. Kitahara, Y. Matsumoto, M. Moriyama, Y. Ajioka, and Y. Saijo, "Trachea Engineering Using a Centrifugation Method and Mouse-Induced Pluripotent Stem Cells," *Tissue Engineering Part C: Methods*, vol. 24, no. 9, pp. 524–533, 2018.
- [114] S. Haykal, M. Salna, Y. Zhou, P. Marcus, M. Fatehi, G. Frost, T. Machuca, S. O. Hofer, and T. K. Waddell, "Double-Chamber Rotating Bioreactor for Dynamic Perfusion Cell Seeding of Large-Segment Tracheal Allografts: Comparison to Conventional Static Methods," *Tissue Engineering Part C: Methods*, vol. 20, no. 8, pp. 681–692, 2014.
- [115] F. G. Aoki, R. Varma, A. E. Marin-Araujo, H. Lee, J. P. Soleas, A. H. Li, K. Soon, D. Romero, H. T. Moriya, S. Haykal, C. Amon, T. K. Waddell, and G. Karoubi, "De-epithelialization of porcine tracheal allografts as an approach for tracheal tissue engineering," *Scientific Reports*, vol. 9, Aug. 2019.
- [116] E. Y. Salinas, J. C. Hu, and K. Athanasiou, "A Guide for Using Mechanical Stimulation to Enhance Tissue-Engineered Articular Cartilage Properties," *Tissue Engineering Part B: Reviews*, vol. 24, no. 5, pp. 345–358, 2018.
- [117] K. Li, C. Zhang, L. Qiu, L. Gao, and X. Zhang, "Advances in Application of Mechanical Stimuli in Bioreactors for Cartilage Tissue Engineering," *Tissue Engineering Part B: Reviews*, vol. 23, no. 4, pp. 399–411, 2017.
- [118] W. Cao, W. Lin, H. Cai, Y. Chen, Y. Man, J. Liang, Q. Wang, Y. Sun, Y. Fan, and X. Zhang, "Dynamic mechanical loading facilitated chondrogenic differentiation of rabbit BMSCs in collagen scaffolds," *Regenerative Biomaterials*, vol. 6, pp. 99–106, Mar. 2019.
- [119] L. Kock, C. van Donkelaar, and K. Ito, "Tissue engineering of functional articular cartilage: the current status," *Cell and Tissue Research*, vol. 347, pp. 613–627, 2012.
- [120] M. C. Jones, F. A. Rueggeberg, A. J. Cunningham, H. A. Faircloth, T. Jana, D. Mettenburg, J. L. Waller, G. N. Postma, and P. M. Weinberger, "Biomechanical changes from long-term freezer storage and cellular reduction of tracheal scaffoldings," *The Laryngoscope*, vol. 125, pp. E16–E22, 2015.
- [121] A. Sotres-Vega, J. Villalba-Caloca, R. Jasso-Victoria, J. R. Olmos-Zúniga, M. Gaxiola-Gaxiola, M. Baltazares-Lipp, A. Santibañez-Salgado, and P. Santillán-Doherty, "Cryopreserved Tracheal Grafts: A Review of the Literature," *Journal of Investigative Surgery*, vol. 19, no. 2, pp. 125–135, 2006.
- [122] Athena Environmental Sciences, Inc., "FNC Coating Mix." <https://athenaes.com/accessory-products.html>, 2020.
- [123] Z. Liu, M. Tamaddon, Y. Gu, J. Yu, N. Xu, F. Gang, X. Sun, and C. Liu, "Cell Seeding Process Experiment and Simulation on Three-Dimensional Polyhedron and Cross-Link Design Scaffolds," *Frontiers in Bioengineering and Biotechnology*, vol. 8, p. 104, 2020.
- [124] M. W. Pot, L. M. de Kroon, P. M. van der Kraan, T. H. van Kuppevelt, and W. F. Daamen, "Unidirectional BMP2-loaded collagen scaffolds induce chondrogenic differentiation," *Biomedical Materials*, vol. 13, Nov. 2018.

- [125] M. W. Pot, *Towards regeneration of articular cartilage. Construction and evaluation of unidirectional collagen scaffolds*. PhD thesis, Radboud University Nijmegen, Apr. 2017.
- [126] S. H. Cartmell, S. Rathbone, G. Jones, and L. A. Hidalgo-Bastida, "3D Sample Preparation for Orthopaedic Tissue Engineering Bioreactors," in *3D Cell Culture. Methods in Molecular Biology (Methods and Protocols)* (J. W. Haycock, ed.), pp. 61–76, Humana Press, 2011.
- [127] Y. Zhong, A. Jiang, F. Sun, Y. Xiao, Y. Gu, L. Wu, Y. Zhang, and H. Shi, "A comparative study of the effects of different decellularization methods and genipin-cross-linking on the properties of tracheal matrices," *Tissue Engineering and Regenerative Medicine*, vol. 16, no. 1, pp. 39–50, 2018.
- [128] C. T. Buckley and K. U. O'Kelly, "Maintaining cell depth viability: on the efficacy of a trimodal scaffold pore architecture and dynamic rotational culturing," *Journal of Materials Science: Materials in Medicine*, vol. 21, no. 5, p. 1731–1738, 2010.
- [129] A. Kurzyk, B. Ostrowska, W. Świążkowski, and Z. Pojda, "Characterization and Optimization of the Seeding Process of Adipose Stem Cells on the Polycaprolactone Scaffolds," *Stem Cells International*, vol. 2019, 2019.
- [130] A. Levin, V. Sharma, L. Hook, and E. García-Gareta, "The importance of factorial design in tissue engineering and biomaterials science: Optimisation of cell seeding efficiency on dermal scaffolds as a case study," *Journal of Tissue Engineering*, vol. 9, 2018.



Optimization of Static Seeding

Static seeding of tissue-engineered constructs is often done to assess cytocompatibility, as scaffolds must be capable of supporting cells in order to be clinically useful [45]. In the seeding optimization experiments conducted in this study, scaffolds were seeded using a static droplet seeding method, in which a concentrated cells suspension was dripped on the surface of the scaffolds. Each seeding method conducted is discussed below. It is important to note that the majority of seeding experiments were carried out before the efficiency of decellularization was assessed, since previous experiments performed by a researcher at the lab evaluating scCO₂ decellularization did not depict the partial decellularization that was seen in this thesis (see Section 3.1).

For each seeding method, cell attachment and proliferation were assessed using the WST-1 assay and H&E staining. For the protocols of the WST-1 assay and H&E staining, the reader is referred to Sections 2.2.3 and 2.1.3.

A.1. Materials and Methods

A.1.1. Static surface seeding with hbSMCs of a dry scaffold

Decellularized tracheal scaffolds (scCO₂(I), scCO₂(II), scCO₂(III) and DEM-ethanol) were seeded with a concentrated cell suspension of hbSMCs ($n = 3$). In brief, scaffolds were cut into 10x20 mm pieces and placed, one scaffold per well, in a 24-well plate with the outer surface turned downwards. A 100 μ L cell suspension containing 5×10^5 human bladder smooth muscle cells (hbSMCs) was pipetted into each well and incubated for 4 hours in a 5% CO₂, 37°C incubator. After 4 hours, 1 mL smooth muscle cell (SMC) medium was added to each well. After 24 hours and after 7 days, constructs were harvested for evaluation.

A PicoGreen DNA assay (Quant-iT PicoGreen dsDNA Assay Kit, Thermo Fisher Scientific) was conducted to obtain the DNA content of the decellularized tracheal constructs. In brief, small pieces (6 mm punches) of decellularized tracheal tissue were cut, weighted, placed in an Eppendorf tube with 1 mL milliQ and incubated at 37°C for 90 minutes. Subsequently, samples were stored at -80°C overnight. Next, 28 μ L of standards and samples were added to a 96-well plate, to which 72 μ L of PicoGreen solution and 100 μ L of Tris-EDTA buffer was added. After the plate was incubated in the dark for 10 minutes, the fluorescence was measured using a microplate reader (Wallac 1420 Victor) at excitation/emission wavelengths of 485/525 nm. DNA contents were determined in relation to the standard curve and normalised to the wet weight of the samples.

A.1.2. Static surface seeding with hbSMCs of a pre-wetted scaffold

The second seeding method compared FNC coating of a tracheal scaffold with pre-wetting the scaffold in medium. For this, FNC coating mix (Athena Enzyme Systems) was used, which is a “*serum-free tissue culture reagent containing fibronectin, collagen and albumin that is used to enhance the attachment of adherent cells to plastic flasks or microplates*” [122]. In brief, a decellularized tracheal scaffold (scCO₂(III)) was cut into approximately 10x10 mm pieces. Half of the pieces ($n = 2$) were rehydrated in FNC mix containing Pen-Strep overnight at room temperature, and the other half of the pieces ($n = 2$)

were rehydrated in SMC proliferation medium without FCS containing P/S overnight at room temperature (on a rollerbank). The next day, scaffolds were placed with the luminal side facing downwards in a 24-well low attachment plate and a 100 μL cell suspension containing 5×10^5 hbSMCs was pipetted on top of each scaffold. Scaffolds were incubated after the seeding procedure in a 5% CO_2 , 37°C incubator for 2 hours to enable cell attachment and transferred to new wells in the 24-well plate, prior to adding proliferation medium. After 24 hours, constructs were analysed to assess the seeding efficiency. Constructs were analysed again at day 7.

A.1.3. Static surface seeding with hADSCs of a pre-wetted scaffold

The third seeding method again compared FNC coating of a tracheal scaffold with pre-wetting the scaffold in medium. However, the duration of coating was extended to 96 h, and instead of using hbSMCs, human ADSCs (hADSCs) were used. Besides, both a cell suspension of 100,000 cells/ cm^2 and a cell suspension of 500,000 cells/ cm^2 were tested. In brief, a decellularized tracheal scaffold (scCO₂(III)) was cut into approximately 10x10 mm pieces and either coated with FNC mix containing P/S overnight or incubated in alphaMEM medium supplemented with 10% FCS and 1% P/S for 96 h (on a rollerbank at room temperature). After 96 hours, constructs were placed in a 24-well low attachment plate and a cell suspension of hADSCs (100 μL with either 1×10^5 cells or 5×10^5 cells) was pipetted onto the constructs. One construct that was incubated in medium was left unseeded as a control. Constructs were incubated in a 5% CO_2 , 37°C incubator for 2 hours and transferred to new wells in the 24-well plate, prior to adding proliferation medium. After 24 hours, constructs were analysed to determine the seeding efficiency. The same analyses were performed after 7 days.

A.1.4. Static seeding with progenitor cells isolated from porcine pleura, trachea, pericard and adipose tissue

Another static seeding experiment was attempted with different progenitor cells. Decellularized tracheal scaffolds were cut with a 12 mm biopsy punch and washed in sterile 0.9% physiological saline solution (at least 2 \times 1 hour and once overnight) followed by incubation in cell culture medium for a minimum of 24 h. Punches from the DEM-ethanol group were also sterilized with 70% ethanol for a minimum of 24 h prior to incubation in 0.9% physiological saline solution and culture medium. Scaffold punches were placed in a 24 well plate and seeded statically with a 100 μL cell suspension containing 5×10^5 cells (which was either isolated from porcine pleura, trachea, pericard or adipose tissue, at passage 4). The metabolic activity of the seeded cells and cellular adherence were measured after 1 and 7 days.

A.1.5. Pre-wetting with FCS

Static surface seeding was carried out as described in section A.1.4. Punches from the scCO₂(III) and DEM-ethanol groups ($n = 1$ per time point) were used, and the punches were seeded with pADSCs (at passage 6) rather than the previously described progenitor cells.

A.1.6. Using Whatman paper

Again, decellularized tracheal scaffolds of the scCO₂(III) and DEM-ethanol groups ($n = 1$ per time point) were cut with a 12 mm biopsy punch and incubated in 0.9% physiological saline solution for a minimum of 24 hours and cell culture medium for a minimum of 24 hours before cell seeding. Punches from the DEM-ethanol group were also sterilized with 70% ethanol for a minimum of 24 hours prior to incubation in 0.9% physiological saline solution and culture medium. Prior to seeding, the tracheal scaffold punches were patted dry with sterile Whatman paper. Subsequently, the scaffold punches were placed in 6-well low attachment plates with on the bottom a double layer of sterile Whatman paper. Subsequently, pADSCs were dripped on the outer layer of the constructs (which was facing upwards) (100 μL per scaffold, 500,000 cells/ cm^2). As soon as the liquid was completely absorbed, the Whatman paper was removed and medium was added gently. After 24 hours of culture, seeded scaffolds were either treated with chondrogenic differentiation medium (high-glucose Dulbecco's Modified Eagle's Medium (Invitrogen) supplemented with 1% insulin-transferrin-selenious acid mix (ITS), 50 nM dexamethasone, 50 $\mu\text{g}/\text{mL}$ L-ascorbic acid 2-phosphate, 40 $\mu\text{g}/\text{mL}$ L-proline, 100 $\mu\text{g}/\text{mL}$ sodium pyruvate, 10 ng/mL TGF- β 3 (Thermo Fisher Scientific) and 1% (v/v) P/S), or were continuously cultured in standard culture medium.

A.2. Results & Discussion

Cell seeding efficiency and distribution play an important role in the *in vitro* and *in vivo* functionality of the cell-seeded scaffold [123]. The first seeding experiment was performed with hbSMCs, which are a fast growing and easy to culture cell line. Prior to cell seeding, scaffolds of the scCO₂ group were dry. This implies that cells were directly seeded on the outer (adventitia) surface of the freeze-dried tissue samples. In Figure A.1 the WST-1 assay and DNA assay for this experiment are depicted. The figure clearly shows that proliferation decreased from day 0 (24 hours after seeding) to day 7. Only the scCO₂(I) group showed an increase in metabolic activity, but this was not reflected in the DNA content of these samples. Histological staining 7 days post-seeding also demonstrated that cells were not able to adhere to the scaffolds (data not shown).

In the second experiment, tissue samples from the scCO₂(III) group were pre-wetted with either FNC mix or SMC medium, to determine if this would have an effect on cell adherence. H&E staining of the constructs showed some cells on the surface of the tissue samples one day after seeding (Figure A.2). However, seven days after seeding no cells could be found on the tissue samples. Furthermore, the WST-1 cell proliferation assay showed a low absorbance signal, both one day after seeding and seven days after seeding, indicating low metabolic activity.

The next step was to determine if cell attachment would be better with a different cell type or lower seeding density. As such, scaffold samples from the scCO₂(III) were pre-wetted with FNC mix or α MED medium, and seeded with either 1×10^5 ADSCs/cm² or 5×10^5 ADSCs/cm². Again, samples were analyzed over the course of one week (1 and 7 days). WST-1 assay showed a very low signal, and the unseeded scaffold sample showed a comparable absorbance value as the seeded samples (Figure A.3.A). ADSCs that were seeded without a scaffold, on the other hand, showed an absorbance value that was around 3-fold the absorbance value of the seeded scaffolds, and thus displayed high metabolic activity (Figure A.3.B). Seven days after seeding, comparable WST absorbance values were seen, again confirming that cells did not adhere to the scaffolds. Subsequently, both decellularized tissue samples from the scCO₂(III) and DEM-ethanol groups were seeded with different progenitor cells. Similar to the previous experiments, a decrease in cell proliferation was observed after 7 days of culture in most samples (Figure A.4.A). After 7 days of culture, histological images revealed no cell attachment. Rehydrating the tissues in FNC mix or medium before cell seeding, as well as using a different cell type and lower seeding density, did thus not improve results.

Next, cell suspensions of pADSCs were pipetted on scaffold punches placed on a double layer of autoclaved Whatman paper. The underlying idea is that the Whatman paper will extract fluids from the scaffold and will allow infiltration of the cells by capillary force [124, 125]. In a previous study, in

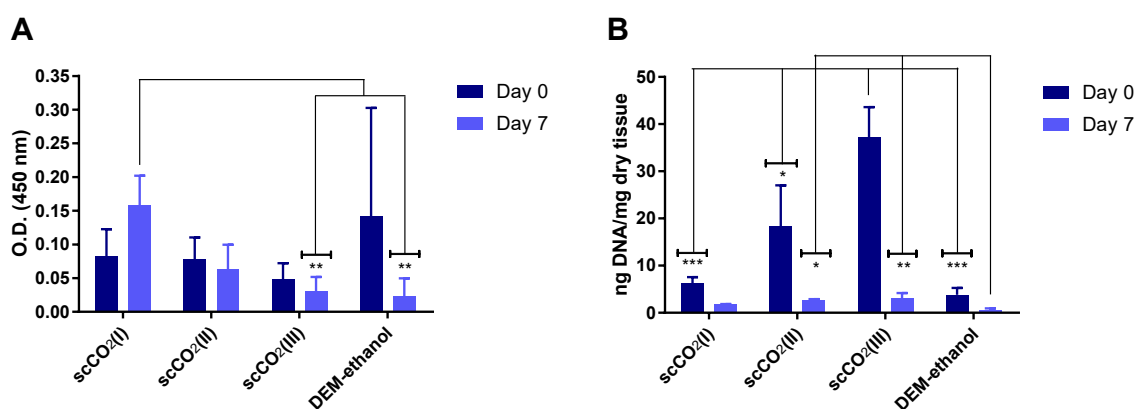


Figure A.1: Human bladder smooth muscle cell (hbSMC) seeding of decellularized tracheal scaffolds. All scaffolds were seeded with 5×10^5 hbSMCs at passages 6 and 9 ($n = 3$ for each group). (A) Metabolic activity (WST-1 assay) and (B) cell proliferation (PicoGreen) were measured and compared on day 0 (24 hours) and day 7 after seeding. Data were expressed as mean \pm SD. Results display that the metabolic activity of the cells is low and did not increase over time, indicating that the cells were not able to adhere on the scaffolds. DNA quantification, which is assumed proportional to cell number, showed a DNA amount of less than 50 ng/mg scaffold in all scaffolds, indicating a low cell number. Besides, DNA content decreased over time in all scaffolds. * $p < 0.05$; ** $p < 0.01$; *** $p < 0.001$.

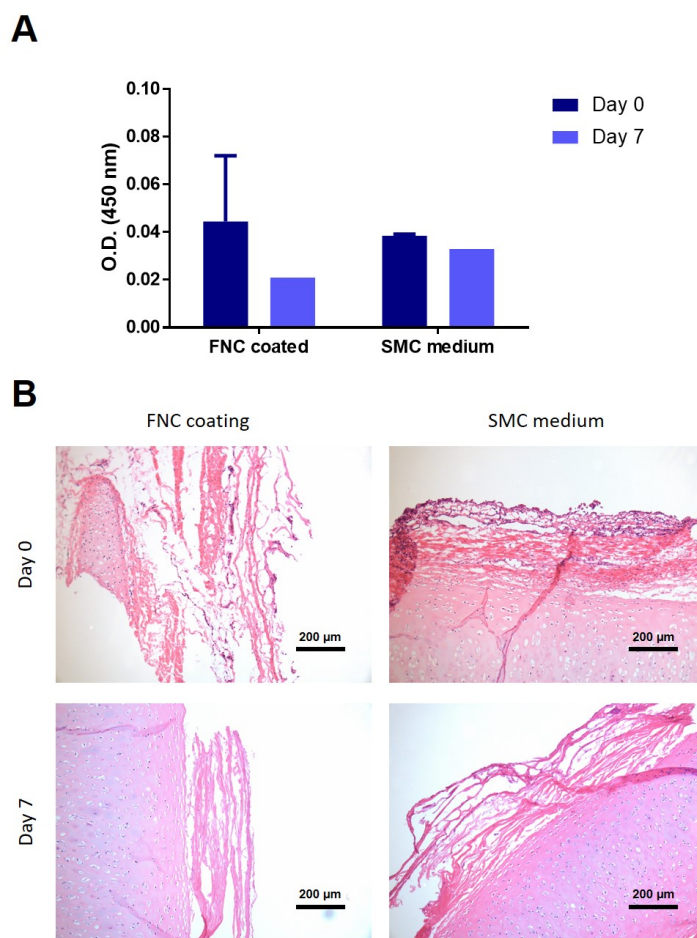


Figure A.2: Human bladder smooth muscle cell (hbSMC) seeding of decellularized tracheal scaffolds pre-wetted in SMC medium or FNC coating mix. All scaffolds were decellularized with the $scCO_2$ (III) method and seeded with 5×10^5 hbSMCs. (A) WST-1 assay displays absorbance values close to zero, indicating low metabolic activity of the seeded cells. (B) After 7 days of culture, H&E staining demonstrated that there were no cells on the surface of the scaffolds.

which collagen scaffolds were seeded, this procedure increased cell influx into the scaffolds [125]. The results depict that some cells adhered to the surface of the DEM-ethanol scaffold. Also, the metabolic activity of cells seeded on the DEM-ethanol scaffold did not decline from day 0 to day 7. Metabolic activity of the cells seeded on the $scCO_2$ (III) scaffold, however, did decrease and no cells were visible on the surface, as assessed by histological staining.

Furthermore, an experiment was conducted with samples that were pre-wetted with 100% FCS overnight. Pre-wetting with FCS, similarly to pre-wetting with medium containing FCS, allows the proteins from the FCS to attach to the scaffold's surface, providing an anchor for the cells to bind to [126]. A higher concentration of FCS was thought to provide a better outcome. Important to note is that in this experiment the complete 12 mm punch was used for the WST-1 assay, and not only a 6 mm biopsy punch. This partly explains the differences in absorbance values seen with the WST-1 assay. As shown in Figure A.6, some cells were able to adhere to the scaffold treated with DEM-ethanol. After 7 days, some cells were still visible on the surface of the DEM-ethanol treated scaffold, but cells were not homogeneously distributed. However, no cells were visible on the surface of the $scCO_2$ (III) scaffold after 7 days. The WST-1 assay validated the histological findings.

After all these attempts, we tried seeding with fibrin-encapsulated porcine ADSCs. With this method, cells did seem to adhere to both scaffold types (Figure A.7). It was therefore decided to repeat this seeding method several times, as discussed in the Results section (Section 3.5).

A number of reasons may explain why the various static seeding methods studied demonstrated poor cell adherence. First of all, seeding efficiency has been shown to be affected by the material of the scaffold, suggesting that the optimal seeding method may be different for each scaffold type. As

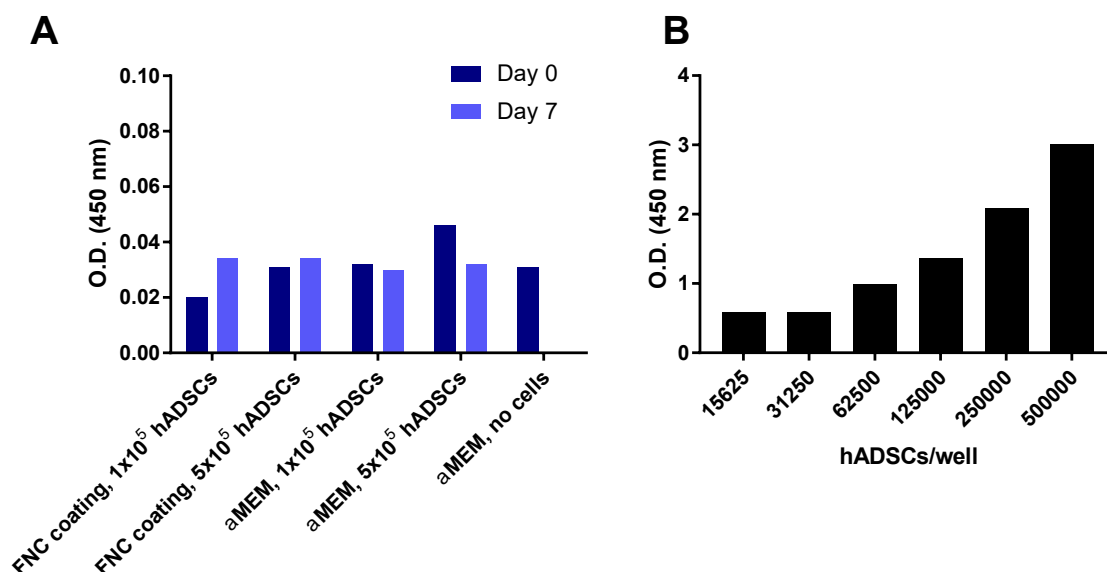


Figure A.3: Proliferation (WST-1 assay) of (A) human adipose derived stem cells (hADSCs) seeded on tracheal scaffolds decellularized with the scCO₂(III) method cultured for up to 7 days and (B) hADSCs seeded in a 24 well plate after 24 hours of incubation. Bars represent the results of one experiment ($n = 1$).

already mentioned in the Discussion (Section 4.3), Hamilton et al., for instance, found that only few cells covered the surface of tracheal scaffolds decellularized with DEM and statically seeded with bronchial epithelial cells, while a large number of live cells were found on the surface of decellularized dermis scaffolds [107], suggesting that cells do not easily adhere to decellularized tracheal scaffolds. In other studies on the decellularization and recellularization of tracheal tissue limited information is provided on cell seeding efficiency and cell adherence after a longer culture period (e.g. 7 days). Butler et al., for instance, only showed cellular adhesion of bronchial epithelial cells for up to 5 days [45]. Whereas Zhong et al., for example, demonstrated that after a culture period of 7 days, the number of cells seeded on the decellularized trachea matrices decreased, but no histological images were displayed [127].

Furthermore, the seeding volume used has been found to affect cell seeding efficiency. In a study by Buckley and O'Kelly, different cell seeding volumes were studied. They showed that the highest seeding efficiency was found using a seeding volume of 25 μ L ($85.4\% \pm 4.9\%$), whereas the lowest seeding efficiency was found with a seeding volume of 100 μ L ($43.8\% \pm 3.2\%$) [128]. Similarly, Kurzyk et al. demonstrated that the seeding efficiency increased when a seeding volume of 35 μ L was used, in comparison to a seeding volume of 50 μ L [129]. In our seeding experiments, we only used a seeding volume of 100 μ L. This could thus have attributed to the limited cell adherence observed. It should be mentioned however, that a test experiment in which pADSCs in a seeding volume of 35 μ L were seeded on a scCO₂(II) scaffold did not display enhanced cell adherence (data not shown).

Besides, the experience of the author could also have played a role. Over time, the author naturally gained more experience with seeding of the scaffolds.

In summary, a variety of variables may have played a part. To further optimize cell seeding efficiency and investigate the effects of various variables on cell seeding of decellularized tracheal matrices, a full factorial design experiment could be conducted, similar to the study of Levin et al. [130]. Variables like cell seeding density, seeding volume, cell passage number, seeding time, cell type and so on could then be investigated further.

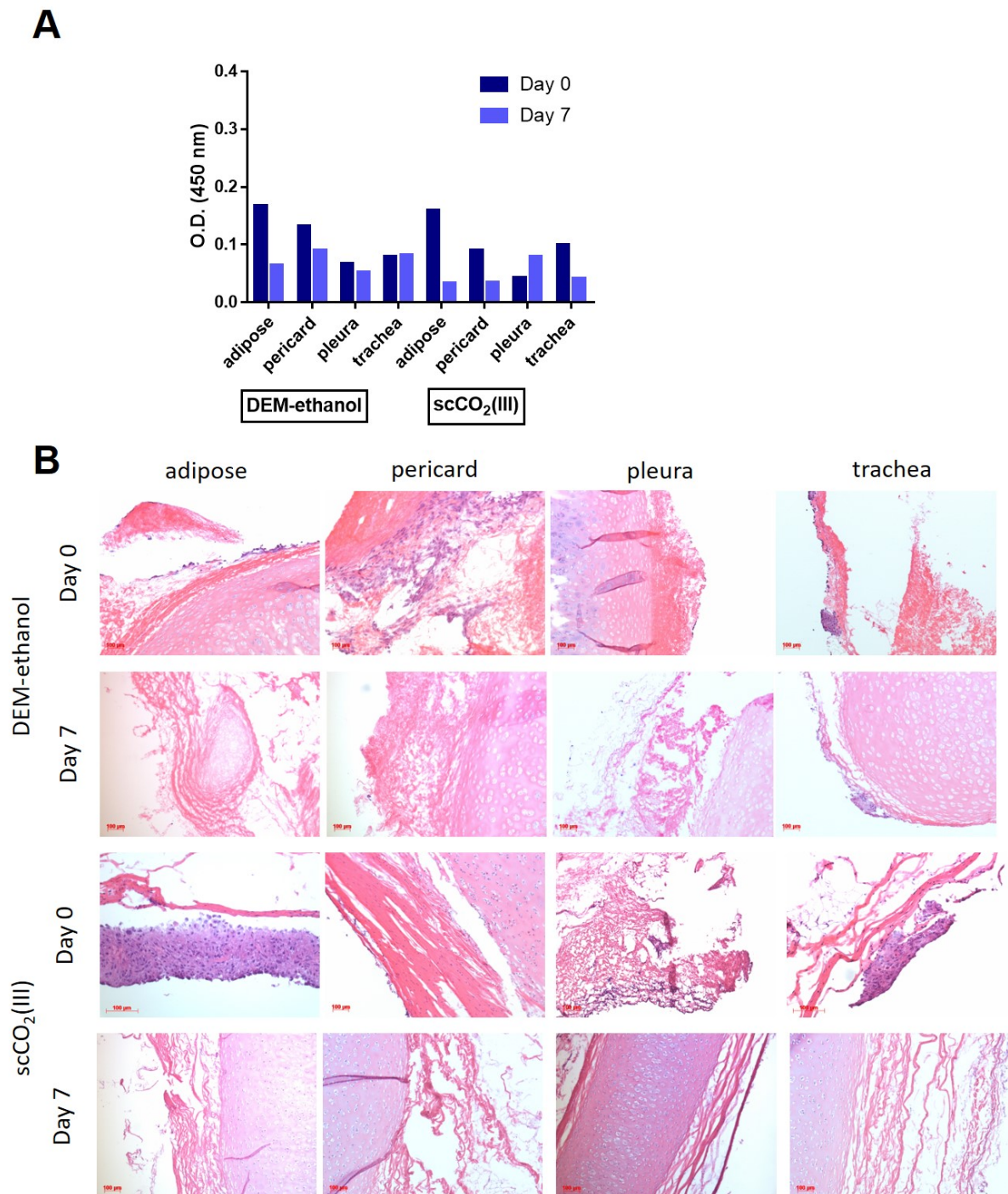


Figure A.4: Proliferation (WST-1 assay) of (A) porcine progenitor cells (isolated from pleura, pericard, trachea and adipose tissue) seeded on tracheal scaffolds decellularized with the scCO₂(III) and DEM-ethanol methods after 1 day and 7 day proliferation. Bars represent the results of one experiment ($n = 1$). (B) H&E staining images of decellularized tracheal constructs seeded with porcine progenitor cells isolated from pleura, pericard, trachea and adipose tissue and cultured for up to 7 days. The images of the DEM-ethanol scaffold seeded with progenitor cells isolated from pericard tissue at day 0 is a top view.

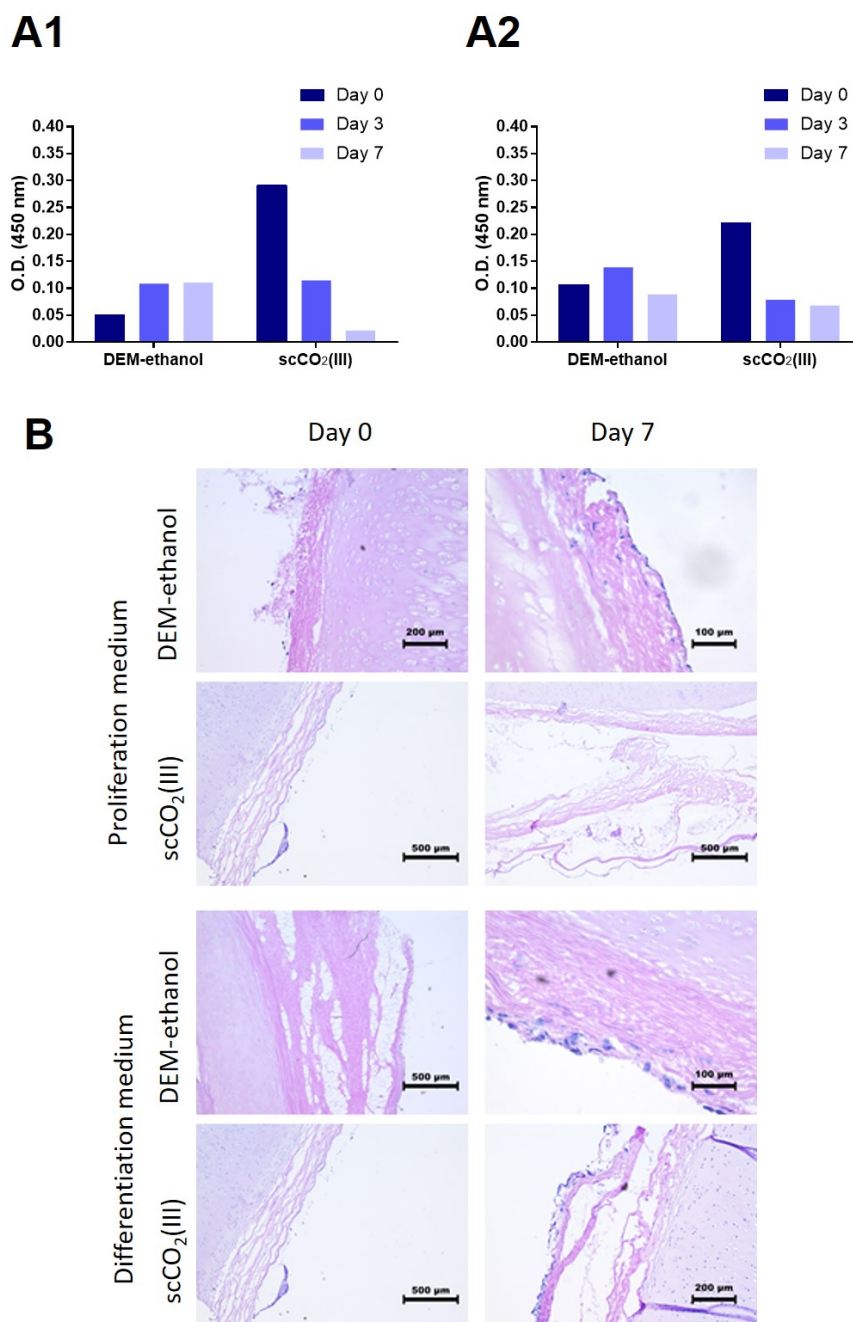


Figure A.5: Comparison of recellularized decellularized tracheal scaffolds with porcine adipose derived stem cell (pADSC). Cell suspensions of pADSCs ($5 \times 10^5 / \text{cm}^2$) were pipetted on scaffold punches placed on a double layer of autoclaved Whatman paper. After 24 hours, medium was changed to differentiation medium or the cell-seeded constructs were continuously cultured in proliferation medium. (A) Proliferation of the seeded cells was assessed with the WST-1 assay. The WST-1 assay mainly shows a decline in metabolic activity from day 0 to day 7, both when cultured in (A1) proliferation medium as well as in (A2) chondrogenic differentiation medium. (B) Images of pADSCs cultured on decellularized tracheal scaffolds at 0 and 7 days and stained with H&E. Some cell adherence on the DEM-ethanol scaffolds after 7 day proliferation was seen. The results of one experiment ($n = 1$) are depicted.

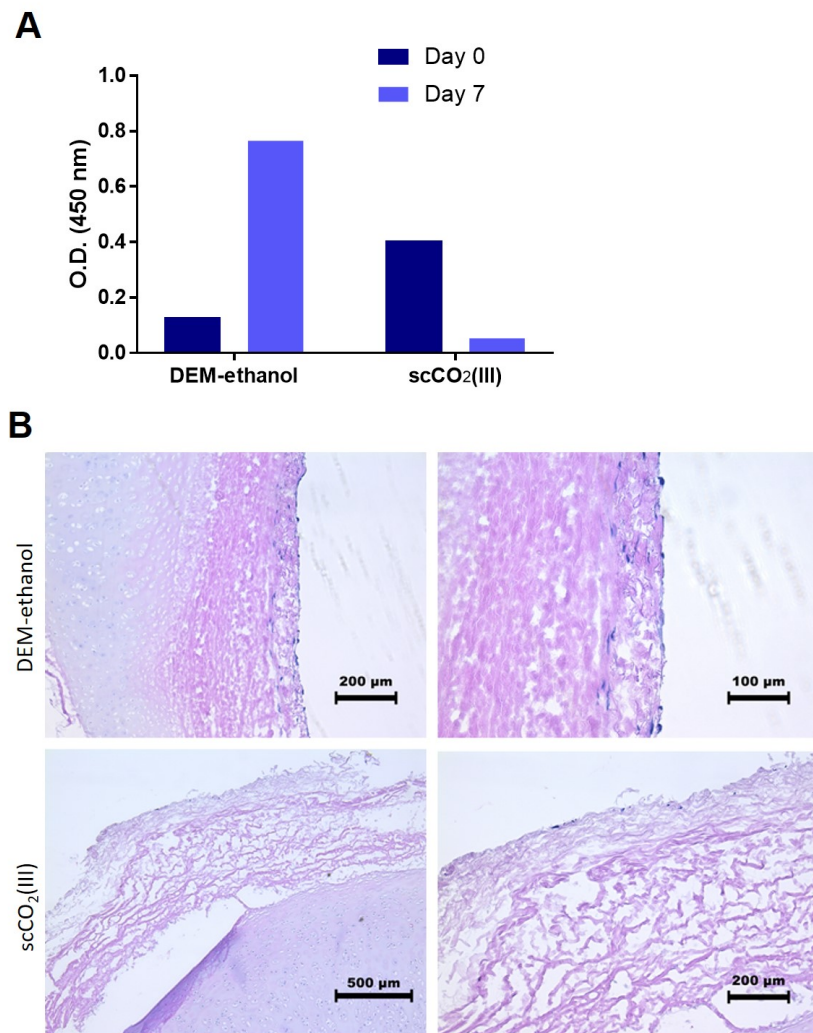


Figure A.6: 24 hours (day 0) and 7 days after porcine adipose derived stem cell (pADSC) seeding onto DEM-ethanol and scCO₂(III) decellularized tracheal scaffolds that were incubated in 100% fetal calf serum (FCS) overnight, (A) the proliferation (WST-1 assay) of the cells was measured and (B) H&E images were taken. The results of one experiment ($n = 1$) are depicted.

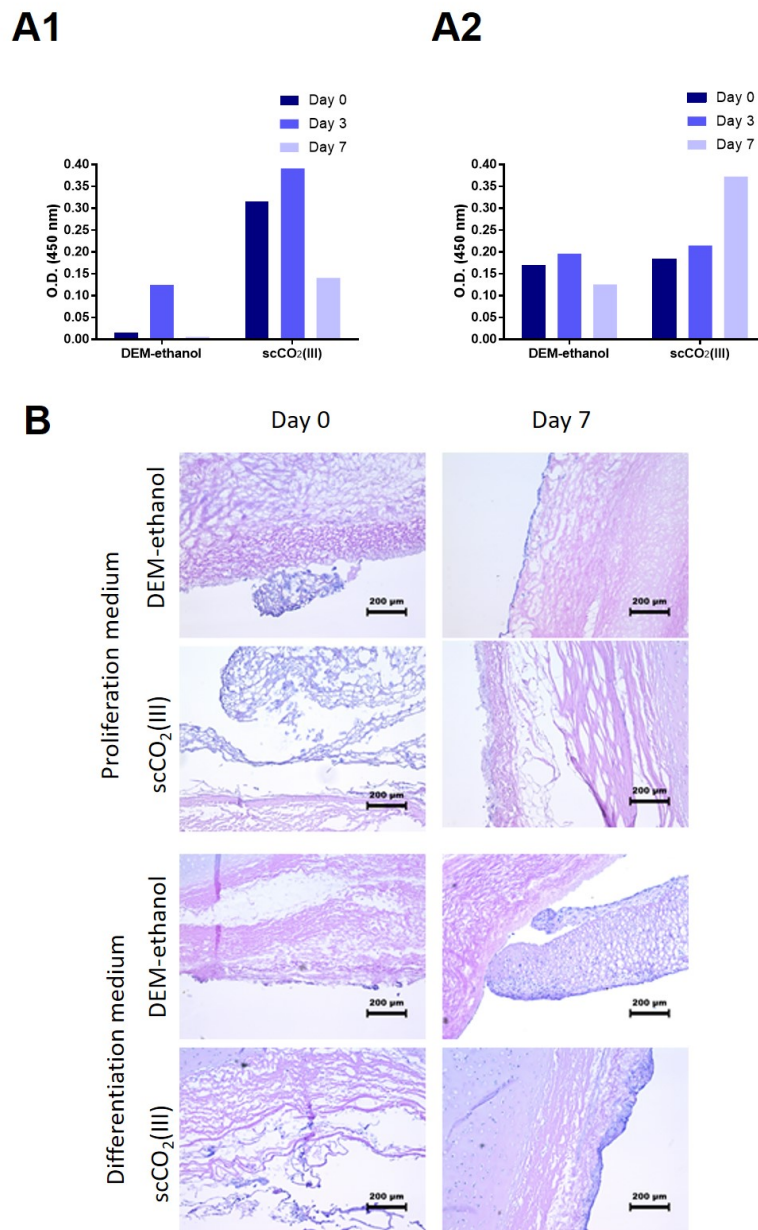


Figure A.7: Comparison of decellularized tracheal scaffolds seeded with fibrin encapsulated porcine adipose derived stem cell (pADSC). pADSCs ($5 \times 10^5 / \text{cm}^2$) were suspended in fibrinogen and, after addition of thrombin, pipetted on scaffold punches. After 24 hours, medium was changed to differentiation medium or the cell-seeded constructs were continuously cultured in proliferation medium. (A) Proliferation of the seeded cells was assessed with the WST-1 assay. Results of the cell-seeded constructs when cultured in (A1) proliferation medium or in (A2) chondrogenic differentiation medium are displayed. (B) Images of fibrin-encapsulated pADSCs cultured on decellularized tracheal scaffolds at 0 and 7 days and stained with H&E. The results of one experiment ($n = 1$) are depicted.